PREPARATION AND CHARACTERIZATION OF DOPED TRANSPARENT ZINC OXIDE THIN FILMS FOR SOLAR CELL APPLICATIONS

BY

REUBEN SETH RICHTER

(10344357)

UNIVERSITY OF GHANA

COLLEGE OF BASIC AND APPLIED SCIENCES

DEPARTMENT OF MATERIALS SCIENCE AND ENGINEERING

THIS THESIS IS SUBMITTED TO THE UNIVERSITY OF GHANA, LEGON IN PARTIAL FULFILMENT OF THE REQUIREMENTS FOR THE AWARD OF MPHIL MATERIALS SCIENCE AND ENGINEERING DEGREE

JULY, 2016.

DECLARATION

Candidate's declaration

I hereby declare that this thesis which is the result of my own original research was prepared in accordance with the University of Ghana's academic regulations and that no part of it has been presented for another degree in this University or elsewhere.

Candidate's name: Reuben Seth Richter

Signature…...……Date……..

Supervisor's declaration

I hereby declare that the preparation and presentation of the thesis were supervised in accordance with the guidelines on supervision of thesis laid down by the University of Ghana.

Supervisor's name: Prof. Boateng Onwona-Agyeman (*University of Ghana*)

Signature…..……Date……

Co-supervisor: Dr. Robinson J. Musembi (*University of Nairobi, Kenya*)

Signature…..……Date……

Head of Department's declaration

I hereby declare that the thesis has been prepared, supervised and accepted in accordance with the guidelines on thesis laid down by the University of Ghana.

Head of Department's name: Dr. David Dodoo-Arhin

Signature……Date……

ABSTRACT

The growing demand for energy has resulted in the research and development of clean and renewable energy technology and related materials. In this work, the effect of acetic acid on the structural, optical and electrical properties of undoped ZnO was studied. Also, the effect of indium and gallium dopants on the structural, optical and electrical properties of ZnO was studied. The ZnO thin films were deposited on glass substrates at 400°C using the spray pyrolysis deposition technique. X-ray diffraction (XRD) results indicated that both undoped and doped ZnO films had (002) preferred orientation. The amount of acetic acid in the precursor solution had an effect on the crystal structure of the undoped ZnO. The undoped ZnO films exhibited high transmittance above 80%. In:ZnO and Ga:ZnO films had transmittance above 60% and 70% respectively. From the Hall Effect measurements, doping improved the conductivity of the ZnO thin films however In:ZnO films showed higher electrical conductivity compared to Ga:ZnO films. Electron probe microanalysis (EPMA) results also confirmed the presence the respective dopants in the thin film samples; indium in In:ZnO and gallium in Ga:ZnO.

DEDICATION

This work is dedicated to my entire family for their numerous contributions to my academic success and especially my best friends Mary-Ann Addo-Mensah and Clement Dzifa Kekessie.

ACKNOWLEDGEMENT

I am most grateful to God for seeing me through this entire research study. I wish to further extend my sincere gratitude to my supervisors, Prof. B. Onwona Agyeman as well as Dr. R. J. Musembi for their expert guidance and inputs to help make this research a success. I acknowledge Dr. George Amoako and the lab technicians at the modern physics laboratory, University of Cape Coast for providing access to electrical characterization equipment and also their support. I further acknowledge my friends and course mates who gave counsel and support in one way or the other to facilitate my work.

I would like to acknowledge the *African Materials Science and Engineering Network (AMSEN) for their financial and technical support of this work.

*African Materials Science and Engineering Network

(A Carnegie-IAS Regional Initiative in Science and Education (RISE) Network)

TABLE OF CONTENTS

LIST OF FIGURES

LIST OF TABLES

LIST OF ABBREVIATIONS

Notation	**Meaning**
TCO	Transparent conducting oxide
ITO	Indium doped tin oxide
FTO	Fluorine doped tin oxide
CdO:In	Indium doped Cadmium oxide
ZnO	Zinc oxide
In:ZnO	Indium doped zinc oxide
Ga:ZnO	Gallium doped zinc oxide
PVD	Physical vapor deposition
CVD	Chemical vapor deposition
PE-CVD	Plasma enhanced chemical vapor deposition
PLD	Pulsed laser deposition
PV	Photovoltaic
SP	Spray pyrolysis
DSSC	Dye-sensitized solar cell
CIGS	Copper indium gallium selenide

EMS	Electromagnetic spectrum
LED	Light emitting diode
LCD	Liquid crystal display
XRD	X-ray diffraction
SEM	Scanning electron microscopy
EPMA	Electron probe microanalysis
FWHM	Full width at half maximum

CHAPTER ONE

1.0 INTRODUCTION

Solar cells are photovoltaic devices used to convert solar energy to electrical energy. The generation of electricity from photovoltaic devices continues as long as light illuminates the surface of the cell. Solar energy is a growing alternative renewable energy source. This growth is due to the abundant and widely accessible fuel source against the diminishing fossil fuels currently being used extensively (Luque & Hegedus, 2011). Unlike fossil fuels, solar energy has less environmental risks such as emission of toxic waste products and environmental hazards associated with spillage of fuel. Solar cells function at ambient temperature and have relatively low operational cost. The major challenges of solar energy are the diffuse nature of the fuel source and lack of economically efficient energy storage systems (Cho, 2011).

The solar cell is made up of various components, each with a given function which contributes to the overall efficiency of the cell. The Transparent Conducting Oxide/Film (TCO) is an important component of the solar cell design. This component is responsible for collecting and transporting electrons generated after the photoexcitation process. This requires that the TCO be optically transparent and electrically conductive. TCOs are used in electronic devices such as light emitting diodes (LED) touch and flat panel displays (Stadler, 2012). Various materials have been used as TCO in solar cells including indium doped tin oxide (ITO), fluorine-doped tin oxide (FTO) and indium-doped cadmium oxide (CdO:In). The above mentioned materials have disadvantages such as high cost, toxicity and unavailability. An alternative TCO material is zinc oxide (ZnO). Zinc oxide is a wide-band-gap semiconductor with a direct band gap of 3.3 eV at room temperature

(Krunks, 1995). The wide band gap makes zinc oxide transparent to light with high transmittance. The lattice parameters 'a' and 'c' of ZnO which has a wurtzite crystalline structure are 3.24 Å and 5.19 Å respectively (Paraguay, 1999). Undoped ZnO has very low electrical conductivity and hence requires doping to improve the conductivity. Factors that influence the choice of dopants include valency, electronegativity and ionic radius. Some of the common dopants used to improve conductivity of ZnO are aluminum and fluorine. Much work has been done to study the effects of these dopants on ZnO (Bedia, 2014; Ding, 2012; Crossay, 2012; Kumar, 2005).

There are several thin film deposition techniques employed in the fabrication of TCOs. These can be classified into three categories namely, physical vapor deposition (PVD), chemical vapor deposition (CVD) and solution growth. Under physical vapor deposition, techniques such as sputtering, pulsed laser deposition (PLD) and molecular beam epitaxy can be used for thin film deposition. Metal organic chemical vapor deposition and low pressure chemical vapor deposition are examples of CVD techniques. ZnO films have been grown by radio frequency (rf) magnetron sputtering (Jeong, 2003), chemical vapor deposition (CVD) (Purica, 2002) and molecular beam epitaxy (Opel, 2013). Most PVD and CVD techniques require complex equipment setup and operate under low pressure or high vacuum conditions. This makes these techniques very expensive. An alternative technique which has a relatively simple setup, operates in atmospheric conditions and can be scaled up easily is spray pyrolysis. Spray pyrolysis has been used to grow ZnO films with very good structural, optical and electrical properties (Crossay, 2012).

1.1 Problem Statement

Energy has become an integral part of our lives and the demand for energy is increasing at a rate faster than the generation rate. The energy crisis faced by some African countries is an indication of this problem. Fossil fuels which stands as the largest energy source is finite and hence there is

a need to find alternative sources of energy most importantly, renewable energy. Solar energy is one of the promising candidates with respect to renewable energy. However, the issue of expense and cost of fabrication hinders the use of solar energy especially in developing countries. The cost of solar cells can be reduced by replacing rare and expensive materials with more available and cheaper materials. Materials such as cadmium are toxic and pose an environmental hazard when decommissioning solar cells. The techniques for fabrication of components are known to affect the final cost of the devices. The manufacturing of TCO and other thin film components of the solar cell require cost intensive equipment which influence cost of photovoltaic devices. New methods of solar cell fabrication need to be investigated which will cut the cost of production.

1.2 Relevance and Justification

Spray pyrolysis is one the cheapest means of thin film deposition and it also has the ability of scaling up for industrial production. The SP method can be integrated into a production chain for the fabrication of photovoltaic device components. The equipment setup necessary for spray pyrolysis is less complex compared to other thin film deposition techniques. Spray pyrolysis is a non-vacuum based deposition technique. Deposition may be carried out under atmospheric conditions. Hence it is necessary to investigate the properties (electrical, structural and optical) of ZnO films grown using the SP technique. Using other dopants such as indium and gallium instead of fluorine or aluminum will also shed more light on the performance of doped ZnO as TCO in solar cells.

1.3 Overall objective

The overall objective of this study is to prepare and optimize doped ZnO thin films for application as TCO in solar cells.

1.4 Specific objectives

The specific objectives for this work were the following:

1. To study the effect of acetic acid concentration on the optical and structural properties of ZnO thin films.
2. To study the electrical properties of In:ZnO (indium-doped zinc oxide) and Ga:ZnO (gallium-doped zinc oxide).
3. To optimize ZnO films which can be used in a dye-sensitized solar cell based on conductivity and transparency.

CHAPTER TWO

2.0 LITERATURE REVIEW

2.1 Solar energy and solar cells

The combustion of fossil fuels for power generation results in emissions into the atmosphere causing serious environmental destruction as well as posing serious health hazards (Krasting, 2014). The fossils fuels are being depleted at fast rate and in near future they will all be gone; renewable energy are the best alternative source which have many advantages over the fossils fuels. Of all the available renewable energy sources which include geothermal, wind, tidal, solar and biofuel, solar energy is the most abundant (Luque & Hegedus, 2011). A solar cell is a device that converts energy from light, usually the sun, directly to electricity. Solar cells are also called photovoltaic devices and they operate by the photovoltaic effect. With respect to photoelectric effect or photoemission, the interaction of light and a material results in the absorption of photons of energy by the electrons. When the energy of the electron exceeds its work function, it is emitted as a photoelectron. The primary functions of the PV cell are to absorb light, generate charge carriers and finally transport the generated charge carriers to the electrodes in the cell. There are many different types of solar cell and classification is based on the type of materials used for the construction of the device as well as the mode of operation. Based on materials for construction, photovoltaic cells are broadly classified as organic or inorganic devices. Inorganic devices are either silicon based or non-silicon based. The silicon based devices make use of the transition element Si (silicon) and can either be crystalline or amorphous (non-crystalline) (Docampo, 2014).

Organic devices make use of organic materials. Examples of such include, organic PV and dye-sensitized solar cells. Figure 2.1 illustrates the classification of photovoltaic cells.

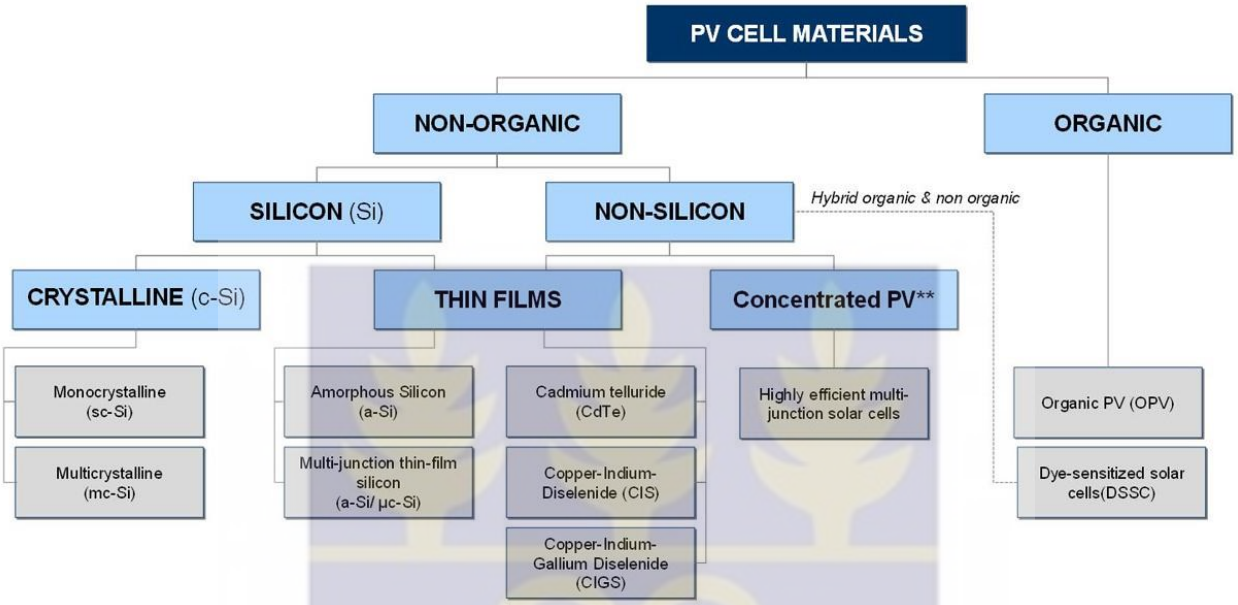

Figure 2.1 Classification of Solar Cells

Silicon photovoltaic devices based on p-n junction module were discovered in 1954 bringing the technology to 60 years of existence in 2014 (Chapin, 1954). Over the years, PV technology and devices have evolved progressively motivated by the need for cheaper, more sustainable and cleaner forms of energy. Chopra reports 2GW of solar cell provided energy being used worldwide for various applications such as stand-alone units, grid-connected power stations and many other low-power electronic devices (Maycook, 2003). For the inorganic class of solar cell devices, mono/polycrystalline silicon, cadmium telluride and copper indium gallium selenide (CIGS) are the common materials used for device fabrication. Wafer-based crystalline-silicon form the majority of all PV modules in use worldwide. Multi-junction photovoltaic (PV) devices fabricated from inorganic materials (semiconductors) have recorded energy conversion efficiencies above 37% with single-junction devices recoding conversion efficiencies of 28%. These energy conversion values were obtained while testing the devices under full sun illumination (Mitchell,

2002). Generally, conversion of solar energy to electrical energy is achieved by a two-step process. Initially, light is absorbed into the system to generate electron-hole pairs. The second step involves the separation of these charges, the electrons and holes to the negative and positive terminals respectively. A typical Si solar cell consists of an antireflective coating, n-type doped Si, p-type doped Si (which forms the bulk of the device), front and rear contacts. Figure 2.2, illustrates the of formation electron-hole pairs (e^-/h^+) in a conventional solar cell.

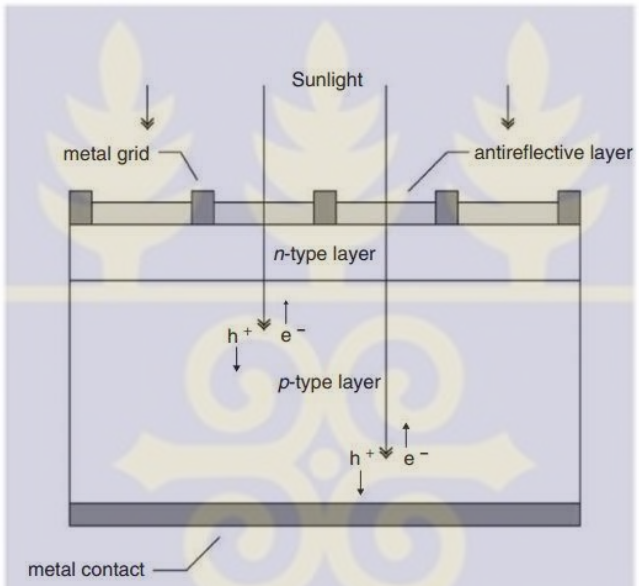

Figure 2.2 A simple conventional solar cell

Preprint of Chapter 1.16 "Crystalline Silicon Solar Cells" published in "Comprehensive Renewable Energy"
ISBN: 978-0-08-087873-7, 2012 by Elsevier - doi:10.1016/B978-0-08-087872-0.00117-7

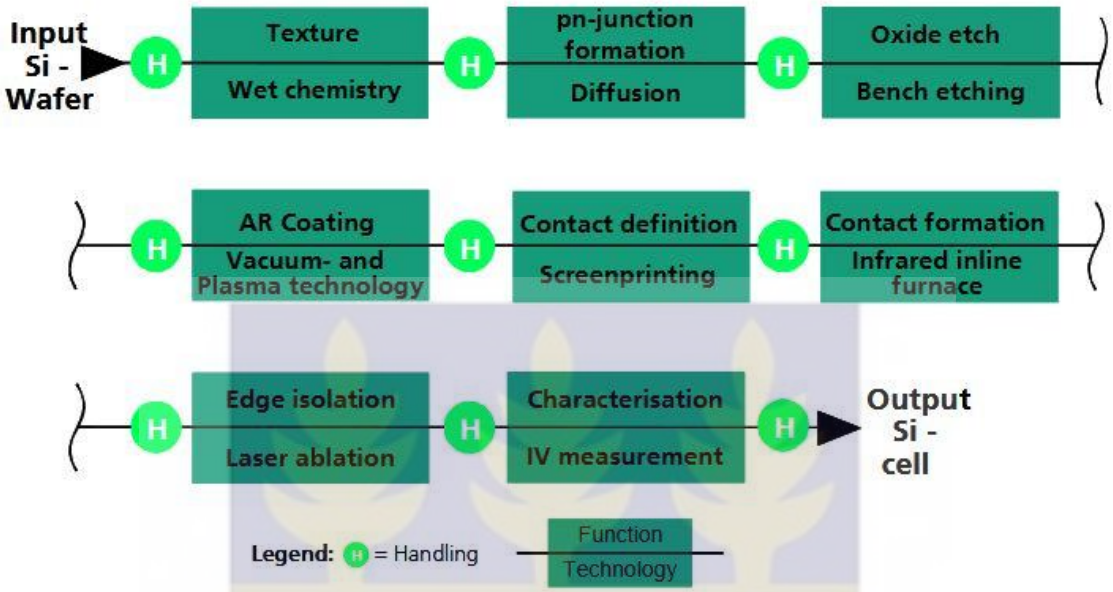

Figure 2.3 Flow diagram for crystalline silicon solar cell industrial manufacturing process

Inorganic PV devices have recorded higher energy conversion values as compared to organic material based devices. The challenge for the inorganic class of PV devices is the high cost of production. This high cost of production can be attributed to the cost of component materials and the related processing methods and techniques (Bhat, 1979). Figure 2.3 illustrates the process flow of Silicon solar cell fabrication. The use of inorganic PV devices requires high initial capital investment which results in a longer recuperation time with respect to finances and energy payback. One solution to this problem associated with inorganic PV devices is the use of relatively cheaper inorganic materials and less expensive processing techniques. This has made solution based processing methods a more viable option (Birkmire, 1997; Zweibel, 2000). Examples of solution based processing techniques include solution bath/growth, spray pyrolysis, spin coating and reel-to-reel printing. Shorter production time, low-cost materials and lower temperature processing are some of the advantages of solution based fabrication methods (Birkmire, 1997).

The dye sensitized solar cell (DSSC) is a solar cell that makes use of inorganic materials. The DSSC working principle is based on photosynthesis. The main components of the DSSC include the transparent conducting oxide (TCO), counter electrode, electrolyte and the metal oxide layer. In order to function correctly, the following processes have to occur in succession without interruption or failure. The first step in the operation of the DSSC is the photoexcitation of the dye. This is followed by the injection of the electron into the metal oxide, transportation to the working electrode and reduction of the electrolyte at the counter electrode. The final steps are diffusion in the electrolyte, regeneration of the oxidized dye and the recombination of acceptor species with the electron charge carriers that were initially injected (Mathew, 2003; Soler, 2003). Some materials used for DSSC transparent conducting oxides are doped zinc oxide (ZnO), fluorine doped tin oxide (FTO) and indium doped tin oxide (ITO). The TCO performs two key functions in the DSSC. The first is to transmit light to the active layer material and subsequently, collect and transport the charge carriers generated by the photoexcitation of the dye. The metal oxide layer material is usually a nanostructure material with significantly large surface area to absorb the photosensitive dye. TiO_2 and ZnO are examples of metal oxides used in DSSC. The dye in the DSSC is excited by photons from the incident light. The absorption range of most dyes for this application begins from 720nm which relates to 1.72eV in terms of photon energy. It is important that the TCO material exhibit high transmittance around the starting point of the dye's absorption range. This ensures that sufficient amount of light reaches the dye to maximize the photoexcitation yield. DSSC dyes may be in the form of metalorganic complexes like Ruthenium polypyridinic complexes or organic substances like Coumarin dyes. To function efficiently, the photosensitizing dye should have a wide absorption region within the visible section of the electromagnetic spectrum and also possess chemical structures that allow it to strongly bind itself to the

semiconducting metal oxide surface. It should also exhibit high photo, electrochemical and thermal stability under various conditions. DSSCs are promising PV devices due to the several reasons which include:

1. Availability of raw materials (Gratzel, 2003).
2. Relatively simpler equipment set up for processing and fabrication (Amin, 2001).
3. Lower cost of production (MaCandles, 1991).
4. Increase flexibility in terms of design and integration into already existing energy systems and devices.

Figure 2.4 illustrates the schematic diagram of a DSSC indicating the various components and mode of operation.

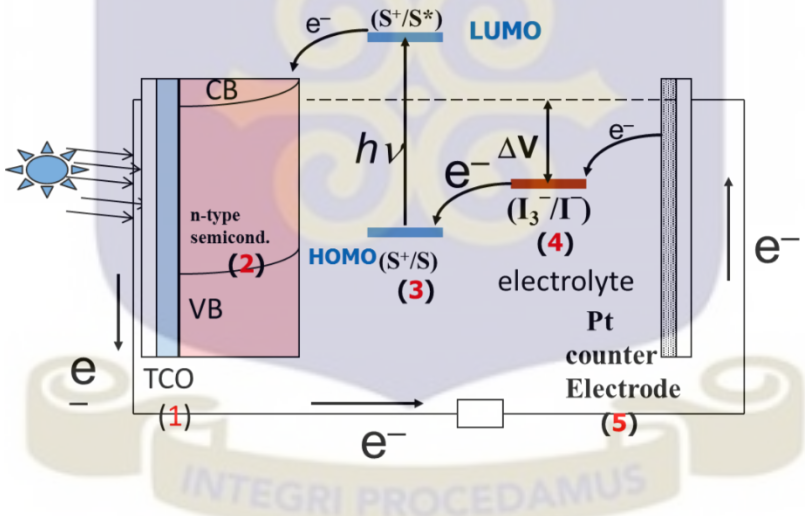

Figure 2.4 Schematic diagram of a dye-sensitized solar cell

2.2 Transparent conducting oxides

The transparent conducting oxide electrode (TCO) is a key component in opto-electronic devices. Devices that make use of TCO include light emitting diodes (LED), liquid crystal displays (LCD), photovoltaic devices, gas sensors, touch and flat panel displays (Godbole, 2011). Generally, TCO materials have two important requirements. The first is they have to be optically transparent with low absorption within the visible section of the electromagnetic spectrum. Also they have to be electrically conducting in order to transport electrons. Figure 2.5 illustrates the electromagnetic spectrum showing the visible light section. Radio waves have lower frequencies and higher wavelengths compared to X-rays and Gamma rays. Visible light occurs approximately between 400nm and 700nm on the electromagnetic spectrum and hence TCOs optical properties are characterized within this range.

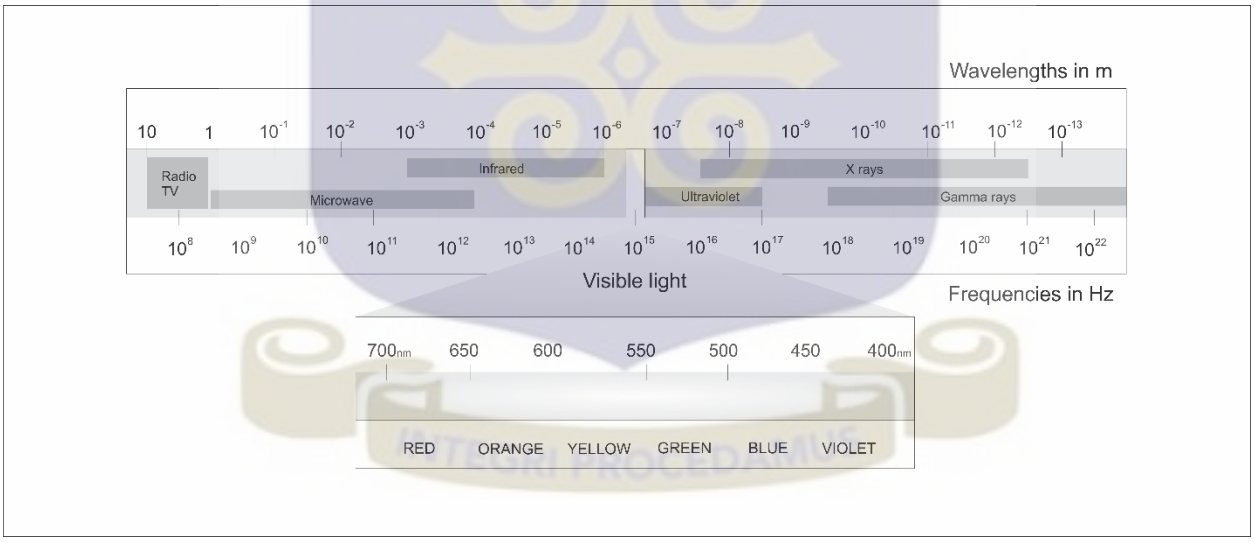

Figure 2.5 The electromagnetic spectrum

TCOs are can be prepared by various thin film technologies such as, sputtering, spray pyrolysis (Rajesh, 2012), thermal evaporation (Horng, 1999) and (plasma enhanced) chemical vapor deposition (PE-CVD) (Groenen, 2001). TCOs may either be binary or ternary compounds with a

metallic component or a combination of metals and non-metallic component which is oxygen. Some examples of TCOs are indium-doped tin oxide (ITO), doped zinc oxide (ZnO), indium-doped Cadmium oxide (CdO:In) and fluorine-doped tin oxide (FTO). In the past decade Zn_2SnO_4, $ZnSnO_3$, $MgIn_2O_4$, $(GaIn)_2O_3$ are some TCOs that have been researched and developed for use as EMI shielding, automobile window deicing and flat panel displays. Other emerging TCO compounds of interest are doped delafossite and mayenite (Stadler, 2012). The electrical and optical properties of TCOs can be further tuned by introducing dopants and varying their concentration. The dopants introduced into TCO materials may be metals, metalloids or halogens. Table 2.1 lists some examples of TCOs and the dopant elements that are introduced for each of them (Shantheyanda, 2010).

Table 2.1 List of TCOs and corresponding dopants (Shantheyanda, 2010)

Binary compound	**Dopants**
In_2O_3	Sn, Ge, Zr, Hf, Nb, Mo, F, Ti, Ta, W, Te
ZnO	Al, , B ,Ga, In, Y, F, V, Si ,Sc, Ge, Ti, Zr, Hf
SnO_2	Sb, F, As, Nb, Ta
CdO	In, Sn

A TCO may either be n-type or p-type depending on the dopant introduced. N-type ZnO can be prepared by doping ZnO with aluminum (Al) or gallium (Ga). Studies have shown that, achieving p-type doped TCOs is technologically more difficult (Stadler, 2012). For the delafossite compounds mentioned earlier, p-type characteristics are observed.

2.3 Zinc oxide as a TCO

Zinc oxide is a water insoluble, inorganic compound of zinc and oxygen with an empirical formula ZnO. It has a wurtzite structure and a wide band gap which influences the optical transparency. ZnO can be described as a multifunctional material due to the various attractive chemical and physical properties. These properties include high chemical stability, a broad range of radiation absorption, high photosensitivity and high electrochemical coupling effect (Jesionowski, 2014), (Lou, 1991). It is a widely studied semiconductor material with a direct band gap of 3.3eV. ZnO has high stability at room temperature and hence makes it an attractive candidate for optoelectronic applications. It can also be used for sensing and biomedical applications because of its good piezoelectric, pyroelectric and non- toxic properties respectively (Chaari, 2012). In the ceramics industry also, hardness, piezoelectric constant and rigidity make ZnO a material of choice. Figure 2.6 details the various applications of ZnO.

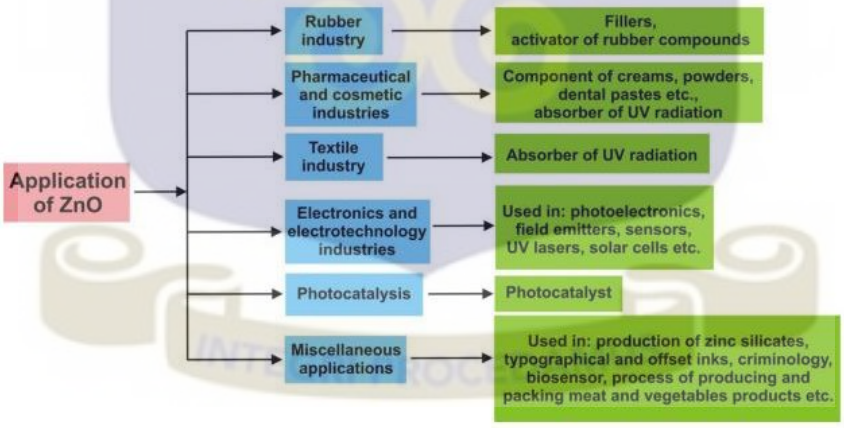

Figure 2.6 Schematic diagram detailing the various applications of ZnO

There are numerous methods of producing ZnO. Examples of such methods include, precipitation in water solution, vapor deposition, hydrothermal synthesis, sol-gel and precipitation from

microemulsion. The various methods of forming ZnO influences the shape of ZnO crystals obtained. Table 2.2 shows various methods of obtaining ZnO.

Table 2.2 Various techniques for producing ZnO (Kolodziejczak-Radzimska, 2014)

Methods	**Precursors**	**Synthesis conditions**	**Properties and applications**
Mechanochemical process	ZnCl2, Na2CO3, NaCl	calcination: 2 h, 600 °C 400 – 800 °C 400°C 0.5h 300-450°C	hexagonal structure; particles diameter: 21–25 nm hexagonal structure; particles diameter: 18–35 nm regular shape of particles; diameter ~27 nm, *BET*: 47 m2/g particles diameter: 27–56 nm particles diameter: ~51 nm, *BET*: 23 m2/g
Precipitation process	Zn(CH3COO)2, and KOH as a water solutions	temperature of process: 20–80 °C; drying: 120 °C	particles diameter: 160–500 nm, *BET*: 4–16 m2/g
	Zn(CH3COO)2, (NH4)2CO3, PEG10000 as a water solutions	drying: 12 h, 100 °C; calcination: 3 h, 450 °C	zincite structure; spherical particles (*D* ~ 30 nm); application: as a photocatlyst in photocatalytic degradation
	Zn(NO3)2	calcination: 2 h, 600 °C; aging: 240 h, 320 °C	wurtize structure; particles diameter: 50 nm; application: as a gas sensor
	Zn(NO3)2, NaOH	synthesis: 2 h; drying: 2 h, 100 °C	particles of spherical size of around 40 nm
	ZnSO4, NH4HCO3, ethanol	drying: overnight, 100 °C; calcination: 300–500 °C	wurtize structure; crystallite size 9–20 nm; particle size *D*: ~12 nm, *BET*: 30–74 m2/g
	Zn(CH3COO)2, NH3 aq.	precipitation temperature: 85 °C; drying: 10 h, 60 °C	hexagonal structure, shape of rods, flower-like particles: *L*: 150 nm, *D*: 200 nm
	ZnSO4, NH4OH, NH4HCO3	reaction: 30 min, 60 °C; drying: 12 h, 100 °C; calcination: 2 h, 400 °C	hexagonal structure, flake-like morphology (*D*: 0.1–1 μm, *L*: 60 nm)
	microsized ZnO powder, NH4HCO3	reaction: ~2 h, 25 °C; drying: 80 °C; calcination:1 h, 350 °C	hexagonal wurtize structure; flower-like and rod-like shape (*D*: 15–25 nm, *BET*: 50–70 m2/g)
	Zn(CH3COO)2, NaOH	reaction: 30 min, 75 °C; drying: overnight, room temperature	hexagonal structure; flower shape (*L*: >800 nm); application: antimicrobial activity
Precipitation in the presence of surfactants	ZnCl2, NH4OH, CTAB	aging: 96 h, ambient temperature, calcination: 2 h, 500 °C	zincite structure; particles diameter: 54–60 nm, BET = ~17 m2/g
	Zn(NO3)2, NaOH, SDS, TEA (triethanolamine)	precipitation: 50–55 min, 101 °C	wurtize structure, shape of rod-like (L: 3.6 μm, D: 400–500 nm) shape of nut-like and rice-like, size: 1.2–1.5 μm

In terms of TCO materials, currently ZnO stands as the most likely replacement candidate for the widely known ITO (Rwenyagila, 2015). Some of the factors that have made ZnO an attractive TCO material include, relatively low cost materials, high stability in several conditions and ease in doping. ZnO for TCO purposes is usually doped with group III elements from the periodic table to provide impurities that offer more electrons to improve the conductivity of ZnO (Wei-Sheng Liu, 2014).

2.4 Deposition techniques for thin films

2.4.1 *Spray Pyrolysis technique (SPT)*

Spray pyrolysis is a deposition technique that can be classified as a solution growth method for thin film formation. Other examples of solution growth methods include spin coating and electrodeposition and chemical bath deposition. Spray pyrolysis is a preferred deposition technique due to the simplicity of the equipment and also the good productivity on a large scale (Patil, 1999; Paraguay, 1999). Other advantages of the spray pyrolysis technique are:

- It provides an easy way of doping almost any material semiconductor material by simply adding the dopant chemicals to the precursor solution.
- This is a non-vacuum processing technique therefore it is less expensive, easier to set up and operate.
- No high quality target are required just the precursor solution with the relevant chemicals
- Large area deposition can be achieved and even for commercial purposes of producing organic solar cells, a production line can be developed based on spray pyrolysis.
- The risk of overheating is virtually non-existent as compared other high-power deposition techniques.

Much work has been done on developing the spray pyrolysis technique and this has led to many different equipment configurations. The general equipment/resources required for spray pyrolysis include spray nozzle, precursor solution, substrate heater, temperature regulator, air compressor and a flow meter. Figure 2.7 illustrates a general setup for the spray deposition equipment and configuration for this work (Patil, 1999).

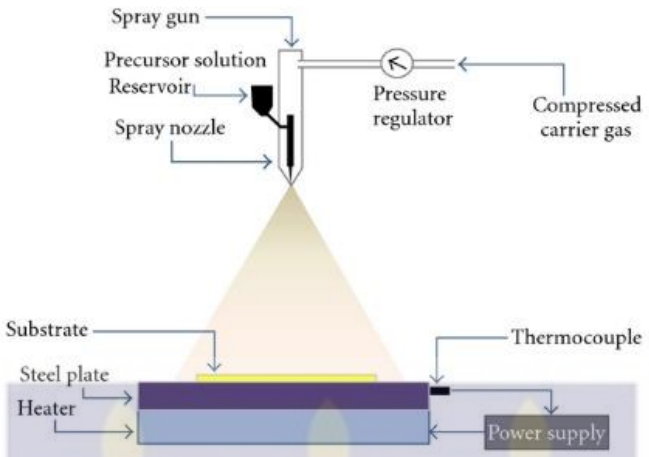

Figure 2.7 A schematic representation of the spray pyrolysis setup

The spray pyrolysis deposition technique involves spraying a precursor solution by means of a spray gun equipped with an atomizing nozzle onto a heated substrate. The precursor solution contains the dissolved chemical sources of the materials to be deposited. The solution is delivered to the substrate in the form of aerosol. The carrier gas carries the droplets from the atomizer and forms the aerosol. As the initial droplets make contact with the substrate surface, they assume circular island shapes and thermal decomposition sets in. During this process, the initial chemical compounds breakdown and fumes of the unwanted by products is released. Some of the products escape from the aerosol as the droplets approach the surface of the substrate due to the temperature. Substances with boiling temperatures above the substrate temperature decompose before the droplets touch the surface of the substrate. This process however depends on the spray rate and the velocity at which the droplets fall onto the substrate surface. As the deposition process continues, the islands aggregate to form a singular mass of thin film on the surface. The thickness of the film increases as the spray deposition continues and more droplets reach the surface. Factors that affect the quality of films obtained by spray pyrolysis include, substrate temperature, precursor solution quality, nozzle-substrate-distance and the spray rate. Various thin films materials with good

electrical, optical and structural properties have been deposited for use as TCO by the spray pyrolysis technique (Chen, 2014; Alaeddine, 2009).

2.4.2 *Chemical Vapor Deposition (CVD)*

Chemical vapor deposition (CVD) is synthesis process where chemical components react chemically in the vapor state to form a solid on a heated substrate (Pierson, 1999). The reaction for the CVD process occur both on the substrate surface and the region immediately above the substrate surface. The driving force behind the chemical reactions may be heat (thermal CV), UV (Ultra-violet) radiation, or plasma (PE-CVD). There are various variations of CVD techniques based on the initiators (thermal-CVD), deposition environment (low-pressure CVD/atmospheric pressure CVD), growth technique (chemical beam epitaxy) or the nature of the precursor components (metal-organic CVD). The process of CVD and the associated equipment is more complex compared to spray pyrolysis deposition. Figure 2.8 illustrates the general equipment set-up for a typical CVD process. The general outline for the CVD process follows these steps. The precursor materials are evaporated and moved into the reactor. The chemical reactions occur in the reactor and produce intermediates and by-products. The reactants and intermediates move to the substrate surface. On the surface, there's adsorption, surface diffusion, nucleation and growth. Further chemical reaction occur on the substrate surface to complete the product formation. The other by-products decompose and drifts away from the substrate (Hitchman, 2009). One of the advantages of CVD is the high deposition rate associated with it. This allows thick coatings to be made in a shorter period of time. CVD require high purity precursor materials and also operates at high temperatures at which certain substrates are not thermally stable and limit their use in this application. CVD however is a common deposition technique for carbon nanotube deposition (Ando, 2010).

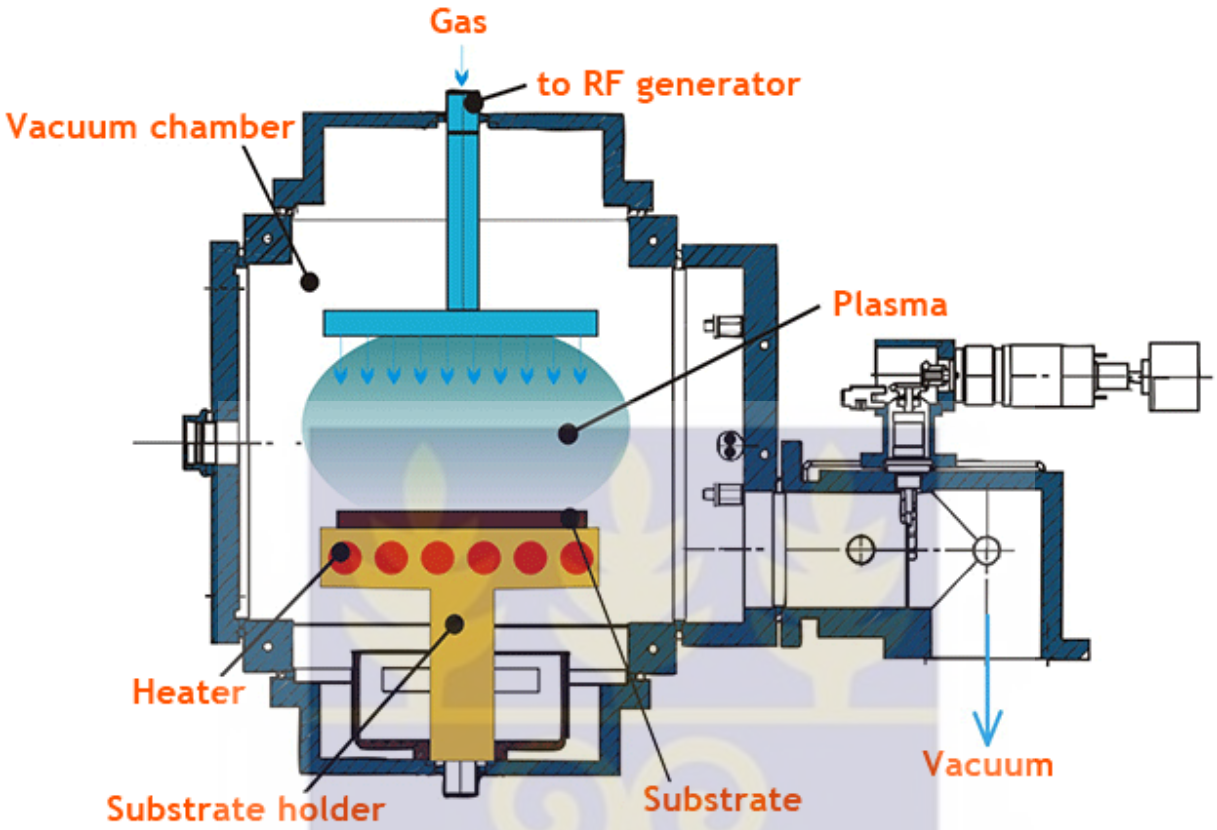

Figure 2.8 General equipment layout for CVD (Zelenograd, 2016)

2.4.3 *Physical Vapor Deposition (PVD)*

Physical vapor deposition (PVD) is a class of vacuum based deposition techniques for thin film fabrication. In PVD, physical processes cause a precursor materials (target) to vaporize and subsequently, be deposited onto a heated substrate. There are various examples of PVD process, some of which are pulsed laser deposition, sputter deposition and cathodic arc deposition. One of the common PVD processes is sputtering. Sputter deposition itself have many variants based on the equipment configuration, deposition environment and initiators. Ion-beam sputtering, dc-sputtering, reactive sputtering, gas-flow sputtering and rf (radio-frequency) magnetron sputtering are some of the examples of sputter deposition techniques. Sputtering may be described as the

ejection of surface atoms from a precursor material (target) using high energy particles. The energy exchange as a result of the bombardment of the surface atoms by these energetic particles causes the surface atoms to dislodge. In reactive sputter deposition, two or more targets are set up within the deposition chamber and the ejected atoms chemically react in a plasma field to from a new compound that is deposited on the substrate. Figure 2.9 illustrates the schematic diagram of a sputter deposition set-up indicating the target, substrate, magnets and pumps to create vacuum in the chamber. Since the PVD process occurs in a vacuum, quality films can be produced without the interference of unwanted particles that may contaminate the thin films and affect its quality and properties.

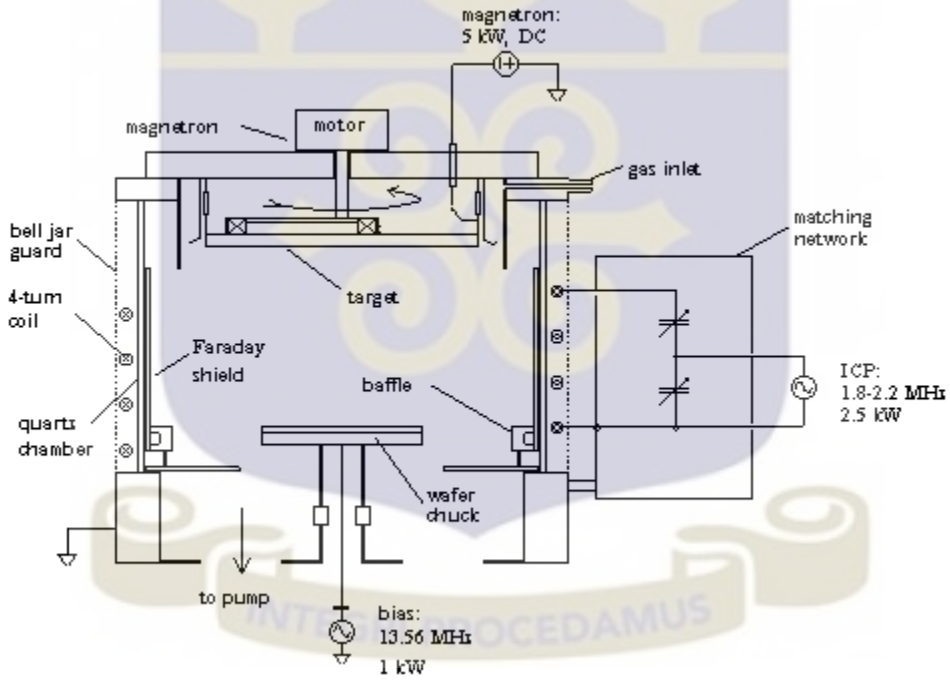

Figure 2.9 Schematic set-up of DC- magnetron sputter system

CHAPTER THREE

3.0 EXPERIMENTAL DESIGN

3.1 Research outline

The entire study has been divided into two phases. The two phases are listed below:

1. Investigation of the effect of acetic acid volume in precursor solution on zinc oxide film structure and optical transmittance within the visible part of the electromagnetic spectrum.
2. Preparation and characterization of zinc oxide films doped with indium and gallium respectively.

Table 3.1 outlines the two phases of this research and the various activities carried out during each phase.

Table 3.1 Activity outline of the experimental setup

Phase	**Title**	**Activities**	
One	Investigation of the effect of acetic acid volume in precursor solution on undoped ZnO thin films	Preparation of undoped ZnO thin films	
		Characterization	XRD
			UV-Vis Spectrophotometry
			Sheet Resistance
Two	Preparation and characterization of Indium	Preparation of doped ZnO thin films (In:ZnO / Ga:ZnO)	
		Characterization	XRD
			UV-Vis Spectrophotometry

	doped ZnO and Gallium doped ZnO thin films		Sheet Resistance
			EPMA
			Hall Effect measurement
			SEM

3.2 Materials and equipment

In this section, Table 3.2 contains a complete list of all the chemicals used for the experimental work. The chemicals used were secured from Sigma-Aldrich.

Table 3.2 List of Chemicals (with details) used for the experimental work

Chemical	**Formula**	**Molar Mass**
Zinc Acetate	$Zn(O_2CCH_3)_2(H_2O)_2$.	219.50 $g \cdot mol^{-1}$
Acetic acid Glacial	$C_2H_4O_2$	60.05 $g \cdot mol^{-1}$
Acetone	C_3H_6O	58.08 $g \cdot mol^{-1}$
Ethanol (99%)	C_2H_6O	46.07 $g \cdot mol^{-1}$
Indium (III) Chloride	$InCl_3$	221.18 $g \cdot mol^{-1}$
Gallium Oxide	Ga_2O_3	187.444 $g \cdot mol^{-1}$

A summary of the equipment used to perform specific activities is given in Table 3.3

Table 3.3 Research work equipment list

Activity	**Equipment**
Substrate Cleaning	Ultrasonic Cleaner
Spray Pyrolysis	Mirage Air Compressor – 2 HP
	Spray gun
	Hot Plate
	Glass substrates
Chemical weighing	AE Adam Nimbus Analytical Balance NBL124e
Characterization	
UV-Visible analysis	Genesys 10S UV-Vis Spectrophotometer
XRD	Empyrean PANalytical X-ray diffractometer
Sheet Resistance	Jandel 4 Point probe
	Keithley 2100 - $6^1/_2$ Digit Digital Multimeter
Hall Effect measurements	Phywe Teslameter/ Current source/ Electromagnets

3.3 Methodology

Doped and undoped ZnO thin films were deposited on soda lime glass substrates by spray pyrolysis. Table 3.3 lists the equipment used at various stages of the thin film preparation and characterization. The experimental procedure is summarized below:

1. Substrate preparation

2. Substrate preheating
3. Precursor solution preparation (Doped and undoped samples)
4. Spray deposition

3.3.1 *Substrate preparation*

The dimensions of the soda lime glass were (25 x 25 x 15) mm. Substrate surface condition is critical to the film structure, growth mechanism and other properties, therefore it was important to ensure that the substrates were clean and well-conditioned before depositing the thin film onto the surface. The first step in substrate preparation was cleaning. The glass substrates were wiped with a clean cloth to remove any smudge or large particle impurities. The second step was to place the wiped substrates into beakers and clean using an ultrasonic cleaner. The solutions used for the cleaning process were acetone, distilled water and ethanol in the stated order. For each solution, the cleaning time was set to 10 minutes on the ultrasonic cleaner. Impurities and other grease stains that may be present on the sample surface were removed after the ultrasonic cleaning process.

3.3.2 *Substrate preheating*

Sample preheating involved setting the sample on the hot plate stage and heating it up to the required spray deposition temperature. The clean substrates were air dried for 5 minutes and set on the hot plate. The hot plate was set to a temperature of 400°C. The same temperature was maintained for the spray deposition process. The substrates were preheated for 45 minutes to ensure uniform distribution of heat across the entire surface of the substrate before spraying and

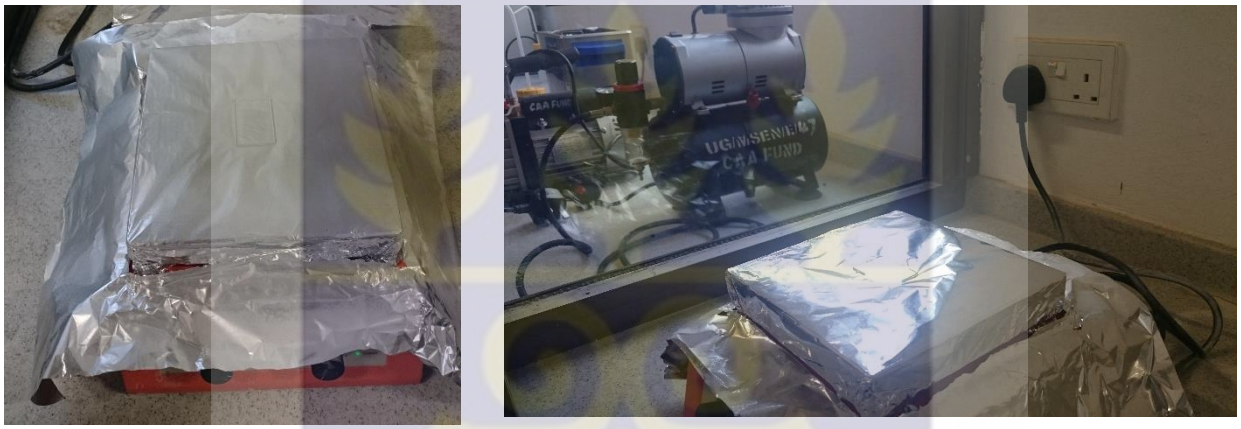

Figure 3.1 The hot plate with glass substrate for preheating

also to burn off any possible remaining carbon compounds that survived the ultrasonic cleaning process.

3.3.3 *Undoped sample precursor solution preparation*

The compound source chosen for ZnO was zinc acetate. 0.2M zinc acetate precursor solution was prepared for the purposes of obtaining ZnO on glass substrates by spray pyrolysis. The required mass of zinc acetate was weighed using a chemical balance and dissolved in equal amount of water and ethanol (99%). Zinc acetate is soluble in water hence a clear colorless solution was obtained when the zinc acetate was dissolved. However, with the addition of ethanol, the solution turned cloudy. The change in the state of the solution was caused by the formation of zinc hydroxide ($Zn(OH)_2$) complexes. To prevent the formation of such complexes which tend to affect the

transparency and conductivity of ZnO films, acetic acid was added. A magnetic stirrer was used to stir the solution for 10 minutes to ensure homogeneity.

3.3.4 *Doped sample precursor solution preparation*

The precursor solution for the doped samples were prepared using the same steps as the undoped samples. For indium doping, the dopant source was indium (III) chloride ($InCl_3$). The solid $InCl_3$ was weighed and dissolved in deionized water. For gallium doping, the dopant source was gallium (III) oxide (Ga_2O_3). The powdered Ga_2O_3 was also weighed and dissolved in deionized water to prepare the dopant solution.

The final step in preparing the precursor solution for the doped samples involved adding the dopant solutions to the zinc acetate solution in drops while stirring. It was important to add in drops and stir continuously to ensure homogeneity in the final solution. This final step differentiated the doped and undoped precursor solution preparation processes.

3.3.5 *Spray deposition*

The entire spray deposition process was carried out in a fume chamber. The fume chamber ensured that the fumes that were released from the decomposition and evaporation processes that lead to the formation of ZnO on the glass substrates, were effectively expelled to reduce risk of respiratory hazards related to working with the chemicals used. Compressed air from an air compressor was used as a carrier gas to transport the precursor solution in the form of aerosol onto the substrate. The deposition was carried out at a temperature of 400°C. The deposition process for a single sample took 45 minutes to complete. During this period the entire precursor solution (100ml) was sprayed at a spray rate of $0.037 mls^{-1}$. The substrate-nozzle distance was kept constant at 30cm. The decomposition of zinc acetate to form ZnO with water and ethanol as solvents is detailed in the following reactions (Vignesh, 2014):

$$Zn(CH_3COO)_2{\cdot}2H_2O + H_2O \xrightarrow{400°C} ZnO\downarrow + 2CH_3COOH\uparrow + H_2O\uparrow \quad \text{(Eqn. 3.1)}$$

$$Zn(CH_3COO)_2{\cdot}2H_2O + 2C_2H_5OH \xrightarrow{400°C} ZnO\downarrow + 2CH_3COOC_2H_5\uparrow + 3H_2O\uparrow \quad \text{(Eqn. 3.2)}$$

Phase one – Investigation of the effect of acetic acid on the structural, electrical and optical properties of ZnO thin films:

In this experiment, the acetic acid volume in the precursor solution was varied from 1ml – 5ml. Two sample sets (Sample Set A and Sample Set B) were prepared for UV-Vis analysis and Sheet resistance measurements. For each sample set, 5 samples (1ml-5ml) were prepared. Table 3.4 shows the various samples prepared and the corresponding sample identification codes. XRD analysis was also carried out investigate the effect of increasing acetic acid volume on the structure of ZnO thin films.

Phase two – Doping of ZnO with Indium and gallium:

In this experiment, ZnO was doped with indium and gallium respectively. The concentration of the dopant was varied from 1wt% - 5wt%. Two replicate samples were prepared for each dopant concentration. Structural analysis was carried out using XRD and SEM to study the effect of the dopants on the structure of ZnO. Sheet resistance, Hall Effect and UV-Vis analysis were also carried out to determine the doped samples electrical and optical properties. EPMA was performed to determine the elements present in the thin film samples. Table 3.4 shows the various samples prepared and the corresponding sample identification codes.

Table 3.4 Thin film samples prepared for characterization

Phase one	**Phase two**	
Undoped	In:ZnO	Ga:ZnO
Sample ID	Sample ID	Sample ID
AC1	IAG-1	GAG-1
AC2	IAG-2	GAG-2
AC3	IAG-3	GAG-3
AC4	IAG-4	GAG-4
AC5	IAG-5	GAG-5

3.4 Characterization

Materials characterization involves the study or investigation of the various properties of materials as predicted by their structure. Material properties that are studied may be classified as optical (UV-Vis analysis, Raman Spectroscopy, Cathodoluminiscence), electrical/magnetic (Sheet Resistance, Hall Effect measurements), mechanical (Tensile/Compressive strength analysis, Flexural strength analysis) and structural (XRD-X-ray Diffraction, SEM-Scanning Electron Microscopy, AFM-Atomic Force Microscopy). For the study of the doped-ZnO thin films prepared in this work, the following characterization techniques will be employed; UV-Vis analysis, XRD, SEM, Hall Effect measurements, EPMA-Electron probe microanalysis and sheet resistance measurement.

3.4.1 *X-ray diffraction (XRD)*

X-ray diffraction is a characterization tool that is used to study the structural properties of materials. Information such as crystalline phases present, unit cell dimensions, lattice parameters and crystal structure can be retrieved from XRD analysis patterns. X-ray diffraction is based on the principle of constructive interference that occurs when monochromatic X-rays interact with crystalline samples. For constructive interference to occur, the conditions must satisfy Bragg's law.

Bragg's law is given mathematically as:

$$n\lambda = 2d \sin\theta \qquad \text{(Eqn. 3.3)}$$

Where: n= positive integer, d= interplanar distance, λ=wavelength and θ=diffraction angle.

The main components of an X-ray diffractometer are the electron gun/source, the lenses, the sample stage and the detector. To generate X-rays, a filament is heated to eject electrons in the X-ray tube. These electrons are accelerated towards a target by applying a voltage. Characteristic X-ray spectra are produced when the accelerated electrons strike and eject inner core electrons from the target. The X-ray spectra produced is filtered and directed towards the sample by an array of lenses. Filtration of the X-ray spectra is achieved by means of crystals or foils. One common target material is copper which produces the characteristic Cu-Kα radiation of wavelength 1.5418Å. This radiation has been used in various works to characterize thin film structures and other crystalline materials (Swanepoel, 1997). The sample to be analyzed is fitted in the sample holder on the sample stage. The intensity of the reflected X-rays from the interaction of the incident X-ray radiation and the sample is recorded, as the sample together with the detector is rotated. As Bragg's law is satisfied and constructive interference occurs, the detector picks up the signals and converts

it to a count rate that is used to generate the XRD pattern. The sample is oriented relative to the incoming X-ray beam and rotates at an angle θ in its path. The detector setup also rotates in accordance with the sample rotation at an angle of 2θ.

The XRD pattern will give primary data about the crystal structure, the lattice parameters and preferred crystallite growth orientation. Further information such as approximate grain size calculation can be done from the XRD data using the Scherrer Equation which is given as:

$$\tau = \frac{K\lambda}{\beta \cos\theta} \qquad \text{(Eqn. 3.4)}$$

Where: τ=mean crystallite size K=dimensionless factor, λ=X-ray wavelength, β=line broadening at FWHM intensity θ=Bragg angle

3.4.2 *Scanning Electron Microscopy (SEM)*

Scanning electron microscopy is a material structure analysis technique that gives information about the structure and surface morphology of materials. The scanning electron microscope (SEM) uses a beam of electrons to analyze surface structure. The use of an electron probe produces a higher resolution compared to light in an optical microscope. The main components of a scanning electron microscope are the electron source (electron gun), electron column, detectors and a vacuum system. The electron gun provides a source of electrons that enter the column. Slits, apertures and lenses help to shape the electron beam and focus it on the sample which is held on a stage in the specimen chamber. Two different types of pumps are used to create vacuum in the specimen chamber. A mechanical pump is initially used to lower the pressure in the chamber to about 5 x 10^{-5} Torr and then a turbo-molecular pump creates and maintains a high vacuum environment. The vacuum environment is necessary to prevent interference with the incident

electrons and create a clean environment to perform the analysis. The capabilities of a scanning electron microscope depends on the detectors mounted around the sample chamber. Various detectors pick up the numerous signals that are generated from the interaction of the electrons with the surface atoms of the material under study. The interaction of the electron and the material surface generate several signals some of which include back scattered electrons, secondary electrons, X-rays and diffracted back scattered electrons. For the purposes of generating an image, a detector is required to pick up and process the back scattered electron and the secondary electron signals (Reimer, 1998).

3.4.3 *Electron Probe Microanalysis (EPMA)*

EPMA is a non-destructive materials analysis technique that works on similar principles as scanning electron microscopy. It is used to analyze small areas of solid material samples. An electron probe microanalyzer is used to perform the analysis. The key parts of this equipment are the electron gun, optical lenses, sample stage, metallographic microscope and X-ray spectrometer.

The X-ray signal detectors pick up X-rays emitted as a result of the electron beam – sample surface interaction. EPMA is a characterization tool that determines the quantitative elemental composition of materials. EPMA is based on the principle of the uniqueness of the atomic structure of every element. When the electron beam incidents on the sample, it may cause an electron to be ejected from the inner shell of the surface atom. When this happens, an electron from the immediate outer shell drops to fill the electron hole created by the ejected electron. As the electron drops, it gives of a characteristic amount of energy as X-rays. The X-ray detector picks up these signals and can determine which element the electron is from as well as the quantitative value in term of mass percent concentration or atomic percent concentration for the given sample.

3.4.4 *UV- Vis analysis*

In thin film characterization, UV-Vis analysis is a key technique. The analysis is done using an ultraviolet – visible (UV-Vis) spectrophotometer. This instrument measures the amount of light absorbed or transmitted at given wavelengths in the UV and visible regions of the electromagnetic spectrum depending on its programed instructions. Other forms of radiation are infrared, radio, x-rays, microwaves and gamma waves. On the electromagnetic spectrum, frequency increases as the wavelength decreases. The visible section of the EMS (electromagnetic spectrum) is found in the mid portion of the spectrum approximately between 400nm and 800nm. The ultraviolet region is also found within 200nm and 400 nm on the EMS. Data that can be obtained from UV-Vis analysis include, transmittance and absorbance readings. A lot of useful information such as absorption coefficient and band gap can be calculated from this data.

Ultraviolet – visible spectroscopy can also be used to study the changes in electronic energy levels in a molecule. These energy level changes may be due to transfer of electrons from π- or non-bonding orbitals (Kumar, 2006). Ultraviolet-visible spectroscopy works based on the principle of Beer-Lambert law, which can be expressed in the form:

$$A = log \frac{I_o}{I} \qquad \text{(Eqn. 3.5)}$$

Where; A – absorbance, I_o – incident light intensity, I – exiting light intensity

The spectrophotometer is used to carry out UV-Vis analysis and it is made up of a light source, a monochromator, sample cell, recorder and a detector. UV spectrophotometers may be single source beam or dual source beam. For single source spectrophotometers, the reference sample is measured first and the actual samples are measured after the reference. For solution based samples,

the reference may simply be the solvent (water, ethanol etc.) in which the material under study was dissolved or suspended in. In the case of thin films, the reference is may be a blank cell or a clean substrate with no film on it. With double beam spectrophotometers, the reference and the samples are measured simultaneously. Figure 3.3 shows the single source beam spectrophotometer used for the UV analysis in this work.

Figure 3.2 A UV-Vis Spectrophotometer

3.4.5 *Hall Effect measurements*

The Hall Effect is based on the theory of separation of charge carriers in conductors when electric current is applied to the material in the presence of a magnetic field (Bracken, 2010). By this means, charge mobility which is denoted 'μ', charge carrier concentration denoted 'n' and the polarity of the charge carriers can be determined. Current is generated by the movement of charge carriers. These charge carriers may either be electrons, holes or ions (ionic conductivity-ceramics). In the presence of a magnetic field, these charge carriers experience a force known as the Lorentz force. This force is responsible for the separation of opposite charge carriers on either side of the test material. An electric field is generated as a result of this charge separation and this causes a steady potential to be established. Figure 3.4 illustrates the theory behind the Hall Effect.

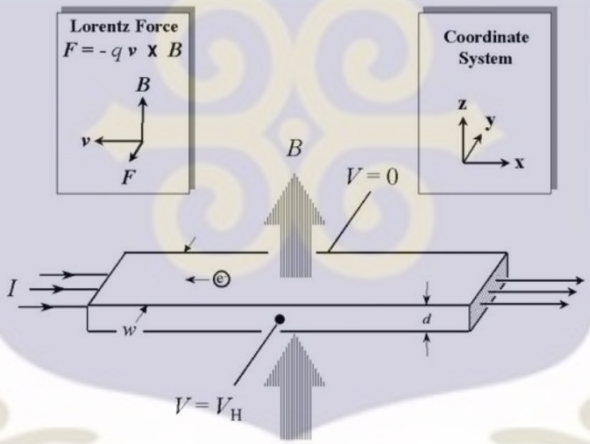

Figure 3.3 Geometry for the Hall Effect measurement

To measure the electrical characteristics of a conducting thin film, contacts are placed on the film surface as indicated in Figure 3.4. The contacts may deposited by spray pyrolysis with the surface of the thin film masked. A common masking material for such deposition is aluminum foil. The nature of the contact deposited determines the type of interface formed between the contact and the film. The interface may be metal-semiconductor or semiconductor-semiconductor. A Hall probe provides the magnetic field around the test sample such that the magnetic field lines are perpendicular the applied current direction. A source meter provides the input current and a digital multimeter or voltmeter is mounted to read the Hall voltage generated. Figure 3.6 illustrates the experimental set up of the Hall measurement equipment.

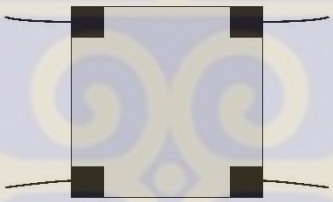

Figure 3.4 Illustration of thin film sample with electrical contacts for Hall measurement

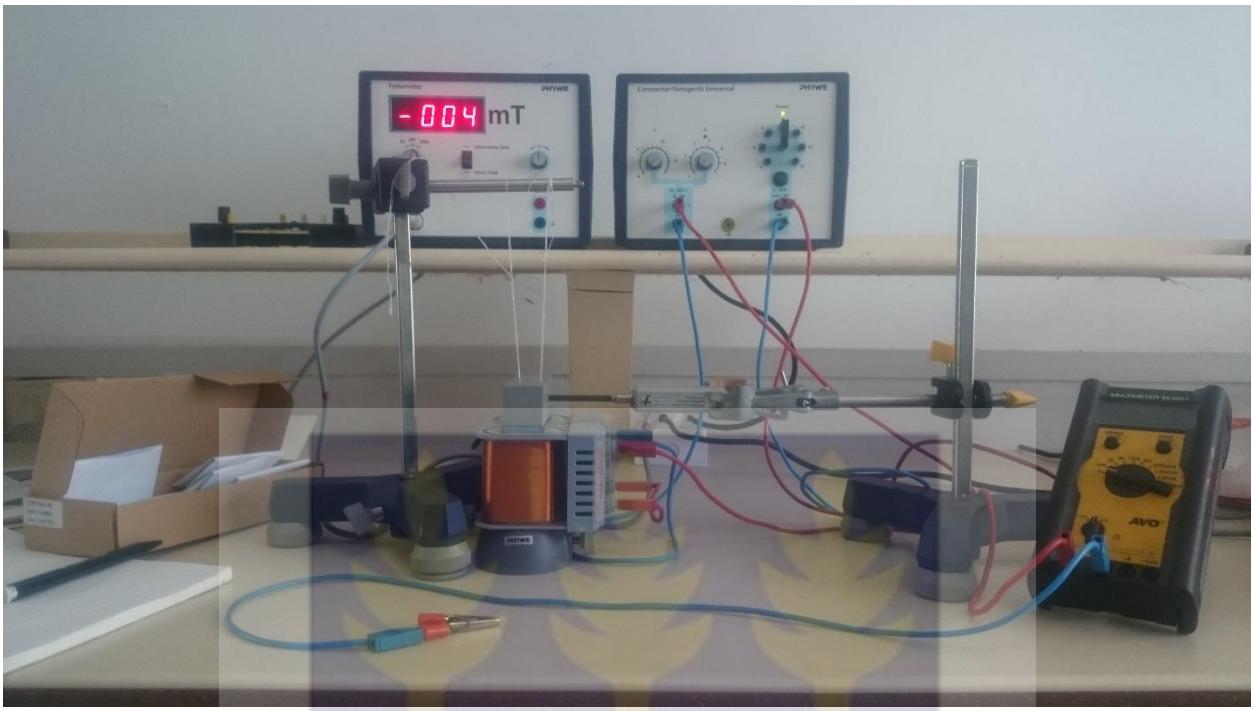

Figure 3.5 Set up for Hall measurement

A mathematical expression that relates Hall voltage, input current and magnetic field intensity is used to calculate for the charge carrier density. The expression is given as:

$$V_H = \frac{IB}{nte} \qquad \text{(Eqn. 3.6)}$$

Where: V_H=Hall voltage, I=current, B=magnetic field intensity, n=charge carrier density, t=film thickness and e=elementary charge.

3.4.6 *Sheet Resistance*

The measure of the electrical resistance in a thin sheet or film of conducting or semiconducting material is termed the sheet resistance, denoted R_s. Sheet resistance can be measured using the 4-point probe. The 4-point probe has four evenly spaced metallic probe heads that make contact with the material under test. Current is passed through the two outer probe heads and the two inner

probe heads measure the resulting voltage as illustrated in Figure 3.7. Resistance is determined by dividing the voltage by the current and the result multiplied by a factor of 4.532 depending on the equipment model and set up.

$$R_s = 4.532 * \frac{V}{I} \quad \text{(Eqn. 3.7)}$$

Where: R_s = sheet resistance, V = voltage and I = current

However, if a digital multimeter is used for the setup, the resistance can be read directly from the display and multiplied by 4.532. The unit for sheet resistance is ohms per square (Ω/sq or Ω/□). From the sheet resistance, the bulk resistivity of the thin film can also be calculated using the mathematical relationship given below:

$$R_s = \frac{\rho}{t} \quad \text{(Eqn. 3.8)}$$

Where: R_s = Sheet resistance, ρ = bulk resistivity and t = film thickness.

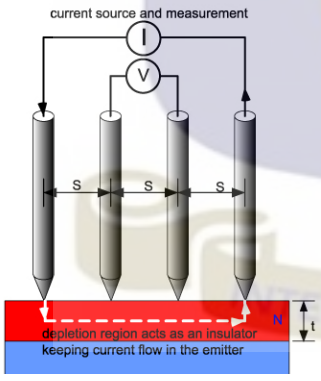

Figure 3.6 Schematic diagram of 4 point probe setup

Bulk resistivity has units of Ω cm. Figure 3.8 illustrates the Jandel Four point probe head and stage setup connected to a Keithley 2100 digital multimeter that was used in this work.

Figure 3.7 A four point probe measurement setup

There are various parameters to consider when measuring sheet resistance of a thin layer of semiconducting material. These parameters include, input current, voltmeter range and the nature of the sample surface. The input current for very high resistivity samples has to be reduced and for very low resistivity samples, the input current increased to prevent overheating of the probe tips which may affect the readings or damage the probe.

CHAPTER FOUR

4.0 RESULTS AND DISCUSSION

4.1 Phase One: Characterization of undoped ZnO thin films

4.1.1 UV-Vis analysis

4.1.1.1 *Transmittance measurements – undoped ZnO*

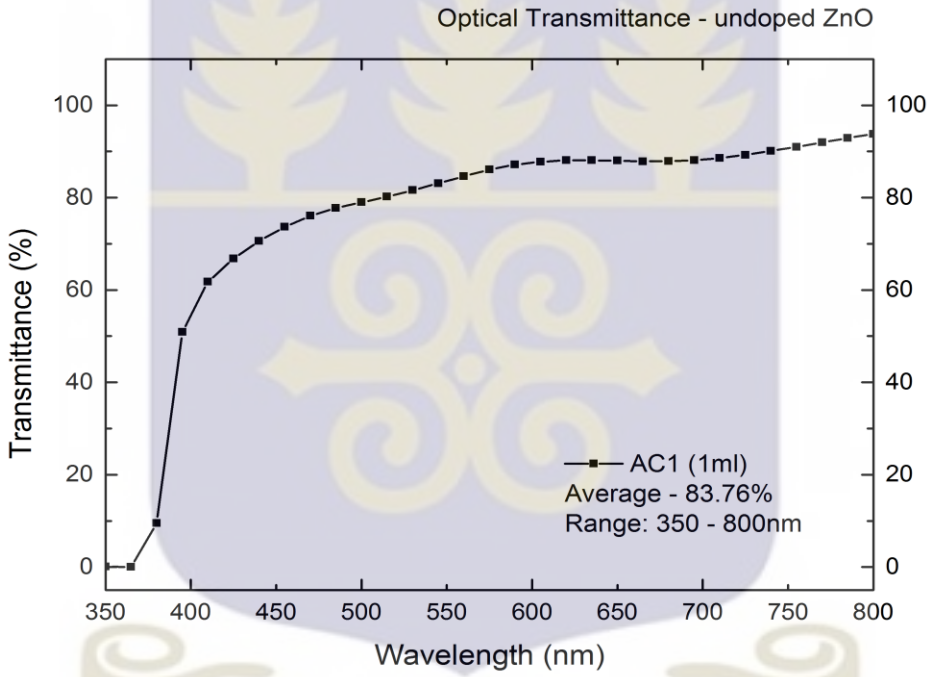

Figure 4.1 Optical transmittance measurements undoped ZnO - 1ml

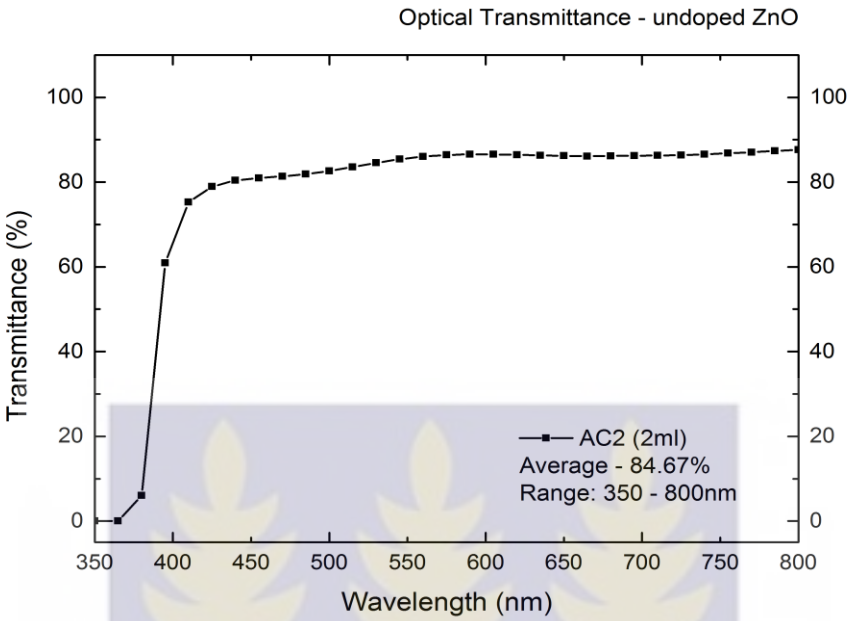

Figure 4.2 Optical transmittance measurements undoped ZnO - 2ml

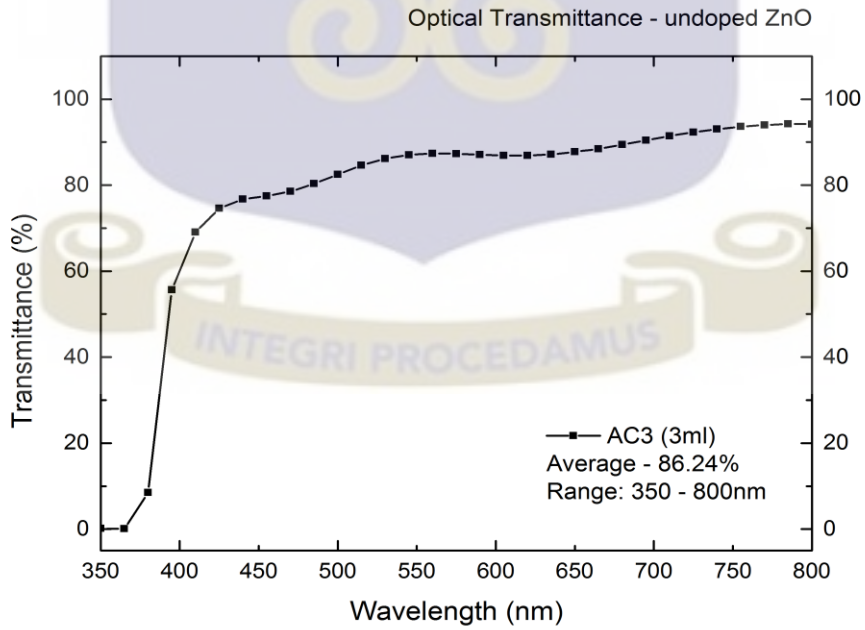

Figure 4.3 Optical transmittance measurements undoped ZnO - 3ml

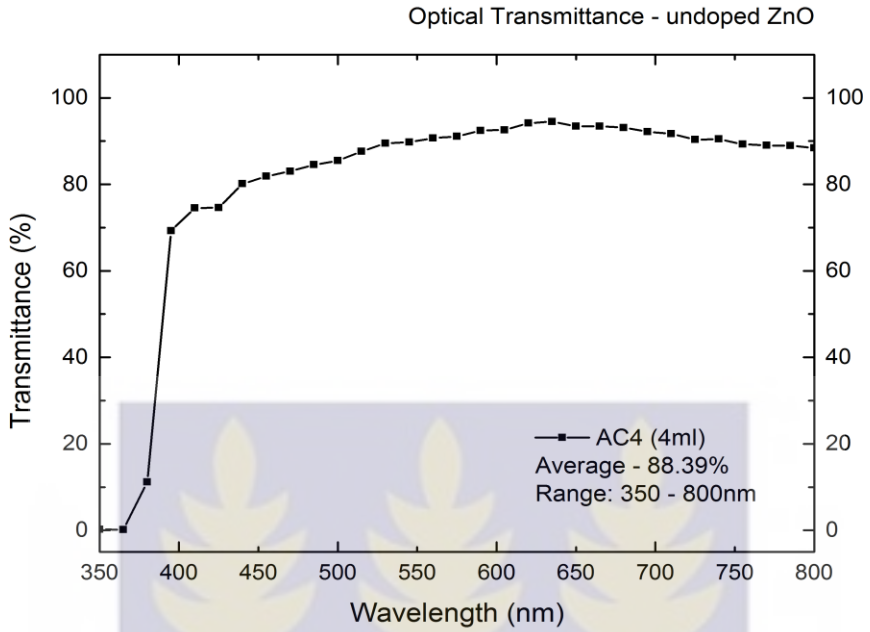

Figure 4.4 Optical transmittance measurements undoped ZnO - 4ml

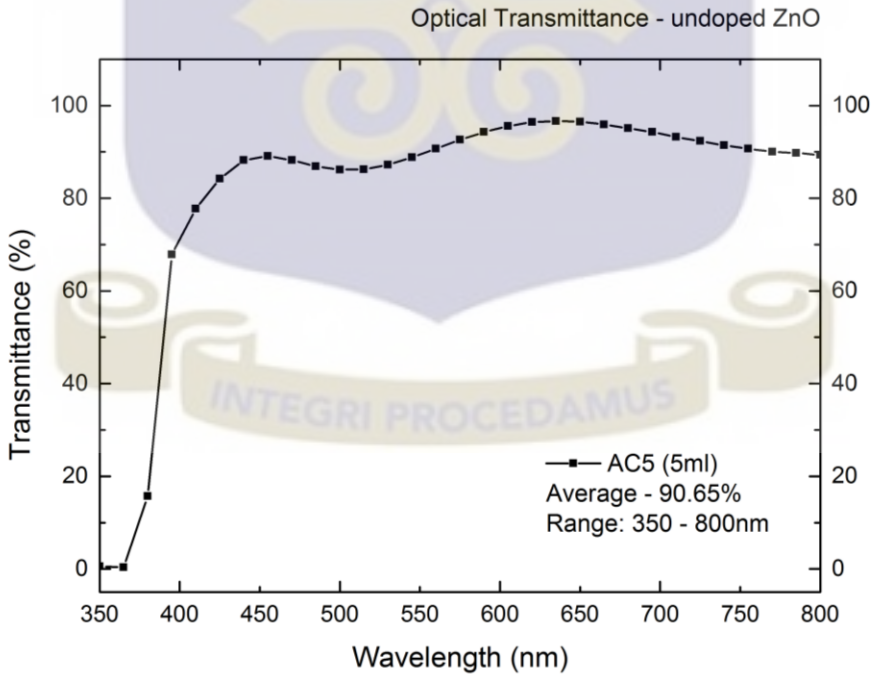

Figure 4.5 Optical transmittance measurements undoped ZnO - 5ml

Optical transmittance measurements undoped ZnO

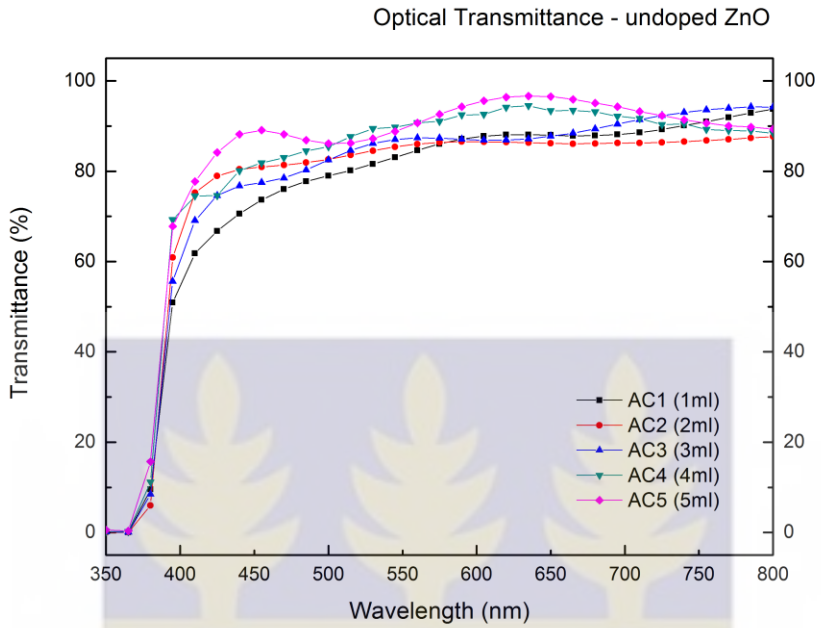

Figure 4.7 Optical transmittance grouped - undoped ZnO

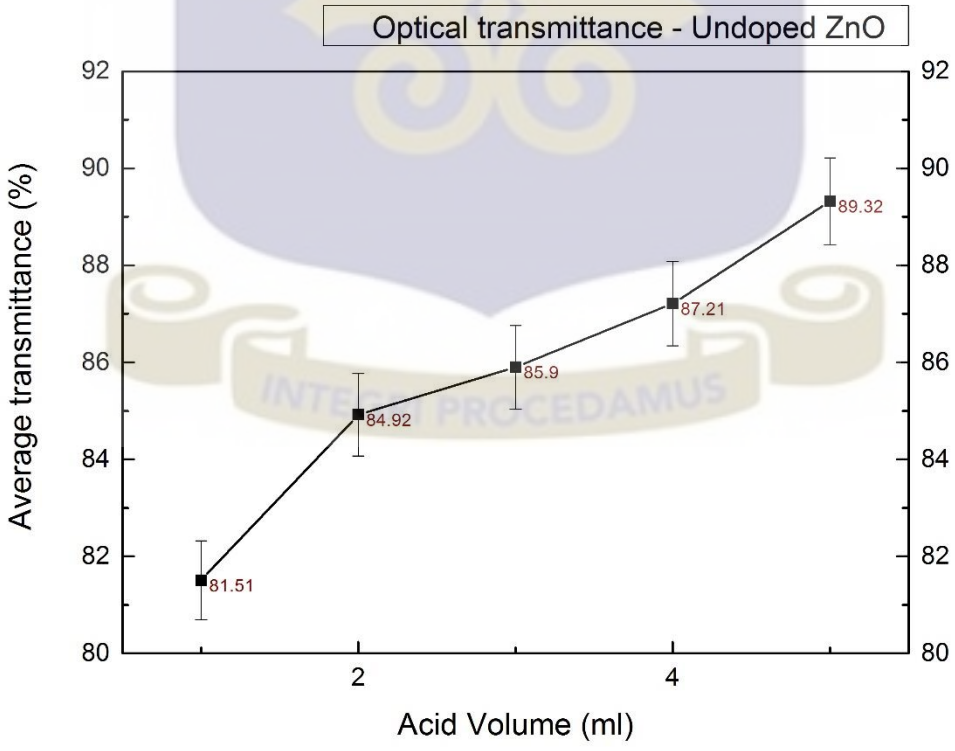

Figure 4.6 Average optical transmittance undoped ZnO

One of the key properties of a good transparent conducting oxide thin film is high transparency. Thin films require substrates for structural support to function. In terms of device physics, the thin film material as well as the substrate has to be of high transparency for optimum device operation and output. For these reasons, the zinc oxide thin films for this study were deposited on clear soda lime glass. To measure the transparency of the thin films, the percentage transmittance data was obtained using a UV-Vis spectrophotometer. The test was conducted within the UV-Visible range of the electromagnetic spectrum ranging from 350nm – 800nm. A step size of 15nm was inputted to generate 31 readings at various wavelengths within the specified range. The average percentage transmittance within the visible section of the electromagnetic spectrum (410nm-800nm) was computed for each sample tested by taking the statistical average of the transmittance values at each wavelength within the given range. The average percentage transmittance for the undoped samples was above 80%. It can be observed from Figure 4.6, that the average percentage transmittance for the undoped ZnO samples increased with increasing acetic acid volume in the precursor solution. The lowest transparency recorded (81.51%) was corresponded to the 1ml acetic acid sample. The 5ml acetic acid sample recording the highest transparency (89.32%). The addition of acetic acid to the precursor solution prevents the formation of zinc hydroxide from hydrolysis reactions. The zinc hydroxide interferes with the overall yield of ZnO on the substrate surface and helps impact the transparency. Increasing the acetic acid volume in the precursor solution effectively eliminates the effects of zinc hydroxide on the structure and hence helps increase the optical transparency of the undoped ZnO thin films. Acetic acid also promotes the solubility of Zn salts in the precursor solution. The dissolution process of these Zn salts occurs within a given pH range. Outside this range, the ability of the acetic acid to suppress the formation

of $Zn(OH)_2$ and promote the dissolution of Zn salts is inhibited hence reducing transparency. (Crossay, 2012).

4.1.1.2 *Absorbance measurements – undoped ZnO*

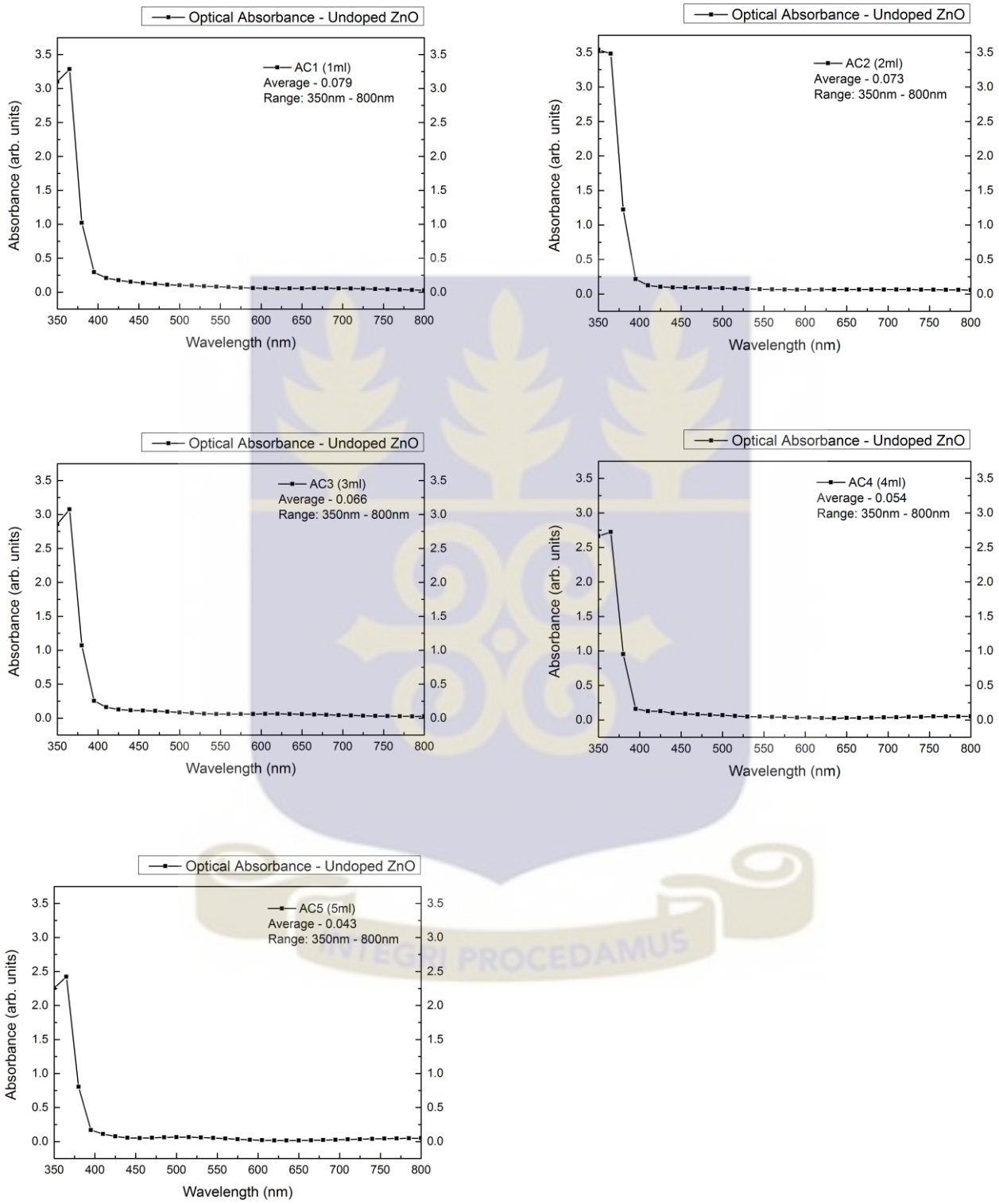

Figure 4.8 Optical absorbance measurements undoped ZnO (1ml -5ml)

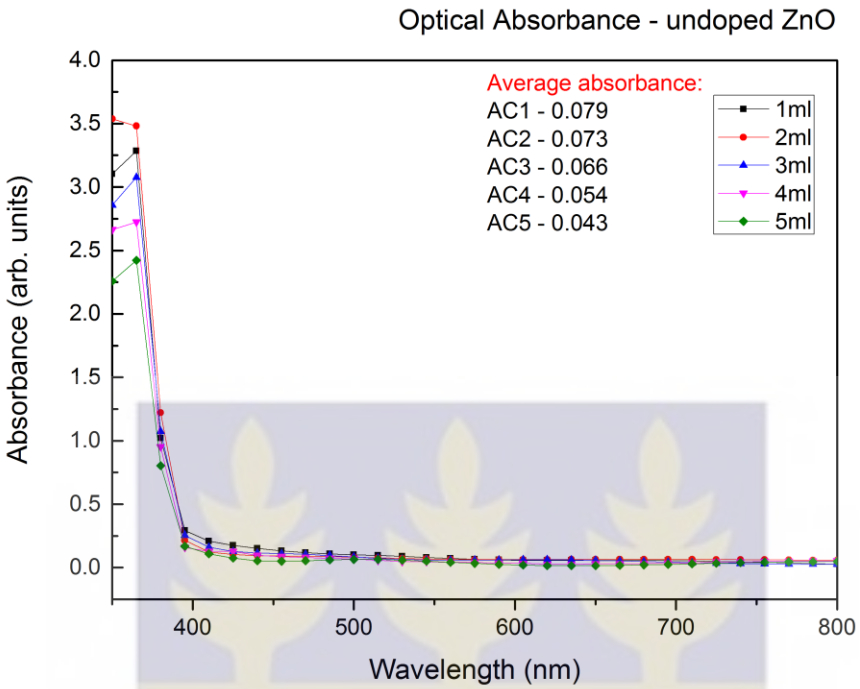

Figure 4.9 Optical absorbance grouped - undoped ZnO

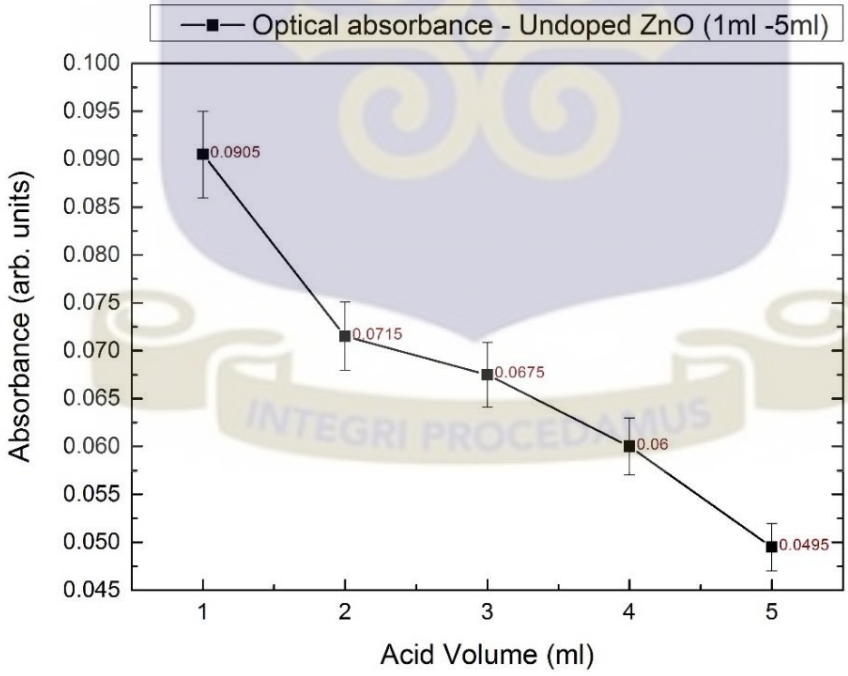

Figure 4.10 Average optical absorbance undoped ZnO

Tauc plot for the optical band gap of undoped ZnO

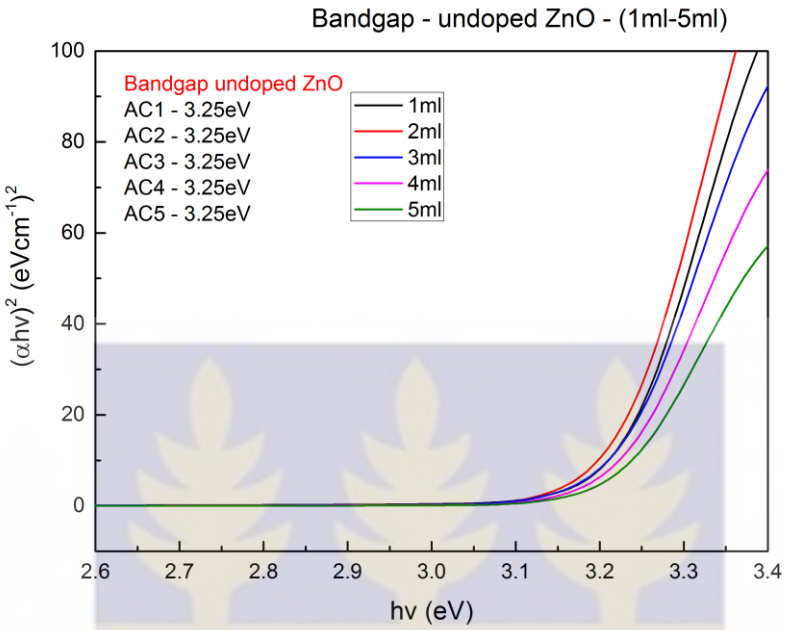

Figure 4.11 Tauc plot - undoped ZnO

Figure 4.10 shows the average absorbance against increasing acetic acid volume for undoped ZnO films. It is observed from the graph (Figure 4.10) that, the average absorbance decreases with increasing acetic acid volume. This is consistent with the data from the transmittance graphs for undoped ZnO Figure 4.6, where the transmittance increased with increasing acetic acid volume. The decreasing absorbance values may be attributed to decreasing film thickness or a complete removal of $Zn(OH)_2$ complexes within the precursor solution. The absorbance data is necessary because it is a key variable used in the estimation of the band gap from the Tauc plot. The optical band gap of the undoped ZnO thin films was calculated by extrapolating the linear portion of the Tauc plot (Figure 4.11). The Tauc plot has $(\alpha hv)^2$ as the ordinate (vertical axis) and hv which is the photon energy as the abscissa (horizontal axis) (Vignesh, 2014). The Tauc's relationship is given as:

$$(\alpha hv) = [A(hv - E_g)]^2 \quad \text{(Eqn. 4.1)}$$

Where: A is a constant; h is Planck's constant, v is the photon frequency and E_g is the optical band gap.

The theoretical estimation of ZnO band gap is 3.37 eV. Experimental values of band gap for ZnO thin films based on the data from Tauc plots range between 3.1 eV to 3.3 eV. Data from Figure 4.11 indicates the band gap of the ZnO thin films prepared by spray pyrolysis was within 3.24eV – 3.26eV. These values are consistent with the expected values of the band gap of undoped ZnO. The increase in acetic acid concentration had no significant effect on the optical band gap of the undoped ZnO films. The film thickness of ZnO films deposited by spray pyrolysis was determined by analyzing the cross section of the film on the substrate. The scale on the resulting micrograph was then used to estimate the thickness. The Tauc equation requires film thickness for the vertical axis coordinates $(\alpha hv)^2$ determination. The band gap was derived by calculating the intercept of the extrapolated linear section of the plot. The average thickness of the films deposited in this work was 500nm and this was used in equation 4.1 to produce the Tauc plots for band gap determination.

4.1.2 X-ray diffraction analysis

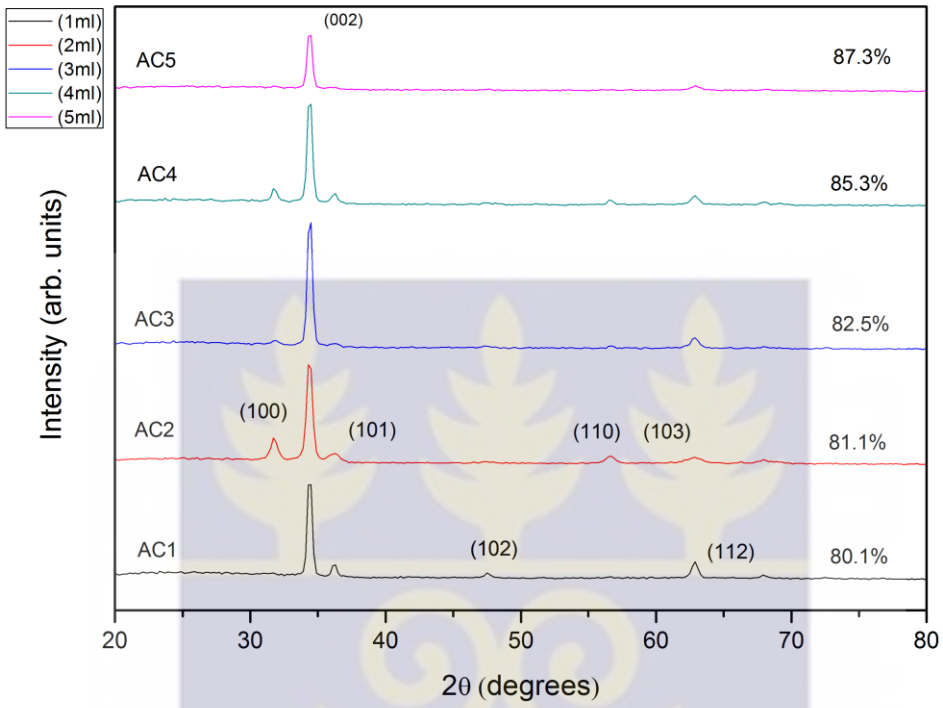

Figure 4.13 X-ray diffraction pattern for undoped ZnO (1ml -5ml)

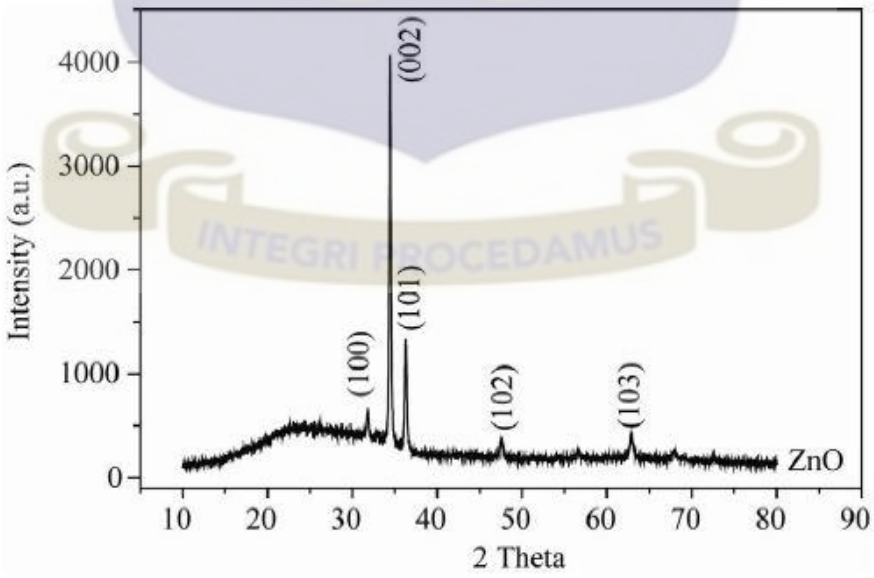

Figure 4.12 Reference XRD pattern for Zinc Oxide (Bhavana Godbole, 2011)

Figure 4.13 shows the X-ray diffraction patter for the undoped ZnO thin films. The XRD analysis was performed using a scan axis of 2θ from 20.00 to 80.00°. A step size of 0.2 was also programmed. The anode material for the X-ray diffractometer was Cu with Kα radiation of 1.54Å. The XRD diffraction peaks occurring at 2θ=31.09, 34.54, 36.34, 47.64, 56.63, 62.94 and 68.2 correspond to the (100), (002), (101), (102), (110), (103), (112), planes of the hexagonal structure of the ZnO analyzed (Bedia, 2014). For all the samples measured, the (002) peak was most dominant indicating that most of the ZnO grains were oriented in that direction with the c-axis of the structure being perpendicular to the sample substrate surface. The pH of the precursor solution used in spray pyrolysis to prepare ZnO thin films has a direct influence on the film structure (Crossay, 2012). Figure 4.14 shows the changes in crystallite size with varying acetic acid volume in the precursor solution. It can be observed that, the crystallite size increases from a minimum of 166Å for 1ml acetic acid to a maximum of 169.9Å for 5ml acetic acid. This indicates that

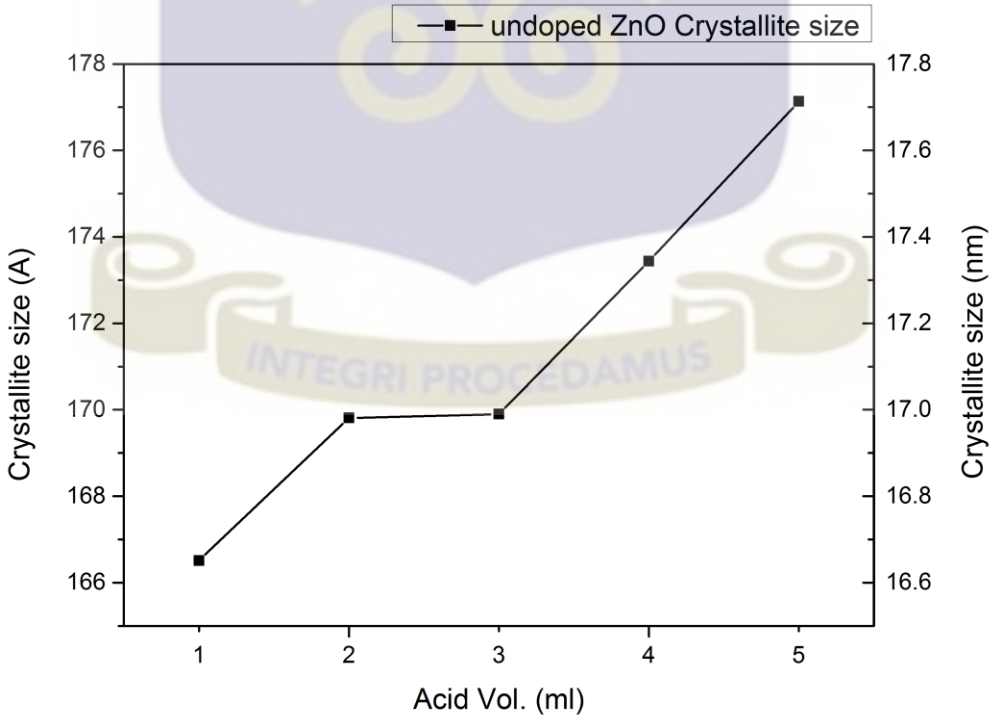

Figure 4.14 Crystallite size (undoped ZnO) trend determined from Scherrer's equation

increasing the acetic acid volume in the precursor solution had an effect on the crystallite size. For the sake of the subsequent doping experiments to be carried out on ZnO, 3ml acetic acid volume was recommended based on the intensity of the peak it showed from the XRD pattern. The 3ml sample showed the highest peak intensity and also more uniform structure based on the relatively lower peaks that showed apart from the preferred (002) peak. The 3ml sample had a corresponding 169.9Å average crystallites size based on the Scherrer equation for crystallites size calculation (Kumar, 2005).

4.1.3 **Sheet Resistance Measurement**

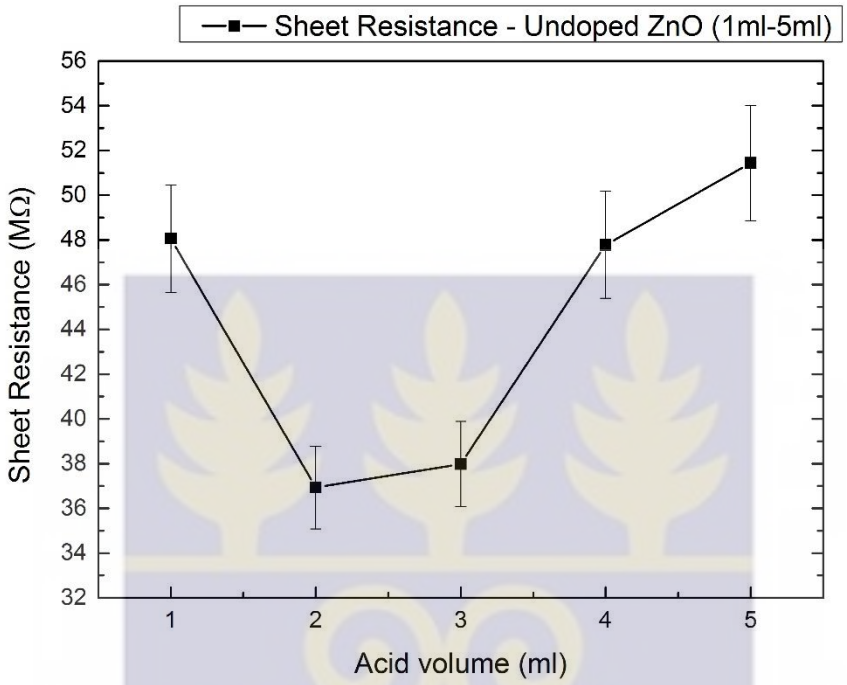

Figure 4.15 Average sheet resistance for undoped ZnO

The electrical resistivity of the undoped ZnO thin films was measured using two probes connected to Keithley 2100 digital multimeter. From literature (Rwenyagila, 2014), it is known that undoped ZnO has very high resistivity usually beyond the sensitivity limits of most conventional four-point probe equipment. The two probes were placed on the surface of the substrate where the film was deposited. The digital multimeter had an automatic 'two wire' function for measuring the resistivity. The two wire resistance function was enabled and the resistances measured. The undoped ZnO films deposited in this research exhibited high resistivity as expected. Figure 4.15 shows a graph of the sheet resistance against increasing acetic acid volume. The lowest resistivity recorded was 36.93MΩ which corresponds to the 2ml acetic acid sample. There was a drop in

resistivity between the 1ml sample and the 2ml sample, however, beyond 2ml, the resistivity increased progressively. The increase in resistivity can be explained by the larger crystallite sizes that formed when the acetic acid volume was increased. The evidence of this is seen from the XRD results in section 4.1.2.

4.2 Phase Two: Characterization of doped zinc oxide thin films

4.2.1 UV-Vis analysis

4.2.1.1 Transmittance measurements for Indium doped ZnO (In:ZnO)

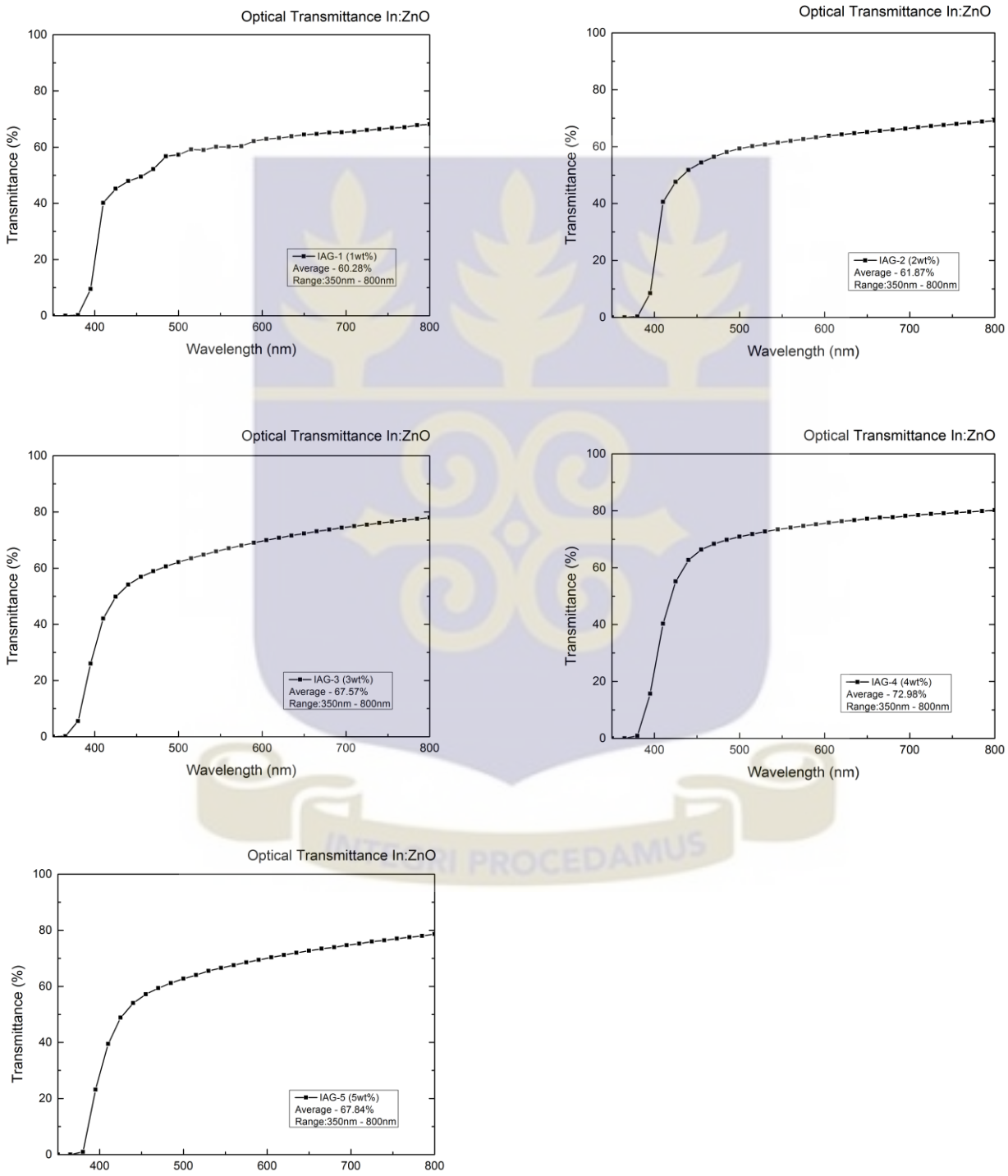

Figure 4.16 Optical transmittance measurements - Indium doped ZnO (In:ZnO)

Optical transmittance measurements Gallium doped ZnO (Ga:ZnO)

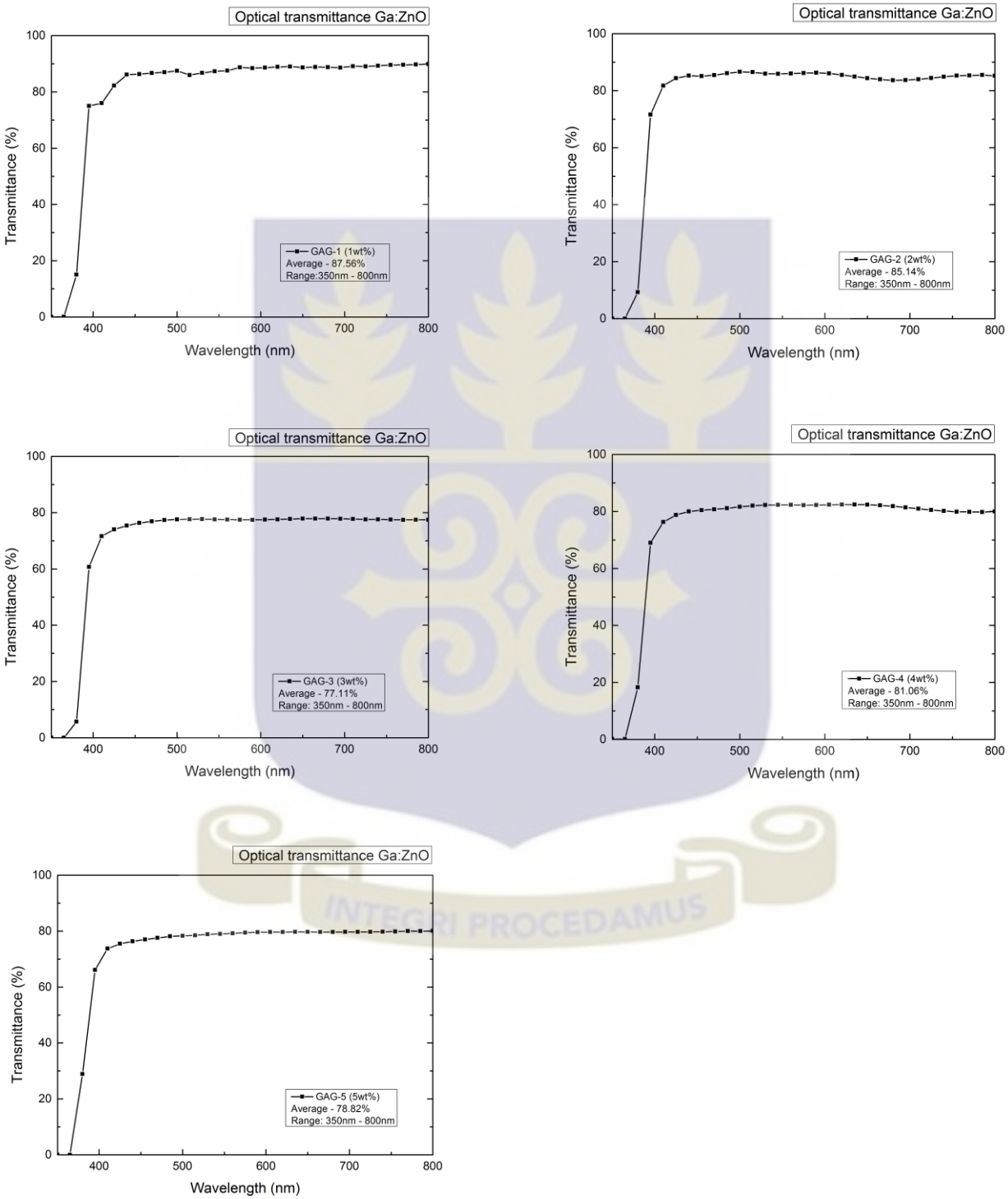

Figure 4.17 Optical transmittance measurements - Gallium doped ZnO (Ga:ZnO)

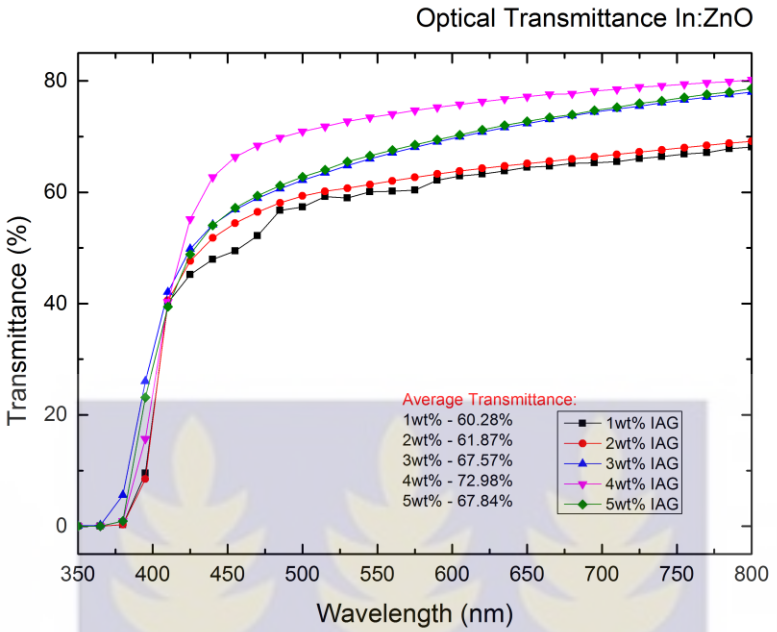

Figure 4.18 Optical transmittance grouped - In:ZnO

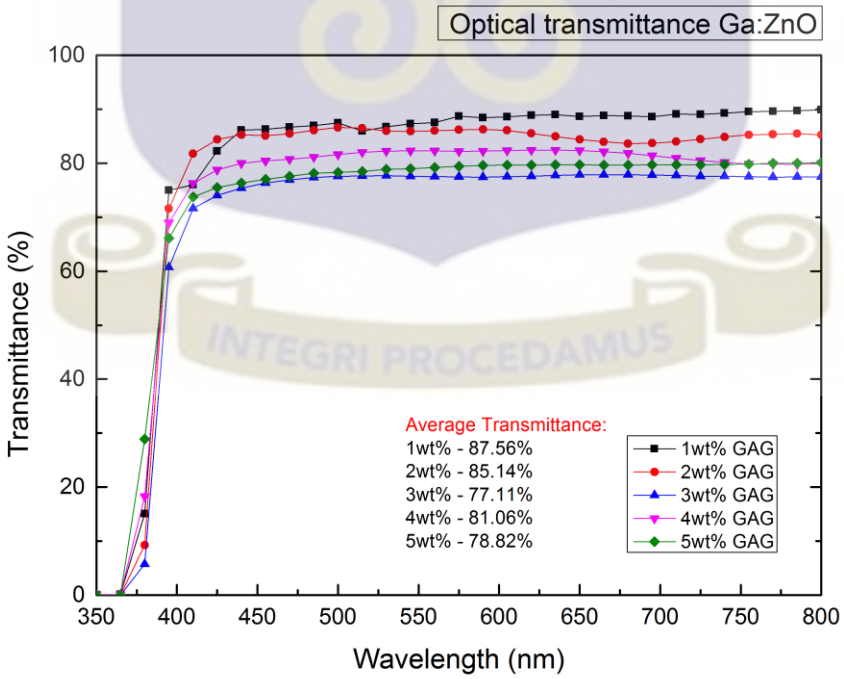

Figure 4.19 Optical transmittance grouped - Ga:ZnO

Average Optical Transmittance In:ZnO / Ga:ZnO

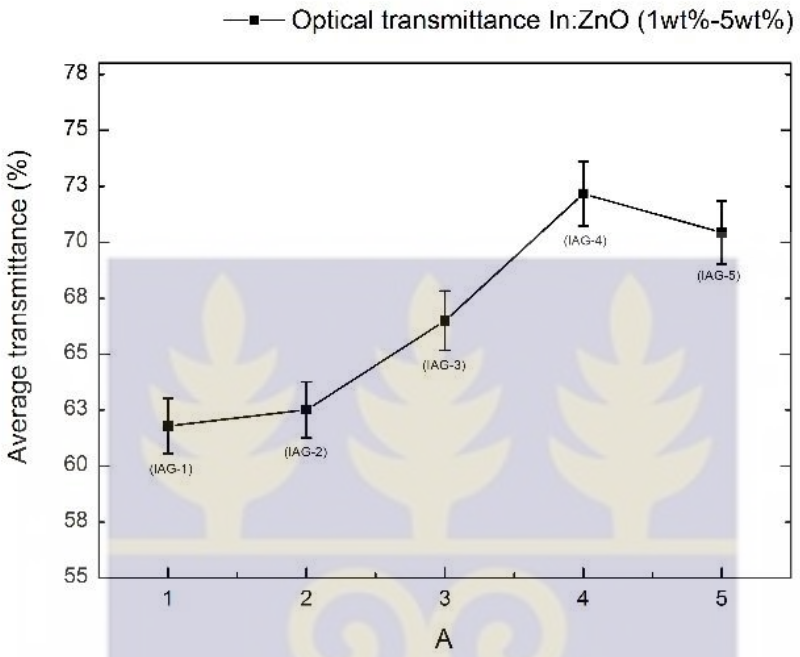

Figure 4.20 Average optical transmittance - In:ZnO

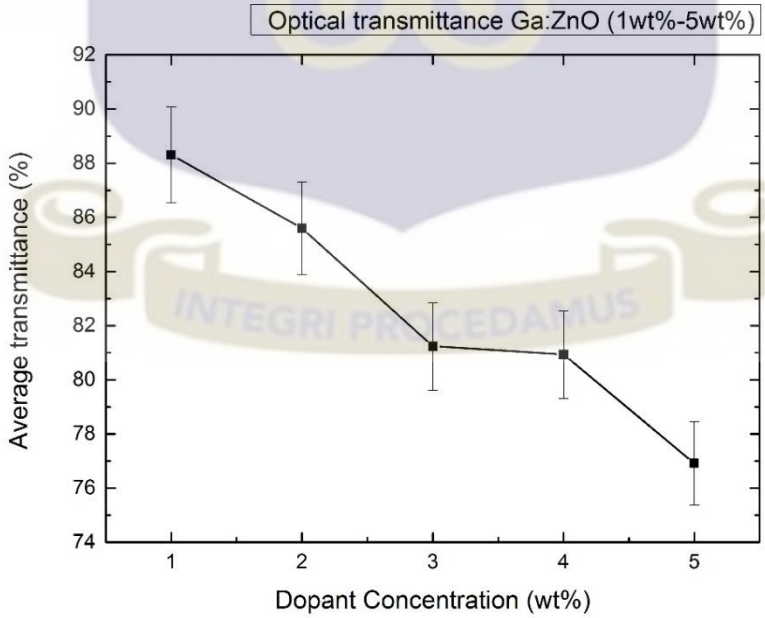

Figure 4.21 Average optical transmittance - Ga:ZnO

The first characterization tool used in the study of doped zinc oxide films was UV-Vis (ultraviolet-visible) Spectrophotometry. The aim of carrying out this characterization was to find out how much light the TCO transmits and absorbs within the ultraviolet and visible range of the electromagnetic spectrum (EMS). A Genesys 10S UV-Vis spectrophotometer was used to analyze the samples. The parameters used were a minimum wavelength of 350nm, step size 15nm and a maximum wavelength of 800nm. A total of 31 readings were recorded for each sample and average transmittance within the range 410nm – 800nm recorded. This was done because all the samples showed low transmittance within this range. 410nm was the cut-off point where spectral peaks emerged. For the In:ZnO samples, the optical transmittance increased steadily until the 5wt% sample where there was a drop. The increase in optical transmittance for the In:ZnO may be attributed to good crystal properties. As the crystallinity of the ZnO structure improves, less scattering of light occurs and the transmittance values increase. The average optical transmittance of the In:ZnO was above 60% with the 4wt% In:ZnO sample recording the highest transmittance value of 72.17%. For the Ga:ZnO thin films, there was a steady decrease in the transparency of the films as the dopant concentration was increased. This results may be explained by a deteriorating structure with increasing dopant concentration. This will cause high light scattering that will affect the transmittance values. Another factor that may have influenced the drop in transmittance is the homogeneity of the precursor solution. As the dopant concentration was increased, incomplete dissolution of the dopant compounds in the precursor solution could have affected the film formation process during the deposition. The 1wt% Ga:ZnO sample recorded the highest transparency (88.31%).

4.2.1.2 Absorbance measurements – Indium doped ZnO (In:ZnO)

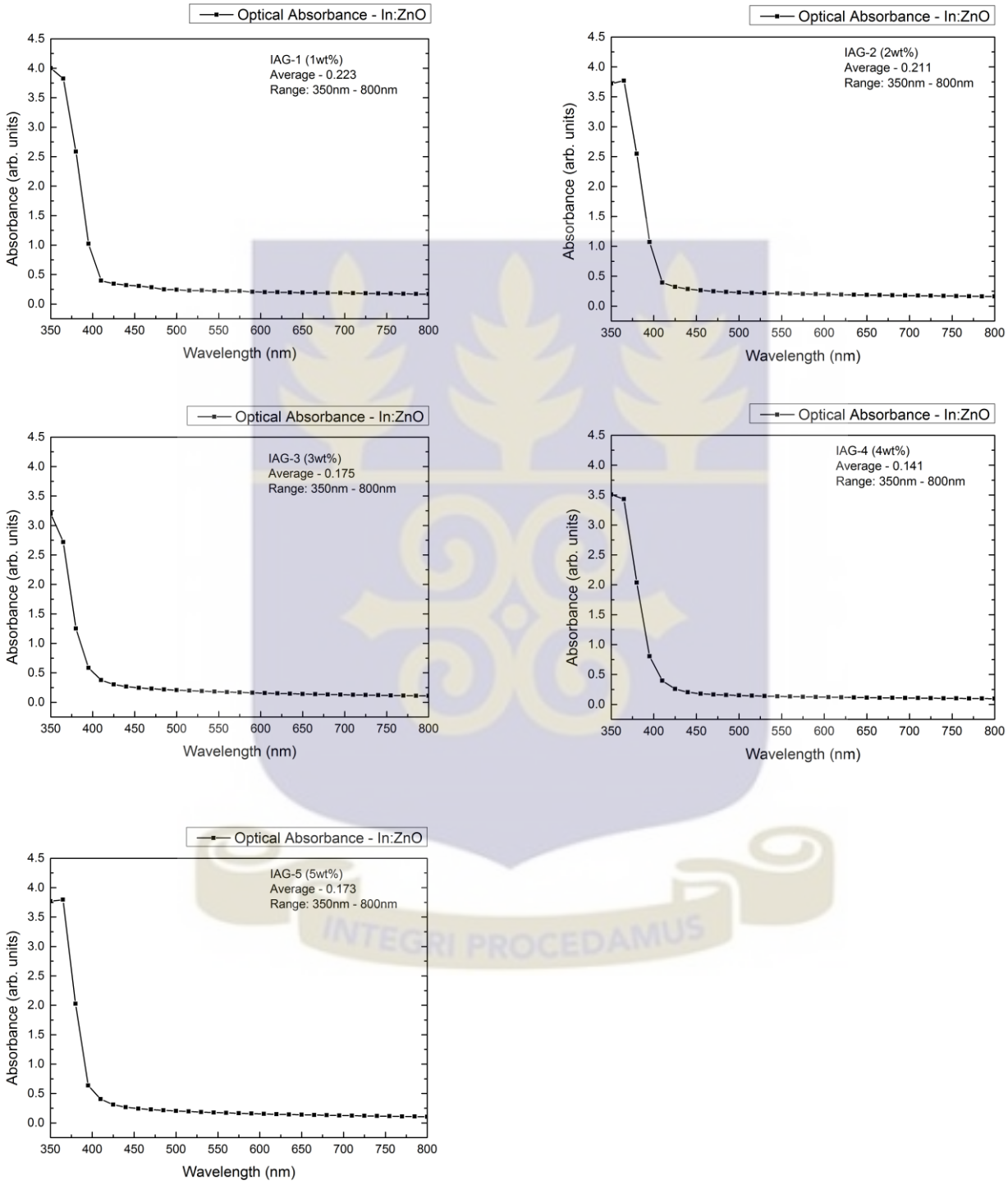

Figure 4.22 Optical absorbance measurements - Indium doped ZnO (In:ZnO)

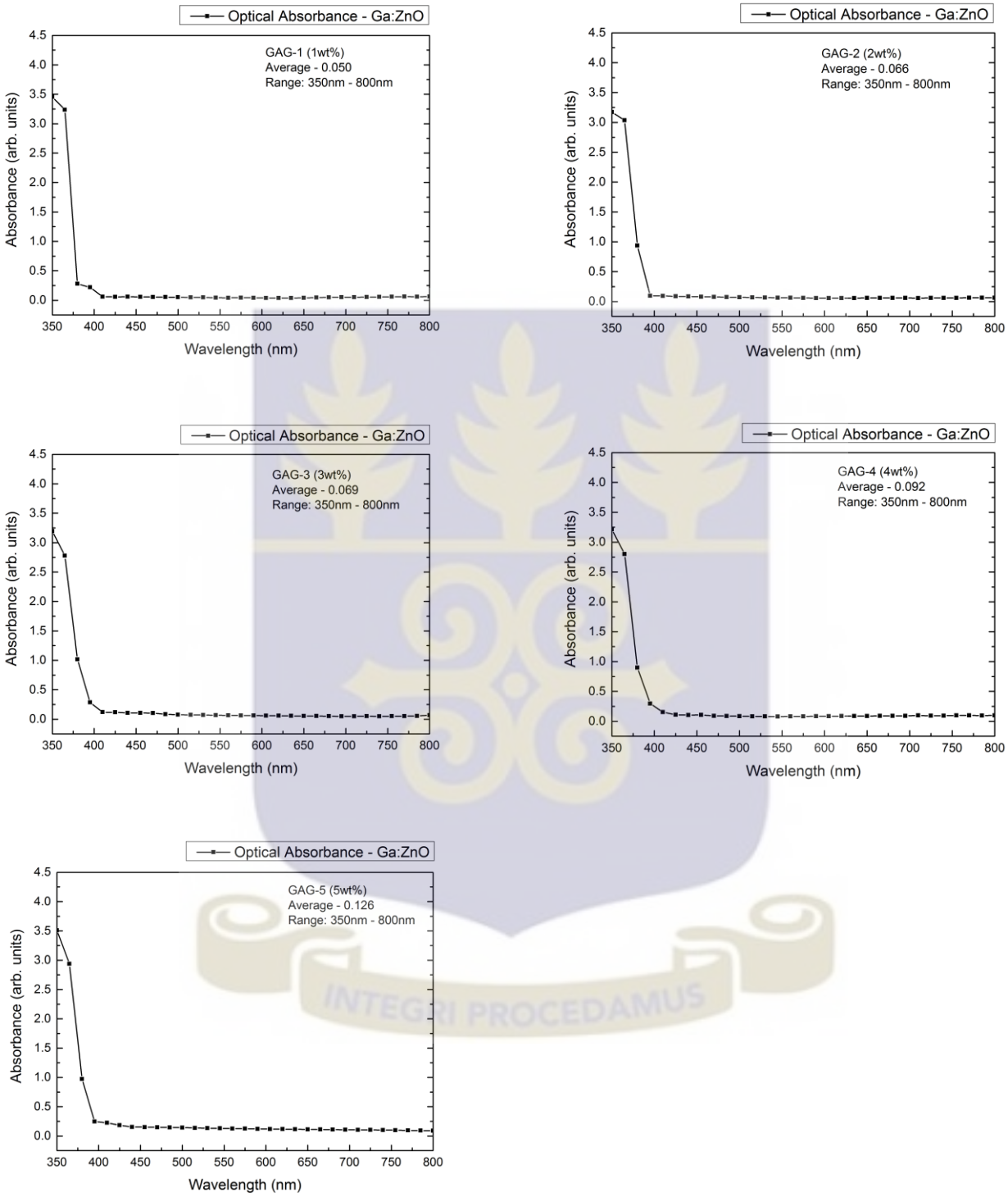

Figure 4.23 Optical absorbance measurements - Gallium doped ZnO (Ga:ZnO)

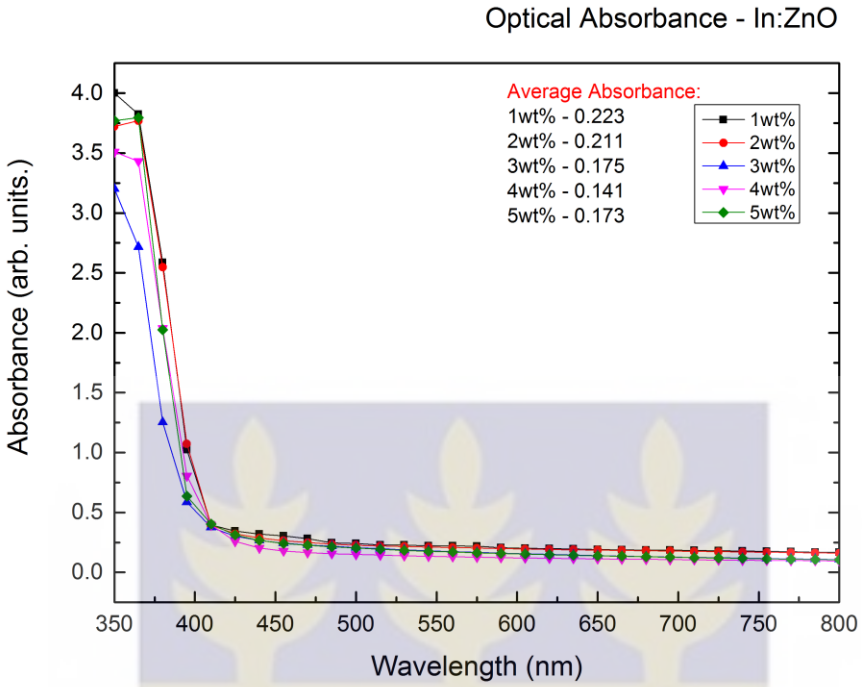

Figure 4.25 Optical absorbance grouped - Indium doped ZnO (In:ZnO)

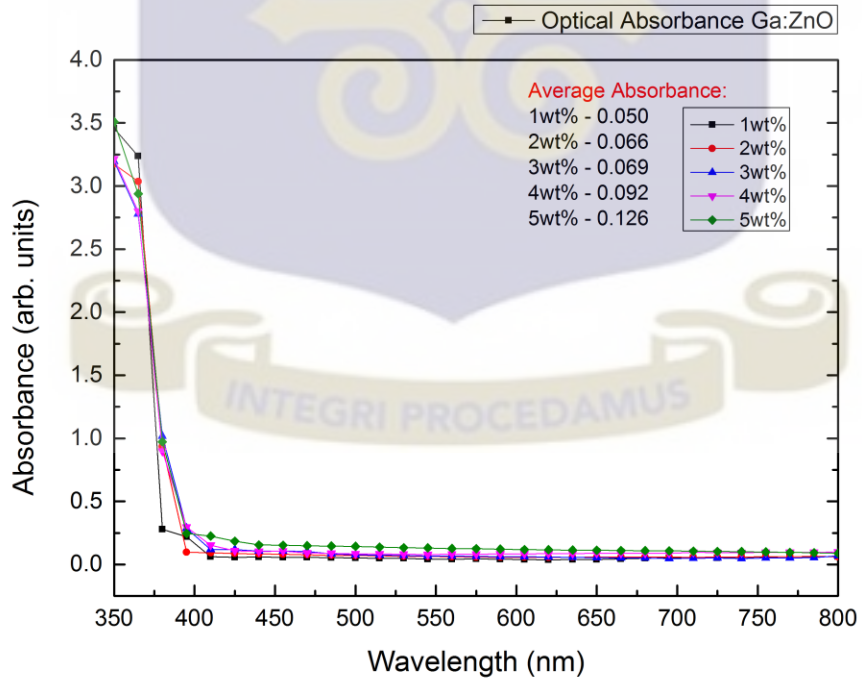

Figure 4.24 Optical absorbance grouped - Gallium doped ZnO (Ga:ZnO)

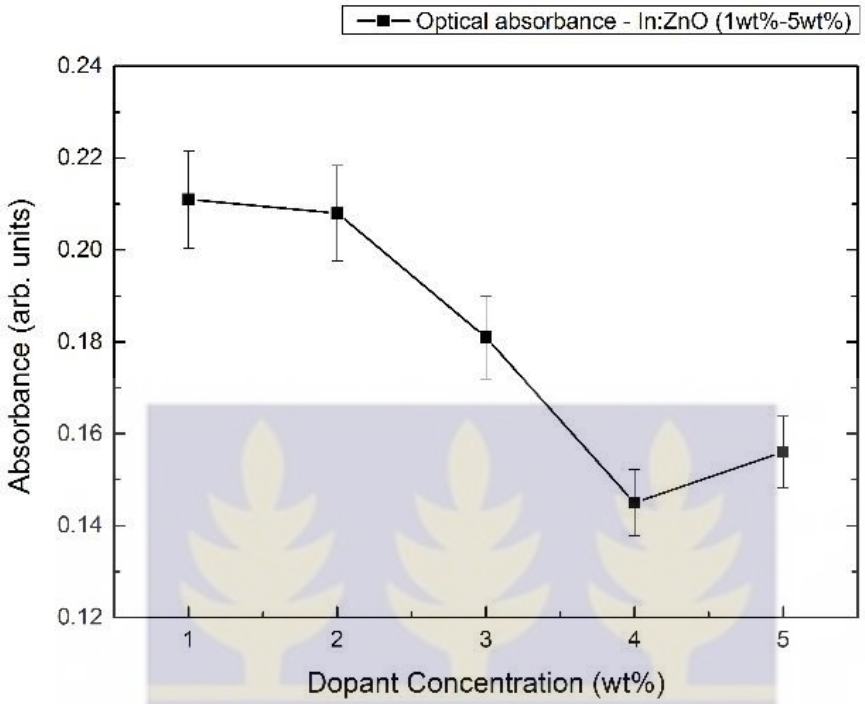

Figure 4.27 Average optical absorbance Indium doped ZnO - In:ZnO

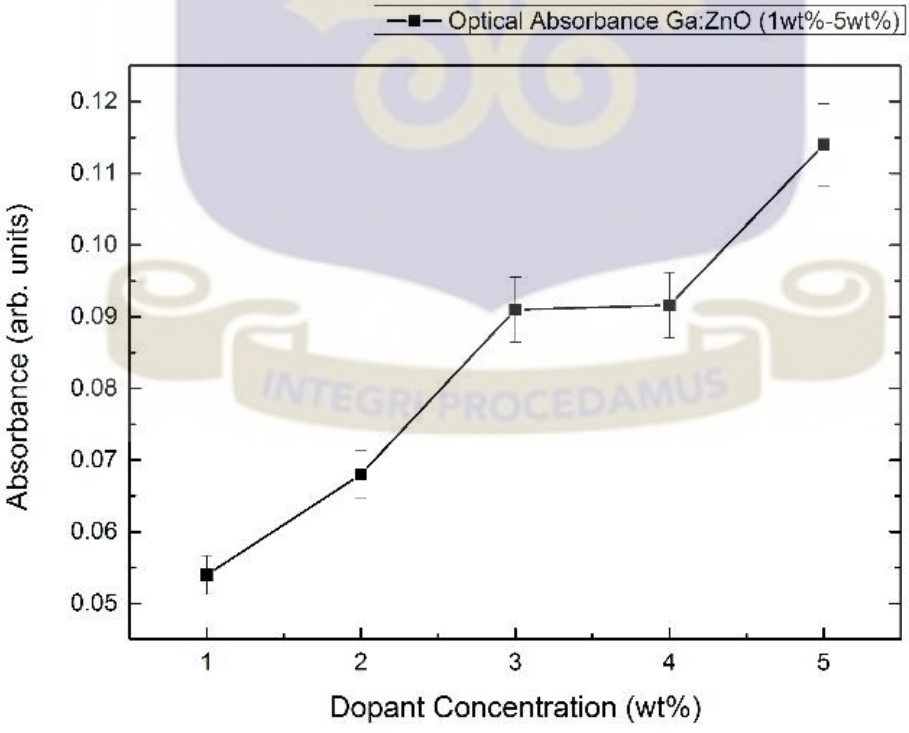

Figure 4.26 Average optical absorbance Gallium doped ZnO - Ga:ZnO

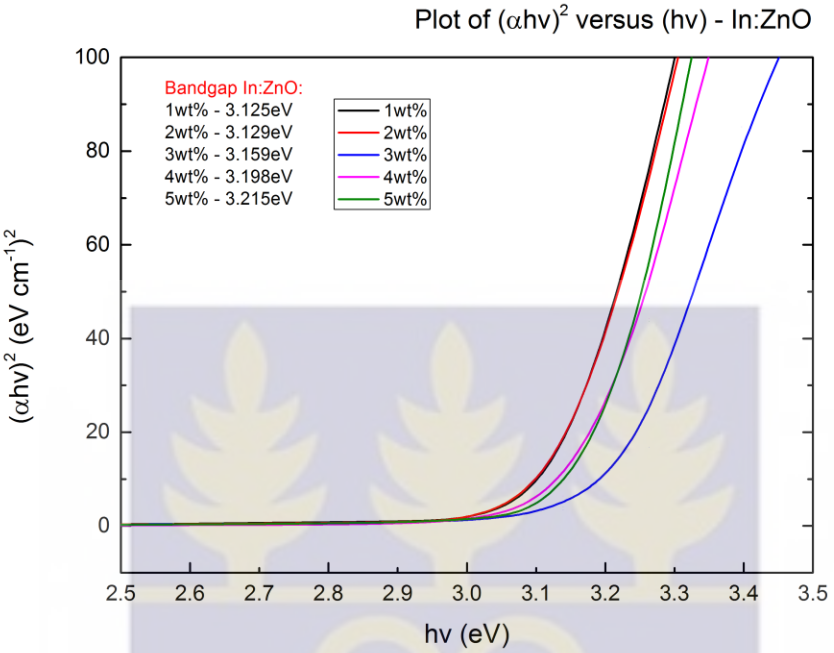

Figure 4.29 Tauc plot - Indium doped ZnO - In:ZnO

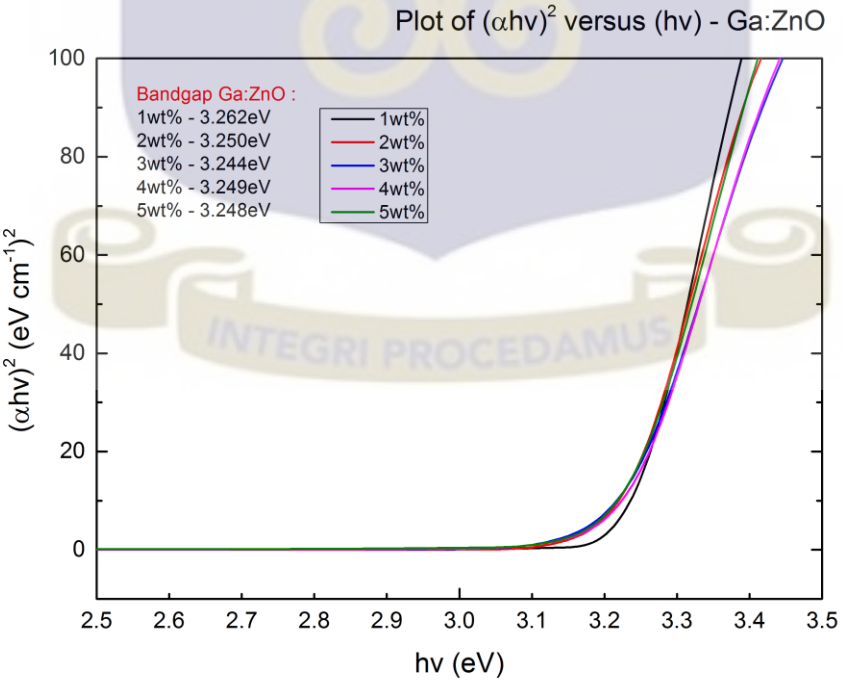

Figure 4.28 Tauc plot - Gallium doped ZnO - Ga:ZnO

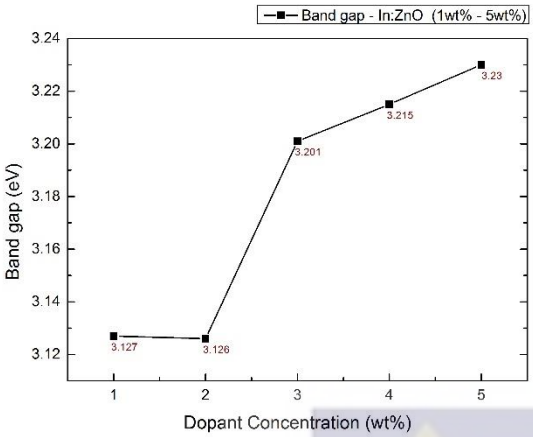

Figure 4.30 Average band gap In:ZnO

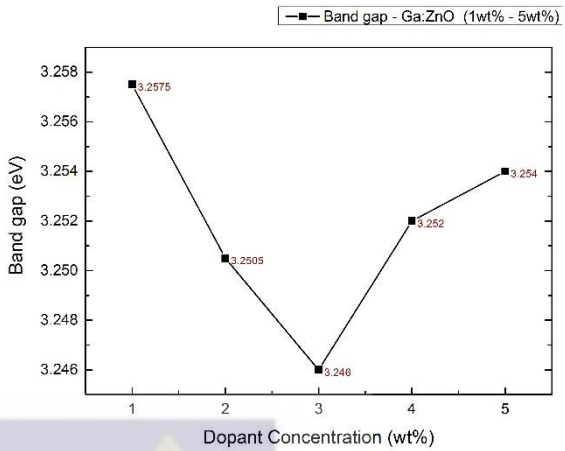

Figure 4.31 Average band gap Ga:ZnO

This section discusses the optical absorbance and band gap data for In:ZnO and Ga:ZnO thin films. The optical absorbance spectra for each doped zinc oxide sample was derived from the optical transmittance data obtained from UV-Vis analysis as described in section 4.211. The optical absorbance trend as seen in Figure 4.26 and Figure 4.27 for both In:ZnO and Ga:ZnO are consistent with expectation and theory based on the optical transmittance data. The band gap for the doped samples was obtained by extrapolating the linear portion of the Tauc plot of $(\alpha h\nu)^2$ against $h\nu$. The band gap in eV is the intercept of the extrapolated line on the x-axis. The undoped ZnO samples had an average band gap of 3.25eV. From Figure 4.30, the band gap of 1wt% In:ZnO and 2wt% were 3.127 and 3.126eV respectively. Increasing the dopant concentration beyond 3wt% resulted in an increase of the band gap values to within 2.201 and 2.230eV. The Ga:ZnO films recorded an average of 3.25eV. Comparing the band gap values for the undoped ZnO, In:ZnO and Ga:ZnO, it was concluded that the reduction in resistivity of the In:ZnO could be attributed to the narrowing of the band gap. Also, the band gap of Ga:ZnO did not change significantly from the undoped ZnO hence the effect of the gallium dopant in reducing the resistivity was not as significant as In:ZnO.

4.2.2 X-ray diffraction analysis

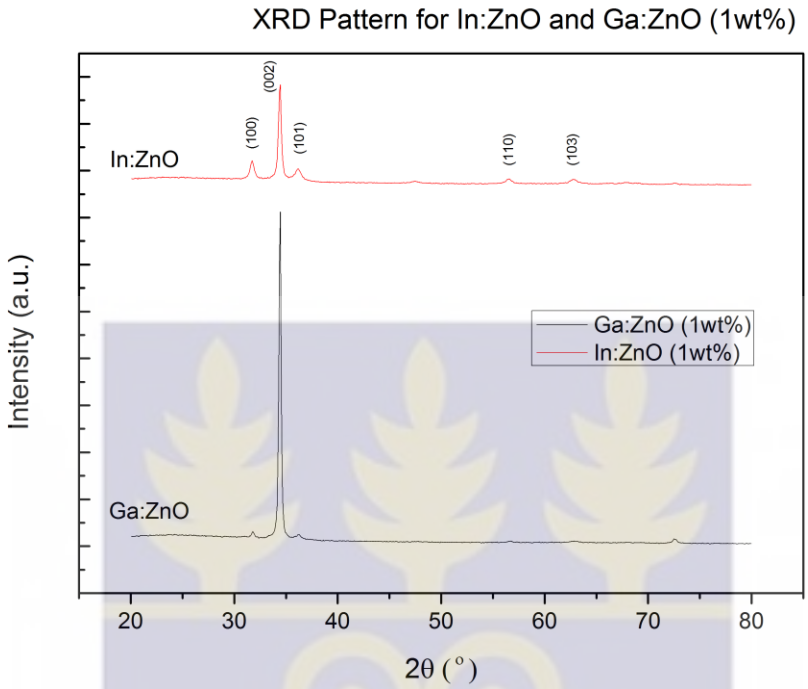

Figure 4.33 XRD Pattern In:ZnO and Ga:ZnO (1wt%)

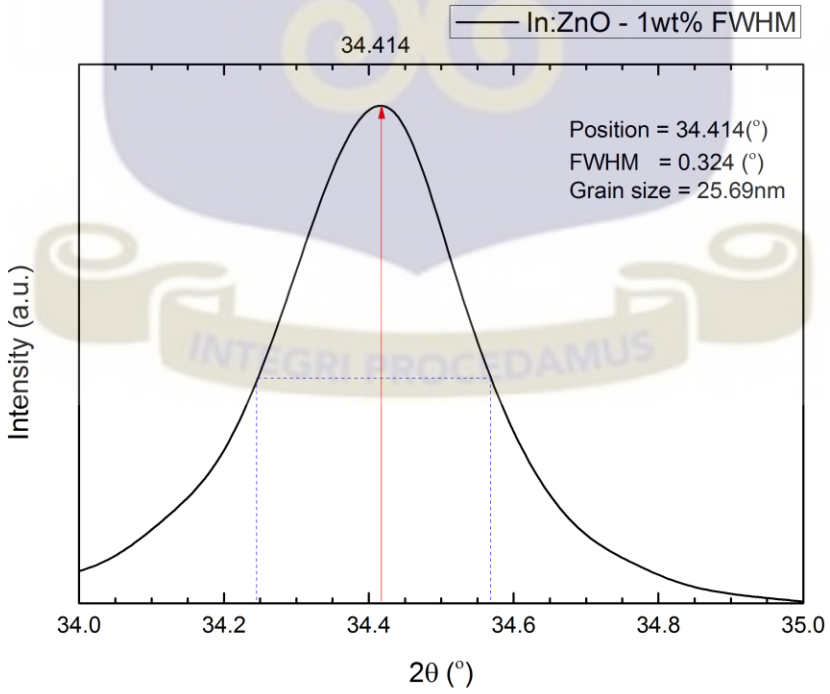

Figure 4.32 FWHM of (002) peak from XRD pattern - In:ZnO

The purpose of the X-ray diffraction analysis was to study the structure of the doped zinc oxide samples and determine if a peak shift occurred as a result of the doping of ZnO. Figure 4.33 shows the X-ray diffraction patter for the doped ZnO thin films. The XRD analysis was performed using a scan axis of 2θ from 20.00 to 80.00°. A step size of 0.2 was also programmed. The anode material for the X-ray diffractometer was Cu with Kα radiation of 1.54Å. The XRD diffraction peaks occurring at 2θ=31.09, 34.54, 36.34, 56.63 and 62.94 correspond to the (100), (002), (101), (110), (103), planes of the hexagonal structure of the doped ZnO analyzed. The most dominant peak for both 1wt% - indium doped zinc oxide (In:ZnO) and gallium doped zinc oxide (Ga:ZnO) was the (002) peak. However, the (002) peak on the Ga:ZnO sample had higher intensity as

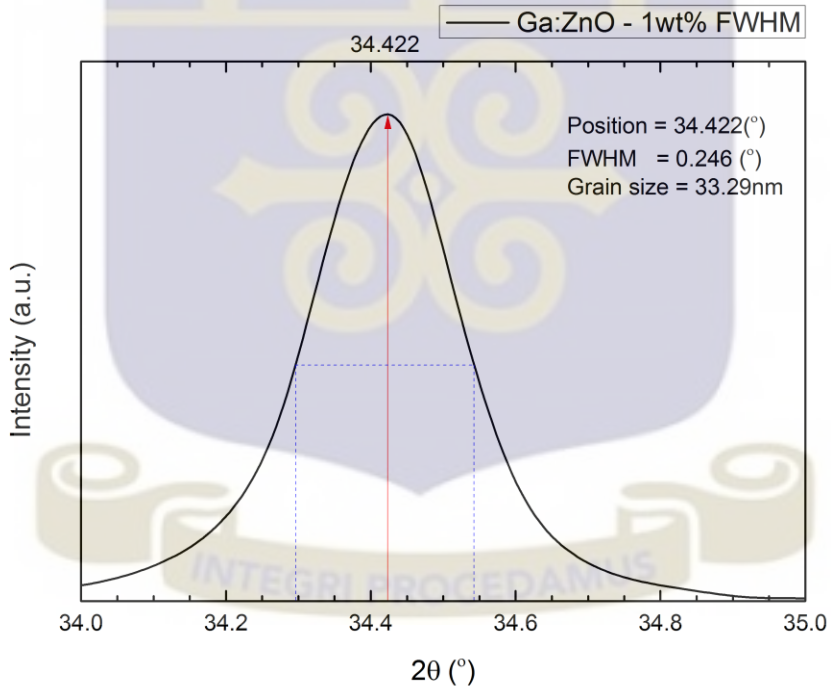

Figure 4.34 FWHM of (002) peak from XRD pattern - Ga:ZnO

compared to the In:ZnO sample. The peak for the preferred (002) orientation occurred at 34.414° and 34.422° for In:ZnO and Ga:ZnO respectively as expected (Rajesh, 2014). From this data, it

can be concluded that there was no peak shift after doping ZnO with indium and Gallium. Other less dominant peaks that showed on the XRD pattern for the In:ZnO sample were (100), (101), (110) and (103). This can be attributed to the difference in atomic radii of indium and zinc. Indium has a larger atomic radius (1.56Å) compared to zinc (1.42Å). The difference in atomic radius causes stress in the ZnO structure when indium replaces zinc. This is seen from the various peaks apart from the preferred (002) peak in the In:ZnO sample. Gallium however has a smaller atomic radius (1.36Å) compared to zinc and indium. From Figure 4.33, it is observed that, the (002) orientation from Ga:ZnO is most dominant and the other peaks have less intensities when compared. The smaller atomic radius of gallium allows it fit with less strain on the zinc oxide structure as compared to indium. This therefore explains the difference in peak intensities for the (002) peaks and the appearance of other peaks and corresponding low intensities for both samples.

4.2.3 Sheet Resistance measurement

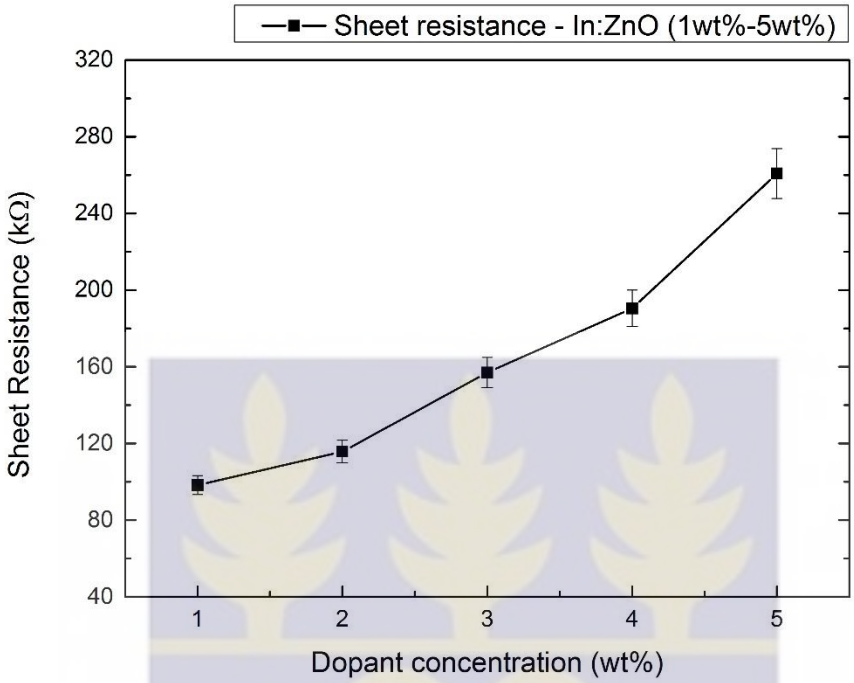

Figure 4.35 Average sheet resistance - In:ZnO

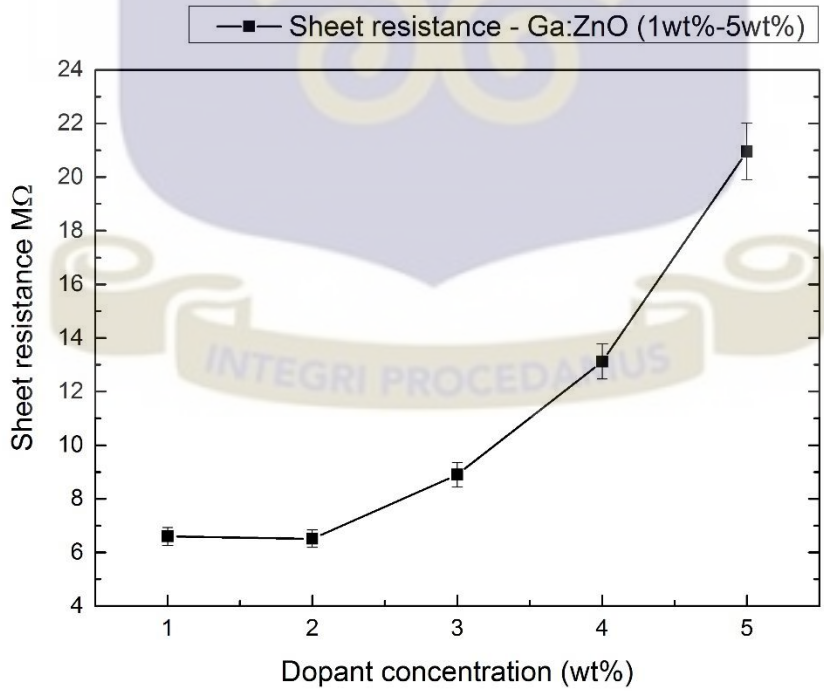

Figure 4.36 Average sheet resistance - Ga:ZnO

The sheet resistance of In:ZnO and Ga:ZnO thin film samples was measured using a four-point probe set-up. The set-up comprised a Keithley 2100 model digital multimeter, a Phywe current source and a probe head supplied by Jandel. The electrical properties of undoped ZnO films could not be measured using the Four-point probe. The resistance values of the undoped films were out of the sensitivity range of the four-point probe device. The doped films however had lower resistivity and hence were characterized using the four-point probe. From Figure 4.35, it is observed that doping ZnO with indium reduced the electrical resistivity of the films. However, increasing the dopant weight concentration in the zinc oxide had a negative effect on the film resistivity. The 1wt% sample recorded a value 7.65kΩ/□, the lowest resistivity for In:ZnO. Increasing the dopant concentration, resulted in an increase in the sheet resistance for the In:ZnO samples. The 5wt% sample exhibited the highest resistivity recording a value of 18.17kΩ/□. A similar trend was observed for the Ga:ZnO samples. There was no significant difference between the 1wt% and 2wt% Ga:ZnO samples in terms of their sheet resistance. The sheet resistance however increased progressively from the 3wt% Ga:ZnO sample up to the 5wt% Ga:ZnO sample which recorded the highest sheet resistance. The increase in sheet resistance values for both In:ZnO and Ga:ZnO samples may be attributed to positioning of the dopant ions within the ZnO lattice. Ideally, the dopant ions are expected to substitute the zinc ions in the lattice. However, increasing the concentration of the dopants caused some of dopant ions to occupy interstitial positions which caused distortions in the ZnO lattice and also increased the efficiency of scattering mechanisms. This can explain the increase in resistivity with increasing dopant concentration for both In:ZnO and Ga:ZnO samples.

4.2.4 Hall Effect measurements

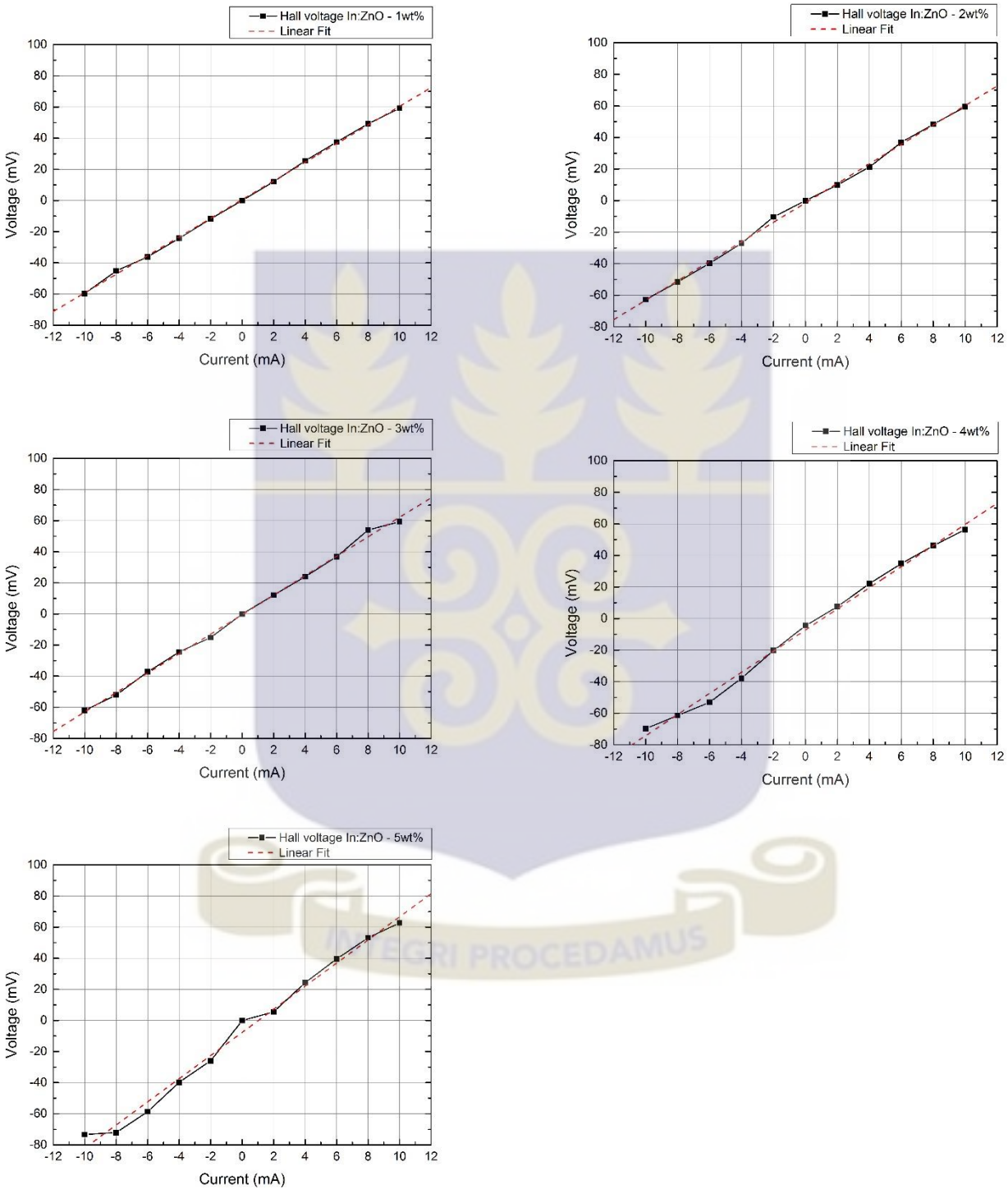

Figure 4.37 Hall Effect measurements - In:ZnO (1wt% - 5wt%)

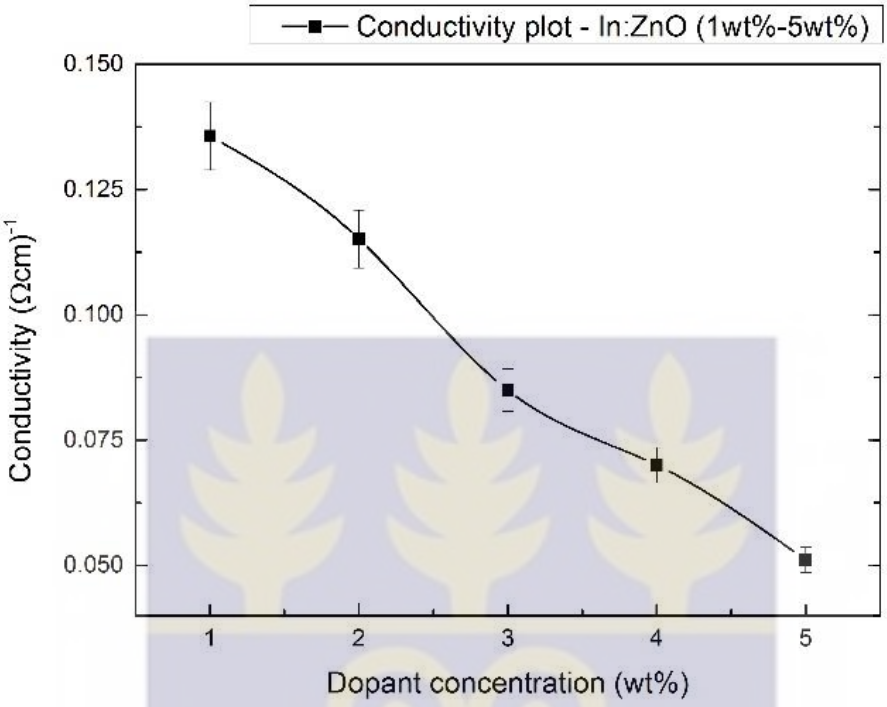

Figure 4.38 Conductivity vs. dopant concentration - In:ZnO

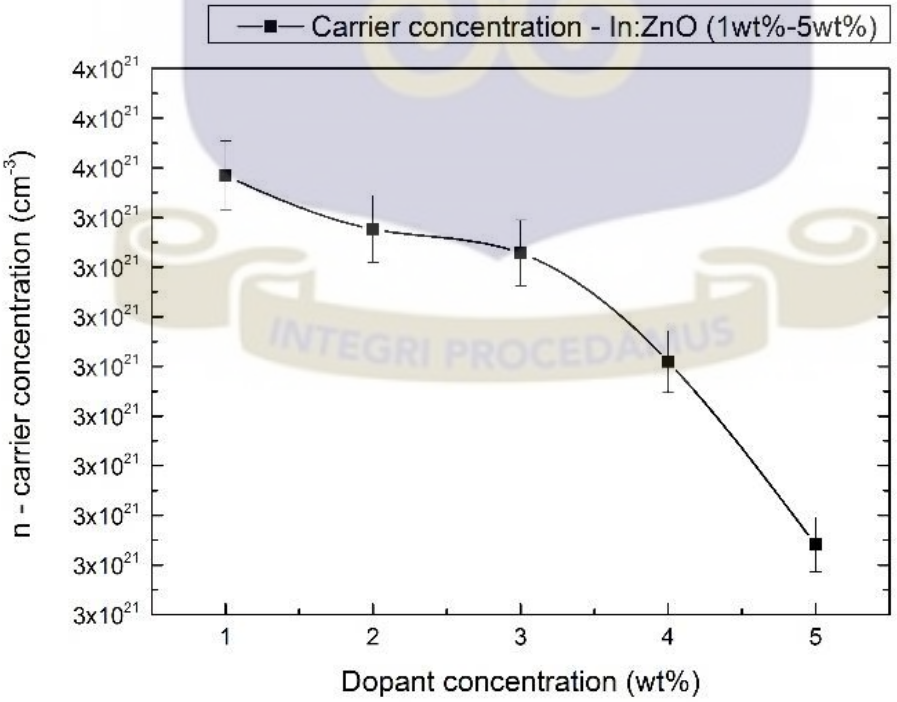

Figure 4.39 Carrier concentration vs. dopant concentration - In:ZnO

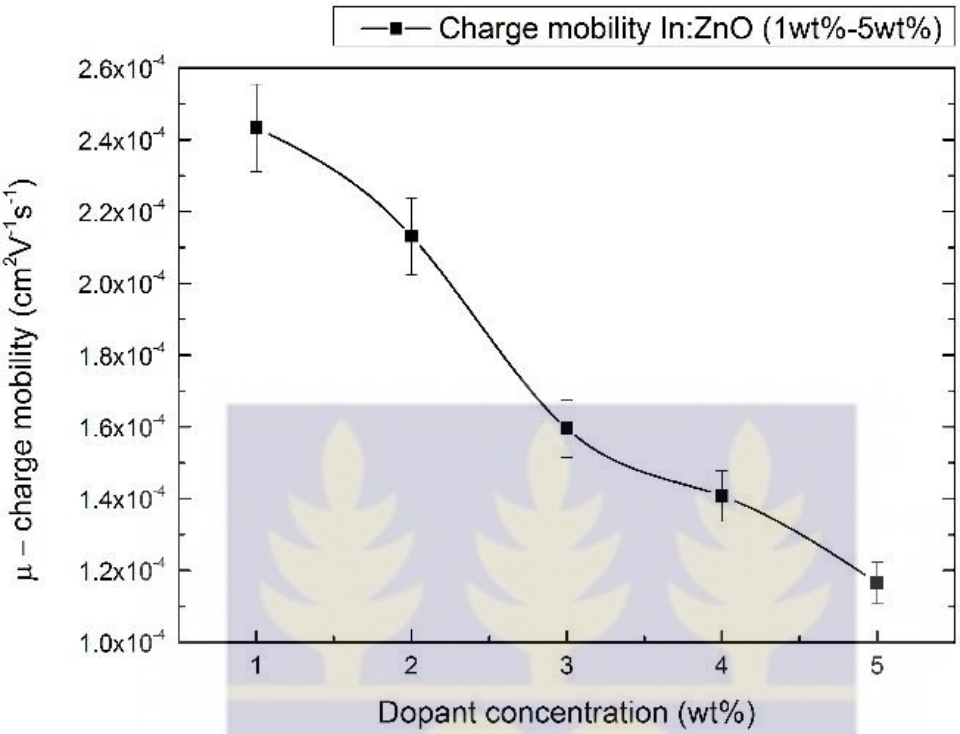

Figure 4.40 Charge mobility vs dopant concentration - In:ZnO

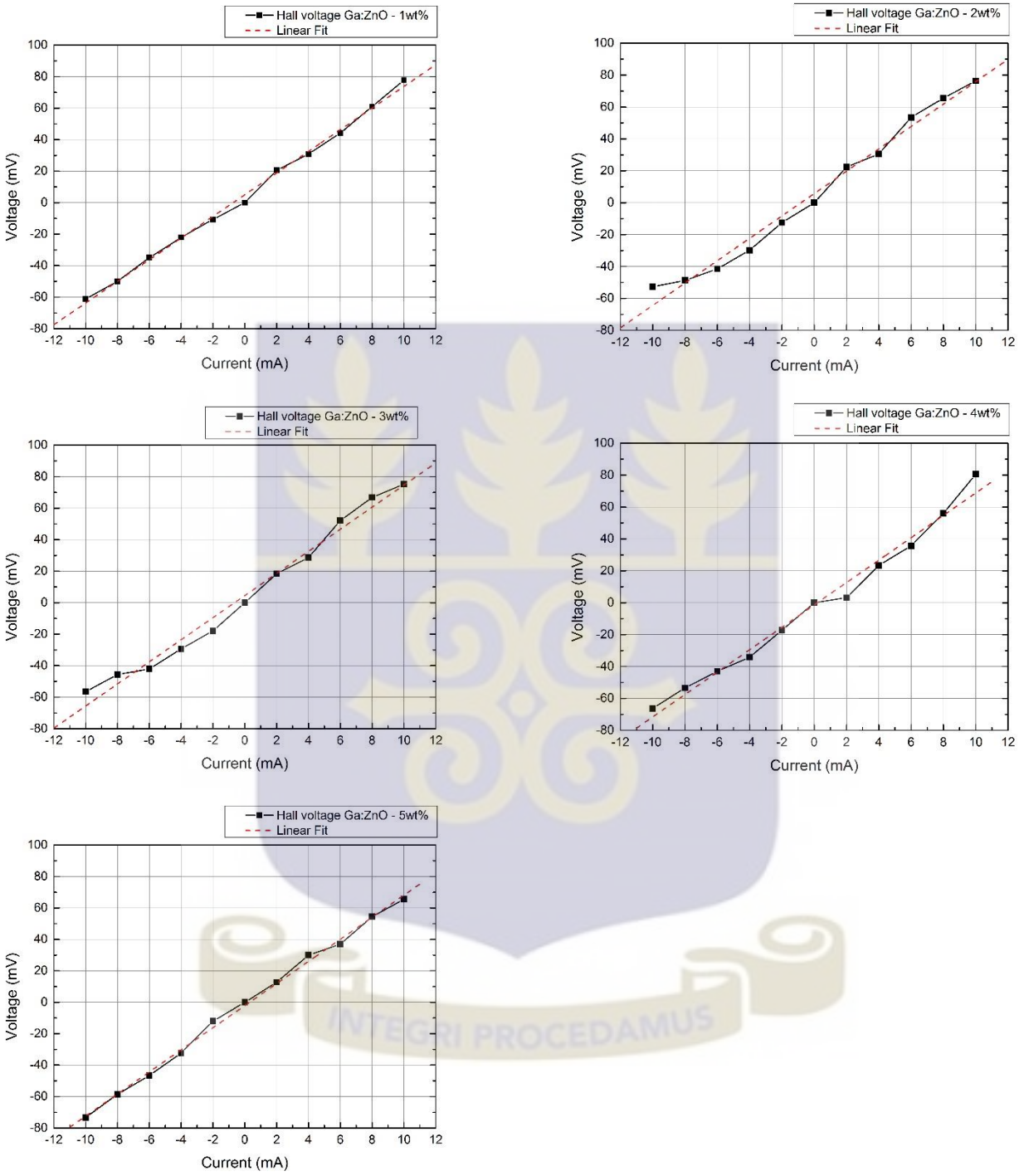

Figure 4.41 Hall Effect measurements - Ga:ZnO (1wt% - 5wt%)

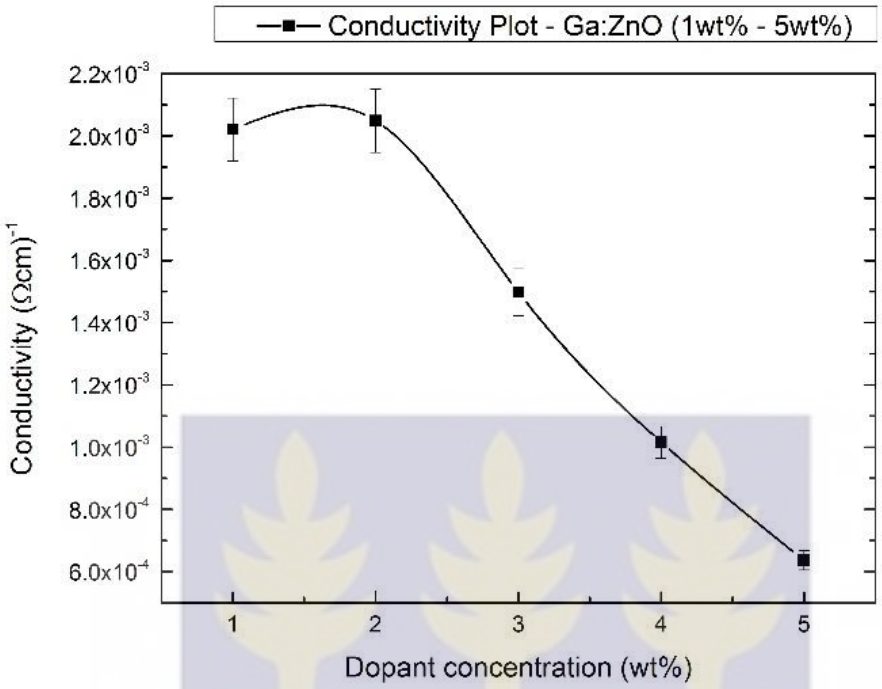

Figure 4.42 Conductivity vs dopant concentration - Ga:ZnO

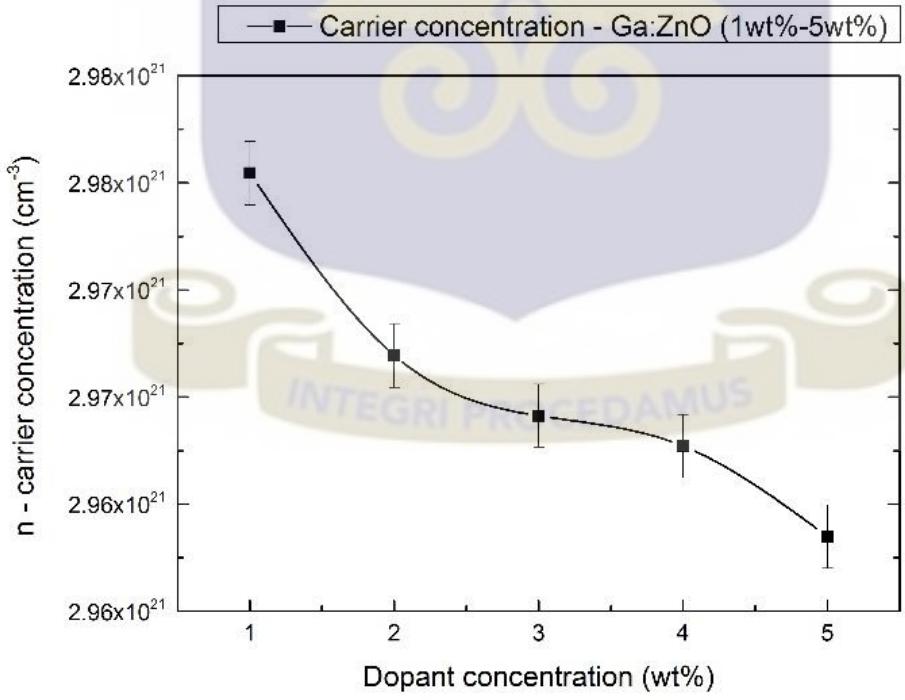

Figure 4.43 Carrier concentration vs dopant concentration - Ga:ZnO

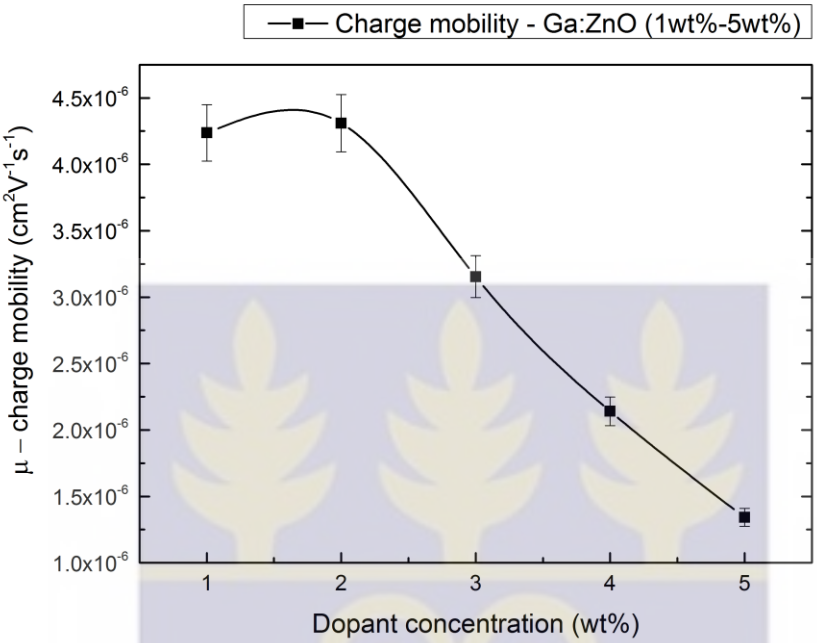

Figure 4.44 Charge mobility vs dopant concentration - Ga:ZnO

The Hall Effect measurement is a characterization technique that can be used to determine the electrical properties of semiconductor materials. The doped zinc oxide thin films that were prepared were subjected to a magnetic field and an electric current was passed through the samples perpendicular to the direction of the magnetic field. There are various configurations that can be employed for Hall measurements. Figure 3.4 illustrates the geometry of the doped ZnO samples that were tested. Molten lead was deposited at the four corners of the sample and allowed to solidify to form contacts. Thin wires were embedded in the lead contacts and these served as ports for the probes. The experiment was carried out a temperature of 300K (27°C). For the purposes of this experiment, a magnetic field of 300mT was created by supplying current to a pair of electromagnets. The magnetic strength was measured with a Phywe Teslameter. For each sample (In:ZnO 1wt% -5wt% / Ga:ZnO 1wt% -5wt%), a minimum current of -10mA (reverse current)

was applied. The current was varied by a step size of 1mA up to a maximum of 10mA. At each current, the corresponding voltage created was recorded using a digital multimeter. Voltage correction was done based on the voltages recorded at 0mA for each sample to attain the actual Hall voltages (V_H). A plot of the input current against the Hall voltage was generated and the slope of the graph used to determine the Hall coefficient. Subsequently, the conductivity, mobility and carrier concentration for each sample was determined. The results for the respective dopants are summarized in Table 4.1.

Table 4.1 Electrical properties of In:ZnO and Ga:ZnO thin films with varying dopant conc.

In:ZnO			
Dopant conc. (wt%)	**Resistivity (Ω cm)**	**Mobility (cm^2/Vs)**	**Carrier conc. (cm^{-3})**
1	7.37125	0.000243	3.48×10^{21}
2	8.68375	0.000213	3.38×10^{21}
3	11.7725	0.00016	3.33×10^{21}
4	14.28275	0.000141	3.11×10^{21}
5	19.56075	0.000117	2.74×10^{21}
Ga:ZnO			
Dopant conc. (wt%)	**Resistivity (Ω cm)**	**Mobility (cm2/Vs)**	**Carrier conc. (cm-3)**
1	494.8875	4.24×10^{-6}	2.98×10^{21}
2	488	4.31×10^{-6}	2.97×10^{21}
3	667.375	3.15×10^{-6}	2.97×10^{21}
4	984	2.14×10^{-6}	2.97×10^{21}
5	1571.875	1.34×10^{-6}	2.96×10^{21}

From the results obtained, it can be concluded that both indium doped zinc oxide (In:ZnO) and gallium doped zinc oxide (Ga:ZnO) show n-type conductivity. For indium doped zinc oxide samples, the lowest resistivity recorded was 7.371Ω cm for the 1wt% sample. The resistivity increased with increasing dopant concentration to a maximum of 19.561Ω cm for the 5wt% sample. The mobility and carrier concentration for the indium doped samples decreased with increasing dopant concentration. The resistivity of gallium doped zinc oxide was higher compared to the respective indium doped samples. The resistivity of the gallium doped samples also increased with increasing dopant concentration. The mobility and carrier concentration decreased as the dopant concentration increased. The conductivity of undoped ZnO is improved as a result of the ionization of the dopants (In^{3+} /Ga^{3+}). The ionized dopants have the ability to replace Zn^{2+} in the ZnO lattice structure to provide extra electrons to improve the conductivity. An excess of dopants impurities within the lattice can alter the structure and affect the conductivity immensely. If the dopants do not replace the Zn^{2+} ions and occur in interstitial positions, the effect of the dopants on the electrical conductivity does not show as expected (Onwona-Agyeman, 2013).

4.2.5 Electron Probe Microanalysis (EPMA)

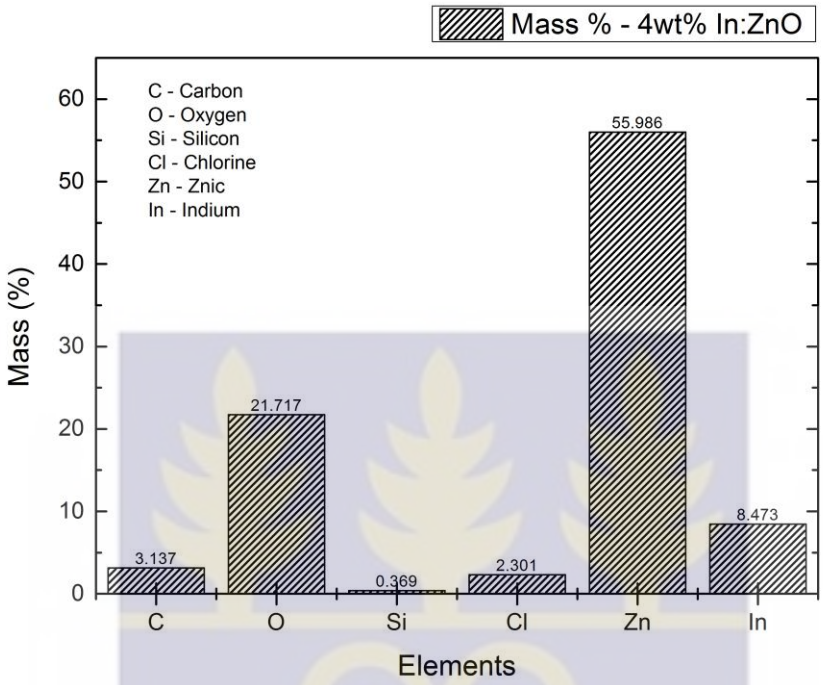

Figure 4.45 EPMA Elemental composition - 4wt% In:ZnO

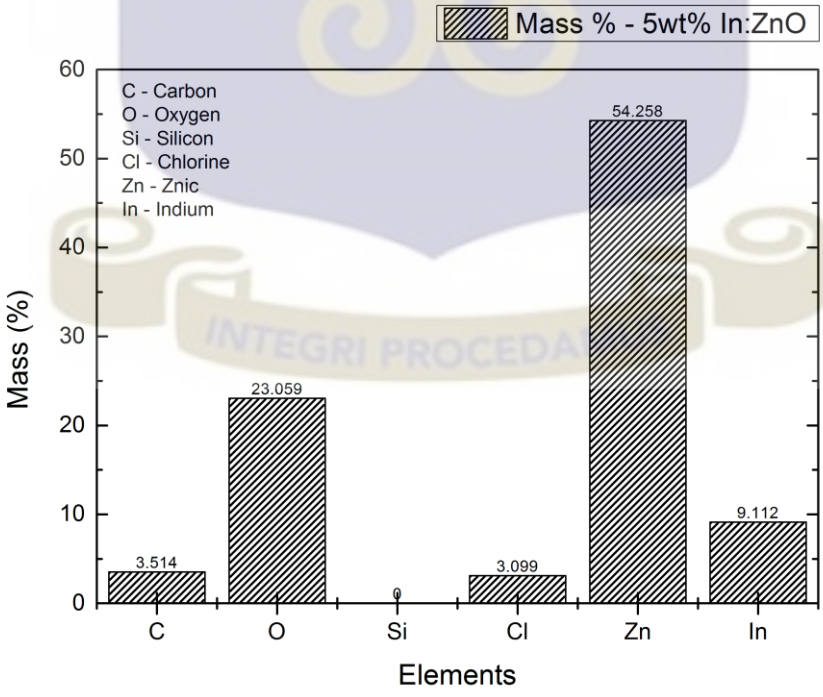

Figure 4.46EPMA Elemental composition - 5wt% In:ZnO

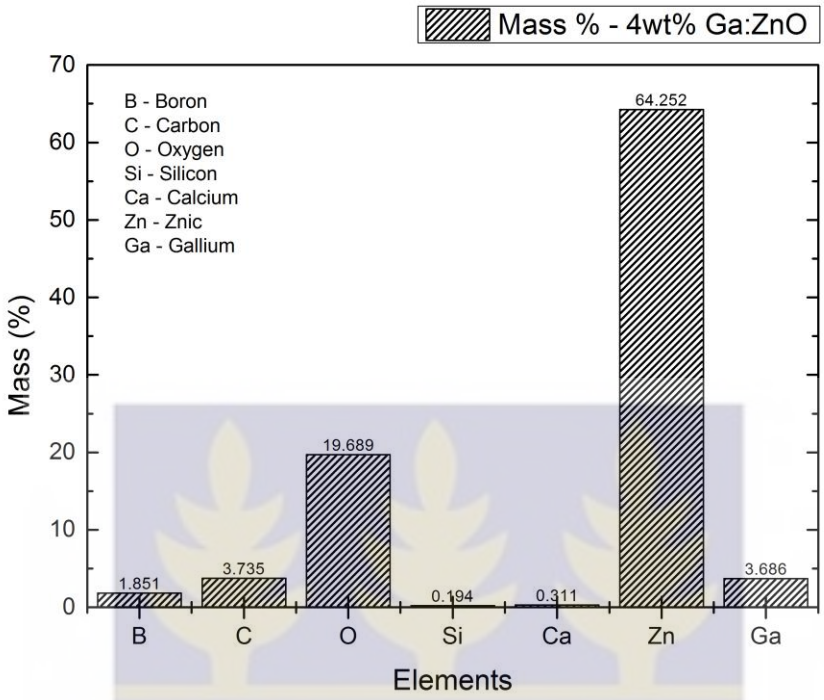

Figure 4.47 EPMA Elemental composition - 4wt% Ga:ZnO

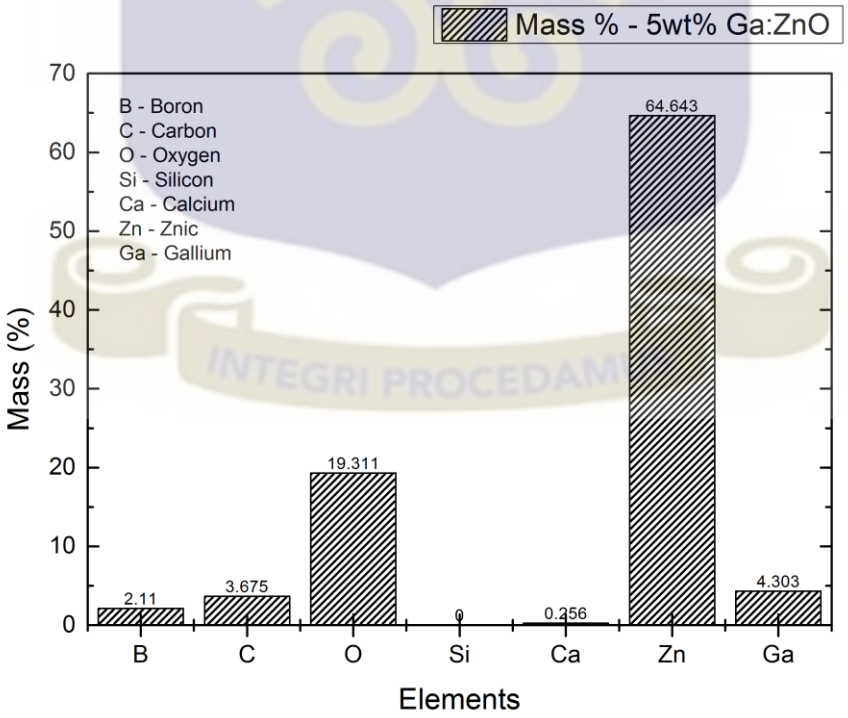

Figure 4.48 EPMA Elemental composition - 5wt% Ga:ZnO

Electron probe microanalysis was carried out on In:ZnO and Ga:ZnO samples to ascertain the presence of the intended dopants and other elements in the ZnO structure. The analysis also gave furthere information about the relative concentration of these elements. The samples analyzed were 4wt% In:ZnO, 5wt% In:ZnO, 4wt% Ga:ZnO and 5wt% Ga:ZnO. The values obtained from the analysis were graphically represented in Figures 4.45, 4.46, 4.47 and 4.48.

It can be deduced from the plot (4wt% / 5wt% In:ZnO), that indium was present in the doped zinc oxide sample. The improvement in the conductivity of these samples can be attributed to the presence on indium. The amount of indium increased from 8.473 (mass%) in the 4wt% sample to 9.112 (mass%) in the 5wt%sample. Similarly, the presence of gallium was detected in the Ga:ZnO samples and hence improvement in the conductivity of the respective samples can be attributed to the presence of gallium. Also, the amount of gallium increased from 3.686 (mass%) in the 4wt% sample to 4.303 (mass%) in the 5wt% sample. The other trace elements such as silicon and boron what were observed in the samples (both In:ZnO and Ga:ZnO) could be from the glass substrate the carried the thin film. Also, chlorine and calcium in both In:ZnO and Ga:ZnO respectively, were from the dopant source compounds. The indium dopant was sourced from indium (III) chloride while gallium was sourced from gallium oxide. The analysis therefore confirmed the presence of both dopants in the respective samples and the deductions made with respect to the electrical properties of doped ZnO samples.

4.2.6 Scanning Electron Microscope Analysis

The surface morphology of In:ZnO and Ga:ZnO films was studied using the scanning electron microscope. The 4wt% In:ZnO, 5wt% In:ZnO, 4wt% Ga:ZnO and 5wt% Ga:ZnO samples were analyzed. Figures 4.49 – 4.52 show the SEM images of the samples analyzed. The sample surfaces were observed at X 250 magnification (probe 100µm) and X 5000 magnification (1µm). The higher magnification (X 5000) produced higher resolution images compared to the X 250 magnification. From Figure 4.50 and 4.51 it is observed that there is a distinct variation in the surface morphology of In:ZnO and Ga:ZnO. Ga:ZnO had cylindrical rod shaped crystallites while the In:ZnO had characteristic hexagonal slices. These plate-like structures spread across the surface fused together and overlapping to give a rough surface. The Ga:ZnO crystallites however were clustered in pockets with varying diameters. The difference in crystallite structure and distribution serves as an explanation for the different optical transparency values.

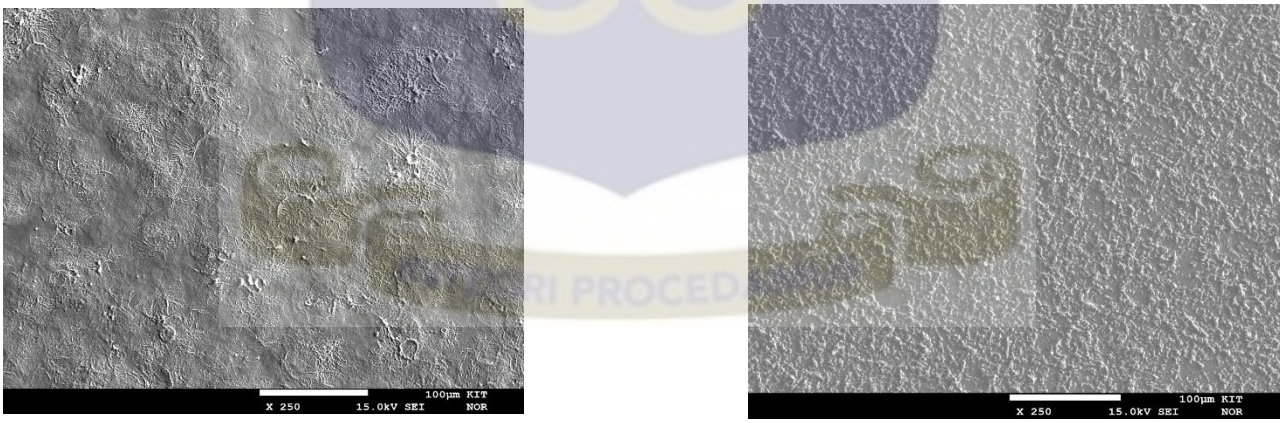

Figure 4.49 SEM images (X 250) 4wt% - In:ZnO (left) and Ga:ZnO (right)

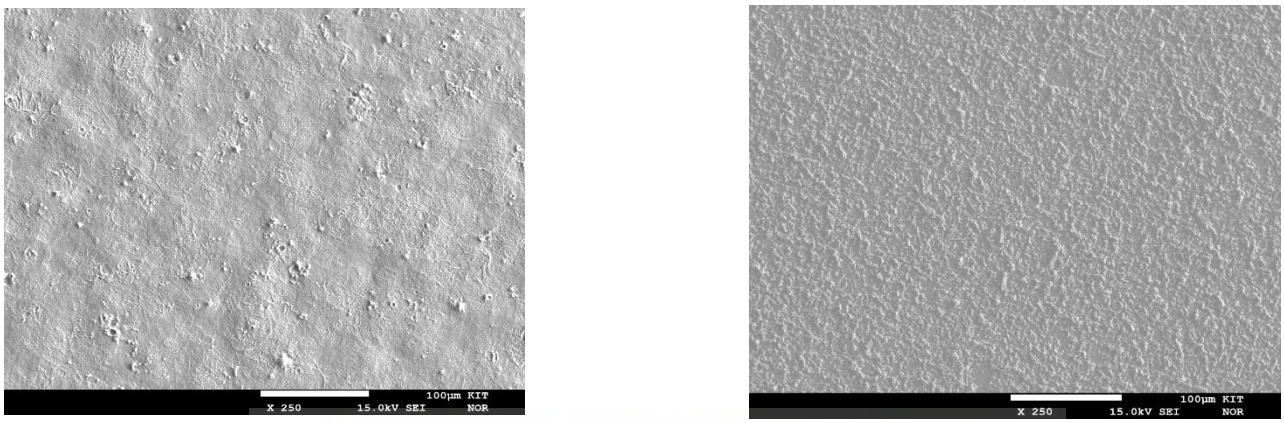

Figure 4.52 SEM images (X 250) 5wt% - In:ZnO (left) and Ga:ZnO (right)

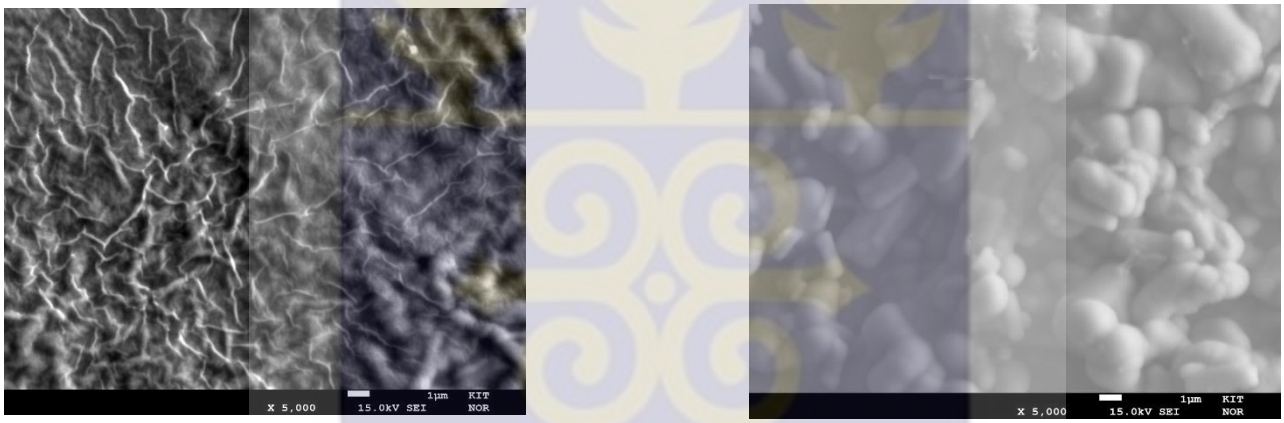

Figure 4.51 SEM images (X 5000) 4wt% - In:ZnO (left) and Ga:ZnO (right)

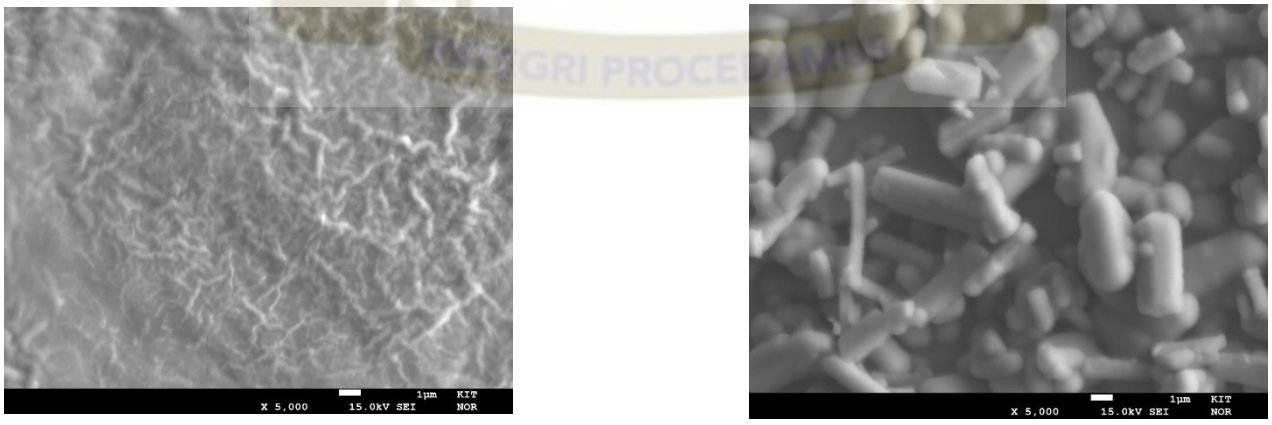

Figure 4.50 SEM images (X 5000) 5wt% - In:ZnO (left) and Ga:ZnO (right)

4.2.7 Optimization process for figure of merit

The two most important properties of a good TCO that enables it to be used in solar cell devices and other opto-electronic devices are high transparency and low sheet resistance. The figure of merit as defined by Haacke (Haacke, 1976) can be calculated to determine the quality and eventual performance of a TCO (Bedia, 2015). The figure of merit is given by the following equation:

$$\varphi = \frac{T\alpha^{10}}{R_S} \qquad \text{(Eqn. 4.2)}$$

Where Tα is the average transmittance and R_s is the sheet resistance.

For this work, the figure of merit would determine the best combination of transparency and low resistivity to determine which dopant concentration would yield the best results. The best TCO dopant concentration corresponds to the highest value in terms of the figure of merit. Table 4.2 lists the doped samples and their respective figure of merit values based on the above mentioned equation.

Table 4.2 Figure of merit for doped zinc oxide TCO samples

In:ZnO		Ga:ZnO	
Dopant concentration	Figure of merit	Dopant concentration	Figure of merit
1 wt%	1.1 x 10^{17}	1 wt%	5.83 x 10^{16}
2 wt%	1.05 x 10^{17}	2 wt%	4.33 x 10^{16}
3 wt%	1.44 x 10^{17}	3 wt%	1.88 x 10^{16}
4 wt%	2.68 x 10^{17}	4 wt%	1.23 x 10^{16}
5 wt%	1.54 x 10^{17}	5 wt%	4.61 x 10^{16}

With respect to indium doped zinc oxide, the highest figure of merit was obtained at 4wt% indium doping. Also, for gallium doped zinc oxide, 1wt% dopant concentration recorded the highest figure of merit. This suggests that these dopant concentrations produce optimized ZnO thin films that can be applied as transparent contact in solar cells.

CHAPTER FIVE

5.0 CONCLUSIONS AND RECOMMENDATIONS

5.1 Conclusions

The first part of this study involved depositing undoped zinc oxide thin films on glass substrates using the spray pyrolysis technique. The zinc oxide was deposited from a precursor solution of zinc acetate, ethanol, deionized water and acetic acid, at a temperature of 400°C. The volume of acetic acid in the precursor solution was varied from 1ml to 5ml. Structural, optical and electrical characterization of the undoped ZnO films were carried out to study the effect of acetic acid volume in the precursor solution. The results are summarized as follows:

- The ZnO thin films exhibited average optical transparency above 80%. Increasing the amount of acetic acid in the precursor solution resulted in an increase in the optical transparency for the range that was studied.
- Further optical characterization showed that, the undoped ZnO thin films had an average band gap of 3.25eV.
- The undoped ZnO thin films also exhibited high resistivity consistent with findings from literature. The lowest sheet resistance measured was 36.93MΩ/□ which corresponds to the 2ml acetic acid sample.
- The XRD analysis of the undoped ZnO showed that, all the films produced had a wurtzite structure and was highly oriented in the (002) plane with good crystal structure parameters. The quality of the crystal structure improved as the acetic acid content increased.

The undoped ZnO thin films cannot be used as a TCO in a solar cell device due to the high resistivity. The 3ml acetic acid film was selected as the best with respect to transparency and structural properties based on the XRD pattern.

The second phase of this study involved studying the effects of dopants (In/Ga) on the structural, optical and electrical properties of zinc oxide. Doping of ZnO was achieved by adding the required amount of the dissolved dopant to a solution of zinc acetate, ethanol, deionized water and acetic acid. The dopant concentration was varied from 1wt% to 5wt% for the respective dopants. The precursor solution (including the dopant) was sprayed on to a glass substrate at 400°C. XRD, SEM, Hall Effect, sheet resistance, EPMA and UV-Vis spectroscopy analysis were carried out on the doped ZnO thin film samples. The results for the various characterization procedures are summarized as follows:

- UV-Vis spectrophotometry analysis showed that the In:ZnO thin films had transparency above 60% and the transparency increased with increasing dopant concentration. For the Ga:ZnO thin films, a maximum transparency of 88% was recorded for the 1wt% sample. The transparency of the Ga:ZnO films decreased with increasing dopant concentration. The effects of indium and gallium dopants on ZnO was attributed to crystal structure and grain distribution.
- From the Hall Effect measurement and sheet resistance analysis, the carrier concentration, conductivity and charge carrier mobility were determined for the respective dopants. For both In:ZnO and Ga:ZnO, the conductivity, charge mobility and carrier concentration, decreased progressively with increasing dopant concentration. The In:ZnO samples however exhibited higher conductivities, mobility and charge concentration compared to the Ga:ZnO.

- The crystal structure of In:ZnO and Ga:ZnO samples was studied using X-ray diffraction. For both samples, the (002) peak occurred at 34.4°C. The XRD pattern for In:ZnO also showed peaks that suggested that, the difference in ionic radius of indium had caused lattice distortions by replacing zinc ions. Both In:ZnO and Ga:ZnO thin films were highly oriented with dominant (002) peaks.
- Electron probe microanalysis was carried out to determine the elemental composition of the doped ZnO thin films. The results showed that, both indium and gallium were present in their respective doped films. The composition of indium in mass percent for both In:ZnO samples was higher than that of gallium in the respective Ga:ZnO samples. This indicated that, more indium dopant had been successfully incorporated in the ZnO during the spray pyrolysis process. This explained why the indium doped samples had higher conductivity compared to the gallium doped samples.

Based on the results obtained from the doped samples that were characterized, it was concluded that the dopant concentration had an effect on electrical, optical and structural properties of both In:ZnO and Ga:ZnO. The figure of merit model was used to select the best dopant concentration. For In:ZnO thin films, 4wt% indium was the optimum dopant concentration that yielded the best results in terms of transparency and conductivity of the TCO. Also, for Ga:ZnO, the results of the computation of the figure of merit model indicated that 1wt% gallium was optimum.

5.2 Recommendations for future research

The following recommendations are made with respect to the results of this study:

- The effects of deposition temperature on the structural, electrical and optical properties of indium and gallium doped zinc oxide deposited by spray pyrolysis can be studied and compared with the results from this work.
- The sources of dopants for the In:ZnO and Ga:ZnO can be varied to investigate the effects of the dopants on ZnO properties. Possible sources include gallium nitride (GaN) and indium (III) oxide (In_2O_3) for gallium and indium doping respectively. Using different dopant sources will result in different reactions during the spray deposition process and may affect the yield of ZnO and also the amount of dopant present in ZnO.

REFERENCES

A. Alaeddine, I. R. (2009). Influence of Al Dopant on the Optical and Electrical Properties of Zinc Oxide Thin Films Prepared by Spray Pyrolysis. *Journal of Applied Sciences, 9*, 1588 - 1592.

A. Crossay, S. B. (2012). Spray-deposited Al-doped ZnO transparent contacts for CdTe solar cells. *Solar Energy Materials & Solar Cells*, 283-288.

A. Kolodziejczak-Radzimska (2014). Zinc Oxide - From synthesis to application: A Review. *MDPI Materials Journal,7, 2833 - 2881.*

Ando, M. K. (2010). Chemical Vapor Deposition of Carbon Nanotubes: A Review on Growth Mechanism and Mass Production. *Journal of Nanoscience and Nanotechnology, 10*, 3739 - 3758.

B. Onwona-Agyeman, M. N. (2013). Preparation and characterization of sputtered aluminium and gallium co-doped ZnO films as conductive substrates in dye-sensitized solar cells. *Chemical Engineering Journal, 219*, 273 - 277.

B.E. MaCandles, S. H. (1991). Influence of CdS window layer on thin-film CdS/CdTe solar cell performance. *Proceedings of the 29th IEEE Photovoltaic Specialists Conference*, 967 - 972.

Bhavana Godbole, N. B. (2011). Growth Mechanism of ZnO Films Deposited by Spray Pyrolysis Technique. *Materials Sciences and Applications, 2*, 643 - 648.

Bracken, P. (2010). A Model for the Quantization of the Hall Resistance in the Quantum Hall Effect. *Journal of Modern Physics*, Vol. 1 pp. 158-162.

Cho, Y. (2011). *Review aand Comparison of Different Solar Energy Technologies.* Gloabal Energy Network Institute (GENI).

D. Soler, M. F. (2003). Substrate influence on the properties of doped thin silicon layers grown by Cat-CVD. *Thin Solid Films, 430 (1-2),* 157 - 160.

D.M. Chapin, C. F. (1954). A new silicon p-n junction photo cell for converting solar radiation into electrical power. *Journal of Applied Physics, 25*, 676.

E.R. Rwenyagila, B. A.-T.-O. (2014). Optical properties of ZnO/Al/ZnO multilayer films for large area transparent electrodes. *Materials Research Society Journal*.

E.R. Rwenyagila, B. A.-T.-O. (2015). Computational modeling of optical properties in aluminum nanolayers inserted in ZnO for solar cell electrodes. *Optics Letters, 40*, 3914 - 3917.

F. Paraguay D., W. E.-Y. (1999). Growth, structure and optical characterization of high quality ZnO thin films obtained by spray pyrolysis. *Thin Solid Films*(350), 192-202.

F.Z. Bedia, A. B. (2014). Al-doped Zno transparent contacts deposited by a spray pyrolysis technique on performance of HIT solar cells. *Energy Procedia*(50), 853-861.

F.Z. Bedia, A. B. (2015). Structural, optical and electrical properties of Sn-doped zinc oxide transparent films interesting for organic solar cells (OSCs). *Energy Procedia, 74*, 539 - 546.

Gratzel, M. (2003). Dye-senstizied solar cells. *Journal of Photochemistry and Photobiology C: Photochemistry Reviews, 4*, 145-153.

Haacke, G. (1976). New figure of merit for transparent conductors. *Journal of Applied Physics, 47*, 4086 - 4089.

Hitchman, A. a. (2009). Overview of Chemical Vapor Deposition. In A. a. Hitchman, *Chemical Vapor Deposition, Precursors, Processes and Applications.* Springer Publications.

J.N. Ding, C. T. (2012). The preparation and properties of Al-doped ZnO thin films as transparent electrodes for solar cell. *Physics Procedia*(32), 789-794.

J.P. Krasting, J. D. (2014). Trajeactory sensitivity of the transient climate response to cumulative carbon emissions. *Geophysical Research Letters, 41*, 2520 - 2527.

Jesionowski, A. K.-R. (2014). Zinc Oxide - From Synthesis to Application: A Review. *MDPI Materials Journal, 7*, 2833 - 2881.

Lou, X. (1991). Development of ZnO series ceramic semiconductor gas sensors. *J. Sens. Trans. Technol., 3*, 1-5.

Lung-Chien Chen, C.-A. H. (2014). Electrical Properties of CZO Films Prepared by Ultrasonic Spray Pyrolysis. *MDPI Materials Journal, 7*, 7304 - 7313.

Luque, A., & Hegedus, S. (2011). *Handbook of Photovoltaic Science and Engineering* (2nd ed.). John Wiley & Sons Ltd.

M. Chaari, A. M. (2012). Electrical conduction and dielectric studies of ZnO pellets. *Physics Condensed Matter B, 407*, 3441 - 3447.

M. Krunks, E. M. (1995). Zinc oxide thin films by the spray pyrolysis method. *Thin Solid Films*(270), 33-36.

M. Opel, S. G. (2013). Laser molecular beam epitaxy of ZnO thin films and heterostructures. *Journal of Applied Physics*(D).

M. Purica, E. B. (2002). Optical and structural investigation of ZnO thin films prepared by chemical vapor deposition (CVD). *Thin Solid Films, 403 - 404*, 485 - 488.

Maycook, P. (2003). Top PV cell/module producers. *Photovoltaic News, 22 (2)*, p. 2.

N. Amin, T. I. (2001). Highly efficient 1 thick CdTe solar cells with textered TCOs. *Solar Energy Materials and Solar Cells, 67 (1-4)*, 195 - 201.

P. Docampo, S. G. (2014). Lessons Learned: From Dye-Sensitized Solar Cells to All-Solid-State Hybrid Devices. *Advanced Materials*. doi:10.1002/adma.201400486

P.K. Bhat, S. D. (1979). Back illuminated high efficiency thin-film Cu2S/CdS solar cells. *Solar Energy Materials, 1 (3-4)*, 215 - 219.

P.M. Ratheesh Kumar, C. S. (2005). Effect of fluorine doping on structural, electrical and optical. *Materials Science and Engineering*(B 117), 307-312.

Patil, P. S. (1999). Versatility of chemical spray pyrolysis technique. *Materials Chemistry and Physics*, 185-198.

Pierson, H. O. (1999). *Handbook of Chemical Vapor Deposition, Principles, Technology and Applications* (2nd ed.). Norwich, New York, U.S.A.: Noyes Publications.

R. Groenen, J. L. (2001). Surface textured ZnO films for thin film solar cell applications by expanding thermal plasma CVD. *Thin Solid Films, 392*, 226 - 230.

R.H. Horng, D. W. (1999). Low-resistance and high-transparency Ni/indium tin oxide ohmic contacts to p-type GaN. *Applied Physics Letters, 79*.

R.L. Mitchell, C. W. (2002). PVMat advances in the photovoltaic industry and the focus of future PV manufacturing R&D. *Proceedings of the 29th IEEE Photovoltaic Specialist Conference*, (pp. 1444 - 1447).

R.W. Birkmire, E. E. (1997). Polycrystalline thin-film solar cells: present status and future potential. *Annual review of Materials Science, 27*, 625 - 653.

Rajesh Biswal, A. M.-P. (2014). Indium doped zinc oxide thin films deposited by ultrasonic chemical spray technique, starting from zinc acetylacetonate and indium chloride. *Materials journals*, 5038-5046.

Rajesh Biswal, L. C.-P. (2012). Formation of Indium-Doped Zinc Oxide Thin Films Using Ultrasonic Spray Pyrolysis: The importance of the Water Content in the Aerosol Solution and the Substrate Temperature for Enhancing Electrical Transport. *MDPI Materials Journal, 5*, 432 - 442.

Reimer, L. (1998). *Scanning Electron Microscopy, Physics of Image Formation and Microanalysis* (2nd ed.). Heidelberg, Germany: Springer.

S.H. Jeong, S. K.-H. (2003). Deposition of aluminum-doped zinc oxide films by RF magnetron sputtering and study of their surface characteristics. *Surface and Coatings Technology*(174-175), 187-192.

Shantheyanda, B. P. (2010). *Characterization of Aluminum Doped Zinc Oxide Thin Films for Photovoltaic Applications.* Orlando, Florida: University of Central Florida.

Stadler, A. (2012). Transparent Conducting Oxides - An Up-To-Date Overview. *MDPI Materials Journal*(5), 661 - 683.

Swanepoel, J. v. (1997). XRD analysis of ZnO thin films prepared by spray pyrolysis. *Thin Solid Films, 299*, 72 - 77.

Vignesh Elavalagan, P. S. (2014). A Simple and Novel Room Temperature Ethanolamine ZnO Nanosensor. *Nanoscience and Nanotechnology Letters, 6*, 1046 - 1052.

Wei-Sheng Liu, S.-Y. W.-Y.-H.-L. (2014). Improving the optoelectronic properties of gallium ZnO transparent conductive thin films through titanium doping. *Journal of Alloys and Compounds, 616*, 268 - 274.

X. Mathew, G. T. (2003). Development of CdTe thin-films on flexible structures a review. *Solar Energy Materials and Solar Cells, 76 (3)*, 293 - 303.

Zelenograd, M. i. (2016, June 8). *MVU TM TIS Compact vacuum chemical vapor deposition (CVD) machine*. Retrieved from MVU TM TIS - vacuum CVD machine: http://www.made-in-zelenograd.com/products/mvu-tm-tis/

Zweibel, K. (2000). Thin-film manufacturing: materials cost and thier optimization. *Solar Energy Materials and Solar Cells, 63 (4)*, 375 - 386.

APPENDICES

Appendix A – UV-Vis Spectrophotometry Analysis

Undoped ZnO – 1wt%

Wavelength (nm)	Transmittance (%)	hv (eV)	Absorbance (arb. Units)	αhv^2 $(eVcm^{-1})^2$
350	0.079	3.542857	3.102373	120.8079
365	0.052	3.39726	3.283997	124.4695
380	9.527	3.263158	1.021044	11.10107
395	50.918	3.139241	0.293129	0.846771
410	61.79	3.02439	0.209082	0.39986
425	66.768	2.917647	0.175432	0.261988
440	70.597	2.818182	0.151214	0.181602
455	73.65	2.725275	0.132827	0.131037
470	76.044	2.638298	0.118935	0.098462
485	77.758	2.556701	0.109255	0.078026
500	78.999	2.48	0.102378	0.064464
515	80.194	2.407767	0.095858	0.05327
530	81.597	2.339623	0.088326	0.042704
545	83.09	2.275229	0.080451	0.033505
560	84.642	2.214286	0.072414	0.025711
575	86.063	2.156522	0.065184	0.01976
590	87.126	2.101695	0.059852	0.015823

605	87.774	2.049587	0.056634	0.013474
620	88.082	2	0.055113	0.01215
635	88.068	1.952756	0.055182	0.011612
650	88	1.907692	0.055517	0.011217
665	87.819	1.864662	0.056412	0.011065
680	87.891	1.823529	0.056056	0.010449
695	88.115	1.784173	0.05495	0.009612
710	88.57	1.746479	0.052713	0.008476
725	89.224	1.710345	0.049518	0.007173
740	90.095	1.675676	0.045299	0.005762
755	90.988	1.642384	0.041016	0.004538
770	91.932	1.61039	0.036533	0.003461
785	92.909	1.579618	0.031942	0.002546
800	93.767	1.55	0.02795	0.001877

Undoped ZnO – 2wt%

Wavelength (nm)	Transmittance (%)	hv (eV)	Absorbance (arb. Units)	αhv^2 $(eVcm^{-1})^2$
350	0.029	3.542857	3.537602	157.0816
365	0.033	3.39726	3.481486	139.8901
380	6.001	3.263158	1.221776	15.89497
395	60.928	3.139241	0.215183	0.456316
410	75.256	3.02439	0.123459	0.139418
425	78.934	2.917647	0.102736	0.089848

440	80.421	2.818182	0.094631	0.071121
455	80.967	2.725275	0.091692	0.062443
470	81.357	2.638298	0.089605	0.055887
485	81.902	2.556701	0.086705	0.049142
500	82.631	2.48	0.082857	0.042224
515	83.573	2.407767	0.077934	0.035211
530	84.548	2.339623	0.072897	0.029088
545	85.406	2.275229	0.068512	0.024298
560	86.021	2.214286	0.065396	0.020968
575	86.4	2.156522	0.063486	0.018744
590	86.554	2.101695	0.062713	0.017372
605	86.521	2.049587	0.062878	0.016609
620	86.421	2	0.063381	0.016068
635	86.286	1.952756	0.06406	0.015648
650	86.212	1.907692	0.064432	0.015109
665	86.092	1.864662	0.065037	0.014707
680	86.151	1.823529	0.06474	0.013937
695	86.229	1.784173	0.064347	0.01318
710	86.264	1.746479	0.06417	0.01256
725	86.382	1.710345	0.063577	0.011824
740	86.553	1.675676	0.062718	0.011045
755	86.814	1.642384	0.06141	0.010173
770	87.045	1.61039	0.060256	0.009416
785	87.38	1.579618	0.058588	0.008565
800	87.649	1.55	0.057253	0.007875

Undoped ZnO – 3wt%

Wavelength (nm)	Transmittance (%)	hv (eV)	Absorbance (arb. Units)	αhv^2 $(eVcm^{-1})^2$
350	0.139	3.542857	2.856985	102.4527
365	0.084	3.39726	3.075721	109.1821
380	8.473	3.263158	1.071963	12.23589
395	55.634	3.139241	0.25466	0.639101
410	69.085	3.02439	0.160616	0.235969
425	74.621	2.917647	0.127139	0.137601
440	76.747	2.818182	0.114939	0.104923
455	77.486	2.725275	0.110777	0.091142
470	78.515	2.638298	0.105047	0.07681
485	80.308	2.556701	0.095241	0.059294
500	82.486	2.48	0.08362	0.043005
515	84.588	2.407767	0.072691	0.030633
530	86.181	2.339623	0.064588	0.022835
545	87.048	2.275229	0.060241	0.018786
560	87.368	2.214286	0.058648	0.016864
575	87.311	2.156522	0.058931	0.016151
590	87.085	2.101695	0.060057	0.015932
605	86.895	2.049587	0.061005	0.015634
620	86.904	2	0.06096	0.014865
635	87.137	1.952756	0.059797	0.013635
650	87.75	1.907692	0.056753	0.011722

665	88.43	1.864662	0.0534	0.009915
680	89.389	1.823529	0.048716	0.007892
695	90.436	1.784173	0.043659	0.006068
710	91.434	1.746479	0.038892	0.004614
725	92.321	1.710345	0.034699	0.003522
740	93.009	1.675676	0.031475	0.002782
755	93.601	1.642384	0.02872	0.002225
770	93.973	1.61039	0.026997	0.00189
785	94.245	1.579618	0.025742	0.001653
800	94.183	1.55	0.026027	0.001628

Undoped ZnO – 4wt%

Wavelength (nm)	Transmittance (%)	hv (eV)	Absorbance (arb. Units)	αhv^2 $(eVcm^{-1})^2$
350	0.217	3.542857	2.66354	89.04834
365	0.189	3.39726	2.723538	85.61002
380	11.158	3.263158	0.952414	9.658894
395	69.267	3.139241	0.159474	0.250626
410	74.52	3.02439	0.127727	0.149225
425	74.612	2.917647	0.127191	0.137715
440	80.129	2.818182	0.09621	0.073516
455	81.843	2.725275	0.087018	0.05624
470	83.011	2.638298	0.080864	0.045516
485	84.519	2.556701	0.073046	0.034878
500	85.45	2.48	0.068288	0.028681
515	87.631	2.407767	0.057342	0.019062
530	89.456	2.339623	0.048391	0.012818
545	89.737	2.275229	0.047028	0.011449
560	90.716	2.214286	0.042316	0.00878
575	91.056	2.156522	0.040691	0.0077
590	92.45	2.101695	0.034093	0.005134
605	92.567	2.049587	0.033544	0.004727
620	94.159	2	0.026138	0.002733
635	94.515	1.952756	0.024499	0.002289
650	93.425	1.907692	0.029537	0.003175

665	93.45	1.864662	0.029421	0.00301
680	93.125	1.823529	0.030934	0.003182
695	92.158	1.784173	0.035467	0.004004
710	91.672	1.746479	0.037763	0.00435
725	90.328	1.710345	0.044178	0.005709
740	90.459	1.675676	0.043548	0.005325
755	89.283	1.642384	0.049231	0.006538
770	89.014	1.61039	0.050542	0.006625
785	88.93	1.579618	0.050952	0.006478
800	88.438	1.55	0.053361	0.006841

Undoped ZnO – 5wt%

Wavelength (nm)	Transmittance (%)	hv (eV)	Absorbance (arb. Units)	αhv^2 $(eVcm^{-1})^2$
350	0.553	3.542857	2.257275	63.95525
365	0.378	3.39726	2.422508	67.7311
380	15.711	3.263158	0.803796	6.879677
395	67.824	3.139241	0.168617	0.280188
410	77.737	3.02439	0.109372	0.109418
425	84.182	2.917647	0.074781	0.047604
440	88.187	2.818182	0.054595	0.023673
455	89.09	2.725275	0.050171	0.018695
470	88.193	2.638298	0.054566	0.020725
485	86.903	2.556701	0.060965	0.024295
500	86.152	2.48	0.064735	0.025774
515	86.233	2.407767	0.064327	0.023989
530	87.215	2.339623	0.059409	0.019319
545	88.797	2.275229	0.051602	0.013784
560	90.692	2.214286	0.042431	0.008827
575	92.6	2.156522	0.033389	0.005185
590	94.283	2.101695	0.025567	0.002887
605	95.595	2.049587	0.019565	0.001608
620	96.404	2	0.015905	0.001012
635	96.646	1.952756	0.014816	0.000837

650	96.521	1.907692	0.015378	0.000861
665	95.901	1.864662	0.018177	0.001149
680	95.079	1.823529	0.021915	0.001597
695	94.288	1.784173	0.025544	0.002077
710	93.223	1.746479	0.030477	0.002833
725	92.338	1.710345	0.03462	0.003506
740	91.406	1.675676	0.039025	0.004276
755	90.674	1.642384	0.042517	0.004876
770	90.04	1.61039	0.045565	0.005384
785	89.779	1.579618	0.046825	0.005471
800	89.328	1.55	0.049012	0.005771

Indium doped ZnO (In:ZnO) – 1wt%

Wavelength	Transmittance	hν	Absorbance	$\alpha h\nu^2$
(nm)	(%)	(eV)	(arb. Units)	$(eVcm^{-1})^2$
350	0.01	3.542857	4	200.8294
365	0.015	3.39726	3.823909	168.7612
380	0.259	3.263158	2.5867	71.2473
395	9.511	3.139241	1.021774	10.28866
410	40.154	3.02439	0.396271	1.436351
425	45.214	2.917647	0.344727	1.011617
440	47.957	2.818182	0.319148	0.808951
455	49.483	2.725275	0.305544	0.693375
470	52.201	2.638298	0.282321	0.554798
485	56.762	2.556701	0.245942	0.395391
500	57.331	2.48	0.24161	0.359033
515	59.224	2.407767	0.227502	0.300055
530	58.989	2.339623	0.229229	0.287628
545	60.094	2.275229	0.221169	0.25322
560	60.158	2.214286	0.220707	0.238835
575	60.362	2.156522	0.219236	0.223529
590	62.15	2.101695	0.206559	0.188463
605	62.903	2.049587	0.201329	0.170272
620	63.251	2	0.198933	0.158297
635	63.823	1.952756	0.195023	0.145033

650	64.456	1.907692	0.190737	0.132399
665	64.693	1.864662	0.189143	0.124388
680	65.186	1.823529	0.185846	0.11485
695	65.305	1.784173	0.185054	0.109011
710	65.51	1.746479	0.183692	0.102922
725	66.061	1.710345	0.180055	0.094837
740	66.411	1.675676	0.17776	0.088725
755	66.835	1.642384	0.174996	0.082605
770	67.108	1.61039	0.173226	0.077819
785	67.814	1.579618	0.168681	0.070996
800	68.131	1.55	0.166655	0.066727

Indium doped ZnO (In:ZnO) – 2wt%

Wavelength (nm)	Transmittance (%)	hv (eV)	Absorbance (arb. Units)	αhv^2 $(eVcm^{-1})^2$
350	0.019	3.542857	3.721246	173.8138
365	0.017	3.39726	3.769551	163.9974
380	0.283	3.263158	2.548214	69.14294
395	8.487	3.139241	1.071246	11.30908
410	40.561	3.02439	0.391891	1.404776
425	47.644	2.917647	0.321992	0.882582
440	51.802	2.818182	0.285653	0.648063
455	54.446	2.725275	0.264034	0.517774
470	56.456	2.638298	0.24829	0.429107
485	58.104	2.556701	0.235794	0.363434
500	59.34	2.48	0.226652	0.315954
515	60.165	2.407767	0.220656	0.282267
530	60.736	2.339623	0.216554	0.256698
545	61.389	2.275229	0.211909	0.232461
560	62.043	2.214286	0.207307	0.210715
575	62.667	2.156522	0.202961	0.191573
590	63.267	2.101695	0.198823	0.174611
605	63.816	2.049587	0.19507	0.159851
620	64.285	2	0.19189	0.147288
635	64.729	1.952756	0.188901	0.136071
650	65.142	1.907692	0.186139	0.126093

665	65.547	1.864662	0.183447	0.11701
680	65.977	1.823529	0.180607	0.108467
695	66.369	1.784173	0.178035	0.100898
710	66.795	1.746479	0.175256	0.093686
725	67.229	1.710345	0.172443	0.086988
740	67.609	1.675676	0.169995	0.081144
755	68.006	1.642384	0.167453	0.075637
770	68.41	1.61039	0.16488	0.070502
785	68.811	1.579618	0.162342	0.065761
800	69.145	1.55	0.160239	0.061688

Indium doped ZnO (In:ZnO) – 3wt%

Wavelength (nm)	Transmittance (%)	hv (eV)	Absorbance (arb. Units)	αhv^2 $(eVcm^{-1})^2$
350	0.063	3.542857	3.200659	128.5838
365	0.192	3.39726	2.716699	85.18058
380	5.595	3.263158	1.2522	16.69643
395	26.024	3.139241	0.584626	3.368258
410	42.051	3.02439	0.376224	1.294696
425	49.826	2.917647	0.302544	0.779188
440	54.179	2.818182	0.266169	0.562669
455	56.886	2.725275	0.244995	0.445793
470	58.915	2.638298	0.229774	0.367494
485	60.635	2.556701	0.217277	0.308593
500	62.156	2.48	0.206517	0.26231
515	63.478	2.407767	0.197377	0.22585
530	64.8	2.339623	0.188425	0.194343
545	65.982	2.275229	0.180575	0.168796
560	67.071	2.214286	0.173465	0.147534
575	68.061	2.156522	0.167102	0.129858
590	69.023	2.101695	0.161006	0.114505
605	69.944	2.049587	0.15525	0.10125
620	70.788	2	0.15004	0.090048
635	71.593	1.952756	0.145129	0.080317
650	72.31	1.907692	0.140802	0.072149

665	73.092	1.864662	0.13613	0.064433
680	73.724	1.823529	0.132391	0.058283
695	74.389	1.784173	0.128491	0.052556
710	74.943	1.746479	0.125269	0.047864
725	75.47	1.710345	0.122226	0.043701
740	76.05	1.675676	0.118901	0.039696
755	76.579	1.642384	0.11589	0.036228
770	77.067	1.61039	0.113132	0.033192
785	77.536	1.579618	0.110497	0.030465
800	77.975	1.55	0.108045	0.028046

Indium doped ZnO (In:ZnO) – 4wt%

Wavelength (nm)	Transmittance (%)	hv (eV)	Absorbance (arb. Units)	αhv^2 $(eVcm^{-1})^2$
350	0.031	3.542857	3.508638	154.5199
365	0.037	3.39726	3.431798	135.9256
380	0.916	3.263158	2.038105	44.23124
395	15.678	3.139241	0.804709	6.381566
410	40.282	3.02439	0.394889	1.426349
425	55.197	2.917647	0.258085	0.567008
440	62.684	2.818182	0.202843	0.326783
455	66.332	2.725275	0.178277	0.236054
470	68.373	2.638298	0.165115	0.189768
485	69.803	2.556701	0.156126	0.159335
500	70.909	2.48	0.149299	0.137093
515	71.797	2.407767	0.143894	0.120036
530	72.711	2.339623	0.1384	0.104849
545	73.416	2.275229	0.134209	0.093243
560	74.032	2.214286	0.130581	0.083603
575	74.679	2.156522	0.126802	0.074775
590	75.228	2.101695	0.12362	0.067503
605	75.775	2.049587	0.120474	0.06097
620	76.275	2	0.117618	0.055336
635	76.72	1.952756	0.115091	0.050511
650	77.171	1.907692	0.112546	0.046097

665	77.593	1.864662	0.110177	0.042207
680	77.701	1.823529	0.109573	0.039924
695	78.201	1.784173	0.106788	0.036301
710	78.481	1.746479	0.105235	0.033779
725	78.876	1.710345	0.103055	0.031068
740	79.106	1.675676	0.101791	0.029093
755	79.378	1.642384	0.1003	0.027136
770	79.638	1.61039	0.09888	0.025356
785	79.874	1.579618	0.097595	0.023766
800	80.215	1.55	0.095744	0.022024

Indium doped ZnO (In:ZnO) – 5wt%

Wavelength (nm)	Transmittance (%)	hv (eV)	Absorbance (arb. Units)	αhv^2 $(eVcm^{-1})^2$
350	0.017	3.542857	3.769551	178.3555
365	0.016	3.39726	3.79588	166.2963
380	0.943	3.263158	2.025488	43.68533
395	23.145	3.139241	0.635543	3.980511
410	39.462	3.02439	0.403821	1.491603
425	48.874	2.917647	0.310922	0.822941
440	54.07	2.818182	0.267044	0.566373
455	57.221	2.725275	0.242445	0.436562
470	59.377	2.638298	0.226382	0.356722
485	61.208	2.556701	0.213192	0.297099
500	62.755	2.48	0.202352	0.251835
515	64.041	2.407767	0.193542	0.21716
530	65.513	2.339623	0.183673	0.184663
545	66.568	2.275229	0.176734	0.161694
560	67.54	2.214286	0.170439	0.142431
575	68.545	2.156522	0.164024	0.125119
590	69.457	2.101695	0.158284	0.110666
605	70.316	2.049587	0.152946	0.098267
620	71.212	2	0.147447	0.086962
635	72	1.952756	0.142668	0.077615
650	72.701	1.907692	0.13846	0.069769

665	73.423	1.864662	0.134168	0.062589
680	73.93	1.823529	0.131179	0.057221
695	74.686	1.784173	0.126761	0.05115
710	75.23	1.746479	0.123609	0.046604
725	75.971	1.710345	0.119352	0.04167
740	76.427	1.675676	0.116753	0.038275
755	77.018	1.642384	0.113408	0.034692
770	77.554	1.61039	0.110396	0.031606
785	78.005	1.579618	0.107878	0.029038
800	78.646	1.55	0.104323	0.026147

Gallium doped ZnO (Ga:ZnO) – 1wt%

Wavelength (nm)	Transmittance (%)	hv (eV)	Absorbance (arb. Units)	αhv^2 $(eVcm^{-1})^2$
350	0.06	3.542857	3.221849	130.2919
365	0.105	3.39726	2.978811	102.4103
380	15.047	3.263158	0.82255	7.204451
395	75.015	3.139241	0.124852	0.153617
410	75.991	3.02439	0.119238	0.130048
425	82.264	2.917647	0.08479	0.061201
440	86.128	2.818182	0.064856	0.033407
455	86.316	2.725275	0.063909	0.030335
470	86.701	2.638298	0.061976	0.026736
485	86.965	2.556701	0.060655	0.024049
500	87.484	2.48	0.058071	0.020741
515	85.991	2.407767	0.065547	0.024908
530	86.734	2.339623	0.061811	0.020913
545	87.33	2.275229	0.058837	0.01792
560	87.522	2.214286	0.057883	0.016427
575	88.701	2.156522	0.052071	0.01261
590	88.451	2.101695	0.053297	0.012547
605	88.618	2.049587	0.052478	0.011569
620	88.882	2	0.051186	0.01048
635	89.001	1.952756	0.050605	0.009765
650	88.643	1.907692	0.052356	0.009976

665	88.806	1.864662	0.051558	0.009242
680	88.786	1.823529	0.051656	0.008873
695	88.625	1.784173	0.052444	0.008755
710	89.119	1.746479	0.05003	0.007635
725	89.029	1.710345	0.050469	0.007451
740	89.302	1.675676	0.049139	0.00678
755	89.563	1.642384	0.047871	0.006182
770	89.615	1.61039	0.047619	0.005881
785	89.713	1.579618	0.047145	0.005546
800	89.921	1.55	0.046139	0.005114

Gallium doped ZnO (Ga:ZnO) – 2wt%

Wavelength (nm)	Transmittance (%)	hv (eV)	Absorbance (arb. Units)	αhv^2 $(eVcm^{-1})^2$
350	0.044	3.542857	3.356547	141.4141
365	0.042	3.39726	3.376751	131.5999
380	9.284	3.263158	1.032265	11.34641
395	71.631	3.139241	0.144899	0.206909
410	81.753	3.02439	0.087496	0.070025
425	84.393	2.917647	0.073694	0.04623
440	85.276	2.818182	0.069173	0.038003
455	85.119	2.725275	0.069973	0.036365
470	85.468	2.638298	0.068196	0.032372
485	86.125	2.556701	0.064871	0.027508
500	86.633	2.48	0.062317	0.023884
515	86.526	2.407767	0.062853	0.022903
530	85.974	2.339623	0.065633	0.023579
545	85.925	2.275229	0.06588	0.022468
560	86.023	2.214286	0.065385	0.020962
575	86.212	2.156522	0.064432	0.019307
590	86.281	2.101695	0.064085	0.018141
605	86.101	2.049587	0.064992	0.017744
620	85.539	2	0.067836	0.018407
635	84.971	1.952756	0.070729	0.019076
650	84.407	1.907692	0.073622	0.019725

665	83.995	1.864662	0.075747	0.019949
680	83.66	1.823529	0.077482	0.019963
695	83.742	1.784173	0.077057	0.018901
710	84.017	1.746479	0.075633	0.017448
725	84.45	1.710345	0.0734	0.01576
740	84.895	1.675676	0.071118	0.014202
755	85.264	1.642384	0.069234	0.01293
770	85.349	1.61039	0.068802	0.012276
785	85.5	1.579618	0.068034	0.011549
800	85.238	1.55	0.069367	0.01156

Gallium doped ZnO (Ga:ZnO) – 3wt%

Wavelength (nm)	Transmittance (%)	hv (eV)	Absorbance (arb. Units)	αhv^2 $(eVcm^{-1})^2$
350	0.027	3.542857	3.568636	159.8497
365	0.02	3.39726	3.69897	157.9135
380	5.739	3.263158	1.241164	16.40342
395	60.732	3.139241	0.216582	0.46227
410	71.62	3.02439	0.144966	0.192223
425	74.059	2.917647	0.130422	0.1448
440	75.427	2.818182	0.122473	0.11913
455	76.352	2.725275	0.11718	0.101982
470	76.927	2.638298	0.113921	0.090335
485	77.352	2.556701	0.111528	0.081308
500	77.573	2.48	0.110289	0.074812
515	77.652	2.407767	0.109847	0.069953
530	77.688	2.339623	0.109646	0.065808
545	77.616	2.275229	0.110049	0.062693
560	77.513	2.214286	0.110625	0.060004
575	77.496	2.156522	0.110721	0.057012
590	77.451	2.101695	0.110973	0.054397
605	77.517	2.049587	0.110603	0.051389
620	77.617	2	0.110043	0.048438
635	77.743	1.952756	0.109339	0.045587
650	77.86	1.907692	0.108686	0.042989

665	77.853	1.864662	0.108725	0.041101
680	77.898	1.823529	0.108474	0.039127
695	77.821	1.784173	0.108903	0.037753
710	77.738	1.746479	0.109367	0.036483
725	77.614	1.710345	0.11006	0.035434
740	77.594	1.675676	0.110172	0.034082
755	77.525	1.642384	0.110558	0.032971
770	77.425	1.61039	0.111119	0.032021
785	77.484	1.579618	0.110788	0.030626
800	77.498	1.55	0.11071	0.029446

Gallium doped ZnO (Ga:ZnO) – 4wt%

Wavelength (nm)	Transmittance (%)	hv (eV)	Absorbance (arb. Units)	αhv^2 $(eVcm^{-1})^2$
350	0.116	3.542857	2.935542	108.1643
365	0.117	3.39726	2.931814	99.2043
380	18.28	3.263158	0.738024	5.799852
395	68.97	3.139241	0.16134	0.256526
410	76.307	3.02439	0.117436	0.126147
425	78.773	2.917647	0.103623	0.091406
440	79.999	2.818182	0.096915	0.074597
455	80.439	2.725275	0.094533	0.066373
470	80.739	2.638298	0.092917	0.060094
485	81.142	2.556701	0.090754	0.053839
500	81.619	2.48	0.088209	0.047855
515	82.034	2.407767	0.086006	0.042883
530	82.237	2.339623	0.084933	0.039486
545	82.304	2.275229	0.084579	0.037032
560	82.295	2.214286	0.084627	0.035114
575	82.227	2.156522	0.084986	0.033589
590	82.246	2.101695	0.084885	0.031828
605	82.366	2.049587	0.084252	0.029819
620	82.445	2	0.083836	0.028114
635	82.447	1.952756	0.083825	0.026794
650	82.39	1.907692	0.084125	0.025756

665	82.136	1.864662	0.085466	0.025398
680	81.86	1.823529	0.086928	0.025127
695	81.387	1.784173	0.089445	0.025467
710	80.982	1.746479	0.091612	0.025599
725	80.518	1.710345	0.094107	0.025907
740	80.163	1.675676	0.096026	0.025892
755	79.907	1.642384	0.097415	0.025598
770	79.843	1.61039	0.097763	0.024786
785	79.794	1.579618	0.09803	0.023978
800	80.007	1.55	0.096872	0.022546

Gallium doped ZnO (Ga:ZnO) – 5wt%

Wavelength	Transmittance	hν	Absorbance	$\alpha h\nu^2$
(nm)	(%)	(eV)	(arb. Units)	$(eVcm^{-1})^2$
350	0.025	3.542857	3.60206	162.8580254
365	0.026	3.39726	3.585027	148.3345843
380	28.923	3.263158	0.538757	3.090732968
395	66.105	3.139241	0.179766	0.318465795
410	73.762	3.02439	0.132167	0.159780509
425	75.502	2.917647	0.122042	0.126788802
440	76.342	2.818182	0.117236	0.109159983
455	77.019	2.725275	0.113402	0.095513104
470	77.565	2.638298	0.110334	0.084736004
485	78.132	2.556701	0.107171	0.075078387
500	78.322	2.48	0.106116	0.069257529
515	78.48	2.407767	0.105241	0.064209441
530	78.878	2.339623	0.103044	0.058121655
545	79.001	2.275229	0.102367	0.05424676
560	79.206	2.214286	0.101242	0.050256015
575	79.44	2.156522	0.099961	0.046469374
590	79.596	2.101695	0.099109	0.043387378
605	79.658	2.049587	0.098771	0.040981516

620	79.694	2	0.098574	0.038867629
635	79.719	1.952756	0.098438	0.036950717
650	79.703	1.907692	0.098525	0.035327464
665	79.689	1.864662	0.098602	0.033804009
680	79.664	1.823529	0.098738	0.032418524
695	79.701	1.784173	0.098536	0.030907625
710	79.717	1.746479	0.098449	0.029563086
725	79.738	1.710345	0.098335	0.028286591
740	79.808	1.675676	0.097954	0.026941421
755	79.829	1.642384	0.097839	0.025821189
770	80.022	1.61039	0.096791	0.024295636
785	79.993	1.579618	0.096948	0.023452109
800	80.119	1.55	0.096264	0.022263607

Appendix B – Sheet resistance measurements

Indium doped zinc oxide (In:ZnO) Sheet resistance – Test 1

Dopant concentration	Sheet resistance	Sheet resistance	Sheet resistance	Average Sheet resistance
(wt%)	(kΩ)	(kΩ)	(kΩ)	(kΩ)
	Reading 1	Reading 1	Reading 1	
1	101.510	993.20	105.380	102.070
2	112.250	120.410	132.010	121.557
3	153.520	158.240	141.010	150.923
4	186.450	192.740	185.440	188.210
5	250.730	235.800	240.310	242.280

Indium doped zinc oxide (In:ZnO) Sheet resistance – Test 2

Dopant concentration	Sheet resistance	Sheet resistance	Sheet resistance	Average Sheet resistance
(wt%)	(kΩ)	(kΩ)	(kΩ)	(kΩ)
	Reading 1	Reading 1	Reading 1	
1	95.710	98.150	89.630	94.497
2	110.620	971.40	122.270	110.010
3	168.140	152.340	168.550	163.010
4	192.560	195.680	189.750	192.663
5	278.160	286.590	273.270	279.340

Gallium doped zinc oxide (Ga:ZnO) Sheet resistance – Test 1

Dopant concentration	Sheet resistance	Sheet resistance	Sheet resistance	Average Sheet resistance
(wt%)	(MΩ)	(MΩ)	(MΩ)	(MΩ)
	Reading 1	Reading 1	Reading 1	
1	7.1	8.15	8.53	7.92667
2	6.43	7.23	6.3	6.65333
3	8.21	9.04	8.57	8.60667
4	12.73	1.4.51	14.86	14.0333
5	18.5	20.13	21.48	20.0367

Gallium doped zinc oxide (Ga:ZnO) Sheet resistance – Test 2

Dopant concentration	Sheet resistance	Sheet resistance	Sheet resistance	Average Sheet resistance
(wt%)	(MΩ)	(MΩ)	(MΩ)	(MΩ)
	Reading 1	Reading 1	Reading 1	
1	5.41	6.02	4.38	5.27033
2	6.14	6.54	6.40	6.36
3	9.05	9.17	9.35	9.19
4	11.28	12.59	12.75	12.2067
5	21.43	22.49	21.72	21.88

Appendix C – Thin Film deposition process

Figure A 1 Weighing of chemicals for precursor solution

Figure A 2 Cleaning of substrates in an ultrasonic cleaner

Figure A 6 Addition of dopant solution to zinc acetate solution

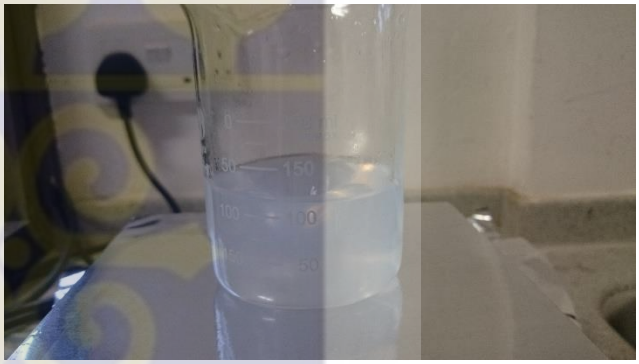

Figure A 5 Stirring of precursor solution

Figure A 4 Spray gun for aerosol formation and delivery

Figure A 7 Air compressor

Figure A 3 Glass slide on hot-plate during spray deposition